THE TEMPERATURE DEPENDENT NON-LINEAR RESPONSE OF A WOOD PLASTIC COMPOSITE

By

DOUGLAS J. POOLER

A thesis submitted in partial fulfillment of
the requirements for the degree of

MASTER OF SCIENCE IN MECHANICAL ENGINEERING

WASHINGTON STATE UNIVERSITY
Department of Mechanical and Materials Engineering

August 2001

To the Faculty of Washington State University:

The Members of the Committee appointed to examine the thesis of Douglas J. Pooler find it satisfactory and recommend that it be accepted.

_____
Chair

_____

_____

ACKNOWLEDGMENT

The author would like to gratefully acknowledge the following for their support and contribution to this work:

- Dr. Lloyd Smith: for serving on my committee, for his insight and expertise in the matters of polymer and composite viscoelasticity, his patience, and his friendship.
- Dr. Michael Wolcott: for serving on my committee, for the time he spent discussing the project, and the guidance he gave me, and for sharing some of his experience with wood and wood-plastic composites.
- Dr. Stephen Antolovich: for serving on my committee, and for his help with damage and fracture of materials.
- David Dostal: for his help mixing and extruding the material used in this work. Also for sharing his contacts with those in the plastics industry.
- Suzanne Peyer: for conducting the DMA analysis of the material.
- Dr. Claude Bathias of ITMA: for Computed Tomography analysis of specimens for failure mechanisms.
- John Grimes, Norm Marcell, and Henry Ruff: for their help with the little things I had to build for this project.
- Robert Lentz: for his help finding equipment and setting up testing apparati.
- The office staff: Jan, Gayle, Margie, Annette and Sarah for their support and keeping my life as simple as possible.

- Scott, Rob, Billy, John, Jens, Ben, and everyone else who stopped by and talked about the weather, movies, the messiness of my desk, farting paper cranes, and anything other than viscoelasticity, time dependent behavior, damage mechanisms, numerical integration, and TTSP, thereby keeping me sane.
- Sarah, my love, for her tender, loving support and understanding, and the flowers that continually brightened my desk. ;)
- My family, for their support and prayers.
- This work is supported by the Office of Naval Research and the Wood Materials and Engineering Laboratory at Washington State University, under contract No. 00014-97-C-0395. Their support is gratefully acknowledged.

THE TIMPERATURE DEPENDENT NON-LINEAR VISCOELASTIC

RESPONSE OF A WOOD PLASTIC COMPOSITE

Abstract

By Douglas J. Pooler, M.S.
Washington State University
August 2001

Chair: Lloyd V. Smith

The present work investigates the effect of temperature on the viscoelastic strain response of a wood-plastic composite. A power law model and a Prony Series model for the viscoelastic strain response were investigated to describe the time dependent behavior of the material at 23^{o}C, 45^{o}C, and 65^{o}C. With application of the time-temperature superposition principle, the Prony Series was found to match more closely with experimental data. While the threshold stress was found to scale with the temperature dependent ultimate strength of the material, the magnitude of damage was found to have a highly non-linear temperature dependence above this threshold stress.

The viscoelastic model developed from the creep analysis was applied to determine the cyclic peak strain response during fatigue loading of the wood-plastic composite. Satisfactory comparisons were achieved with the Prony Series below the threshold stress. The model was found be ineffective in describing the damage caused by cyclic loading above the threshold stress, however. The non-linear temperature dependence of damage observed in creep was also found for fatigue loading.

TABLE OF CONTENTS

Page

LIST OF TABLES

LIST OF FIGURES

Dedication

This thesis is dedicated to Sarah, my wife-to-be,

and to my parents.

CHAPTER ONE

BACKGROUND

1.1 Background

Much of the Navy's waterfront facilities are constructed of treated timber. Due to its treating against water and biological degradation, this material must be disposed of as low level hazardous waste, which is costly, amounting to approximately $40-50 million per year. Extruded wood-plastic composites are an attractive alternative due to their ease of manufacture, and the ability to reduce water adsorption without chemical treatment (which may leach into the water). Wood-plastic composites and plastic lumber have been successfully used in non-structural applications such as decking, but have been limited in their structural use in the commercial sector due in part to the time and temperature dependent nature of the material. Work has been undertaken to improve the mechanical properties and water resistance of the wood-plastic composite for use in structural applications.

Previous work on this subject has considered the effects of water sorption on the mechanical properties and fatigue life of the material. This paper continues the work of developing testing means to evaluate and compare different formulations and materials to facilitate selection of appropriate materials for each specific application within the design of waterfront and private structures. Specifically, this paper deals with the effects of temperature on the viscoelastic response of the wood plastic composite, and the creation of a predictive model of its behavior.

1.2 Literature Review

1.2.1 Classical Viscoelasticity

The study of viscoelastic behavior increased has in fervor as the use of polymeric materials in engineering applications has become more widespread. Viscoelastic materials, must be modeled with both time dependent and elastic components and therefore, cannot be simply represented with Hooke's law. The simplest forms of viscoelastic response involve either stress relaxation, where a specimen is elongated to a prescribed strain and the magnitude of the stress is measured over time; or creep, where the specimen is loaded to a constant stress, and the resulting time dependent strain response is recorded. Compliance, which may be thought of as the inverse of stiffness, embodies the necessary time dependence in the latter of the two methods. It is this rendering which will be utilized in this investigation.

One of the simpler time dependent compliance models is the linear viscoelastic power law model. As presented by Schapery [1], this can be expressed as

$$D(t) = D_o + D_1 t^n \tag{1.1}$$

where D_o and D_1 are the instantaneous compliance and the time dependent compliance respectively and n is an empirically determined material parameter. The viscoelastic behavior of many materials can be described with this model.

In order to describe more complex viscoelastic behavior, models utilizing combinations of springs (Hookeian behavior) and dashpots (time dependent behavior) in parallel or series, or combinations of both have been developed. The Kelvin and Maxwell models are mentioned by Flugge [2] as examples. A Prony Series can be described as N

Kelvin elements (springs and dashpots in parallel) in series with a lone spring, as shown in **Fig. 1.1**. The time dependent compliance of this model can be represented as [3]

$$D(t) = D_o + \sum_{r=1}^{N} D_r \left[1 - e^{\frac{-t}{\tau_r}} \right] \tag{1.2}$$

where D_o and D_i, are positive constants, and where τ_i is the retardation time. The spring-dashpot models are very versatile in that additional stiffness and damping mechanisms can model varying modes of viscoelastic response occurring in long duration tests when compared to the power law model which models only one mode. There are many other forms of the time dependent compliance used to model viscoelastic behavior which will be explored in the next section.

Calculation of the time dependent strain response from the known time dependent compliance may be accomplished utilizing Schapery's application of the Boltzmann superposition principle. This principle indicates that the final stress or strain response of a material to a series of applied displacement or loads is the summation of all the individual stress or strain responses to the individual displacement or loads. This can be graphically represented as in **Fig. 1.2**. In this figure, a second creep stress is applied at 400 seconds. The strain response (dashed line) from that load, as if it were applied to an unstressed specimen, can be added to the strain response from the initial stress. Schapery's application of this principle has been called the convolution integral and may be expressed as

$$\varepsilon(t) = \int_{-\infty}^{t} D(t-\tau) \frac{d\sigma(\tau)}{d\tau} d\tau \tag{1.3}$$

where $\varepsilon(t)$ is the strain response to an applied load, $D(t)$ is the time dependent compliance and $\sigma(t)$ is the applied stress. Eq. (1.4), when used to evaluate the time dependent

compliance given by Eq. (1.1) or (1.2) results in a viscoelastic model for the strain response.

Schapery presents a general form of the time-dependent non-linear compliance, from which linear compliance may be derived, as

$$D(t) = \frac{\varepsilon}{\sigma_o} = g_o D_o + g_1 g_2 \Delta D\left(\frac{t}{a_\sigma}\right) \tag{1.4}$$

where D_o is the instantaneous compliance, and $\Delta D(t)$ is the time dependent compliance. (Note that both Eq. (1.1) and (1.2) can be expressed in the form $D(t)=D_o+\Delta D_1(t)$.) The equation is non-linear due to the presence of g_o, g_1, g_2 and a_σ which are stress dependent parameters, and are related to the stress dependence of Gibb's free energy and other free energy and entropy production concepts. [1] These parameters are not time dependent, and are therefore evaluated after integration has been completed, as seen in Eq. (1.4) A linear viscoelastic model results when $g_o=g_1=g_2=a_\sigma=1$, ie. there is no stress dependence.

1.2.2 Viscoelastic models

Walrath [4] utilized a power law model in his exploration of the behavior of the non-linear strain response of an aramid reinforced epoxy. He incorporated two viscoelastic constituents into the nonlinear viscoelastic parameters, and found that this worked reasonably well for predicting uniaxial creep and recovery response of the composite. He also was able to model temperature dependent strain response using the time-temperature superposition principle (TTSP) manifested in a time shift factor.

Elahi and Weitsman have used the linear power law compliance model with great success in modeling the linear viscoelastic strain response and non-linear response of a random oriented glass fiber/urethane resin composite [5,6]. A damage model with short

and long time dependence was utilized to model the behavior above a threshold stress. Rangaraj and Smith, [7] also utilized a linear power law in their investigation of the creep and recovery behavior of a WPC with the same volumetric constituency as that utilized in this work. This was found to model the strain response to an applied load in creep and recovery reasonably well within stress levels at which damage did not occur (material stiffness did not change after load application). At stress levels where material degradation occurred, use of a damage model applied to the power law was found to account for damage and adequately model strain response. Details of this work will be described further in Chapter 3.

Sain, et. al [8] utilized a similar power law equation in their investigation of PVC based, PE based, and PP based wood-plastic composites,

$$\varepsilon(t) = \varepsilon_o + At^{\tau} \tag{1.5}$$

where A is the amplitude of the transient creep strain, ε_o is the instantaneous strain and τ is the time constant. Testing was conducted between 22°C and 60°C. The time constant τ and the instantaneous strain ε_o were adjusted with temperature based on empirical data to account for the temperature dependence of the modeled strain response. Utilizing flexural testing, they noted the relatively low temperature dependence of the time dependent portion when compared to the temperature dependence of the instantaneous strain. However, as greater loads were applied, the time dependent strain became more influential in the overall flexural creep strain response. It was also noted that the addition of wood into a PE matrix significantly retarded the time dependent strain response when compared to the strain response of virgin PE. It was also found that the response of a

wood-fiber composite could not be predicted based on a rule of mixtures combination of the properties of the constituents.

Other investigators have utilized other models to describe the time dependent response of viscoelastic materials. The Nutting equation mentioned by Neilsen and Landel [9] has been used to describe the uniaxial strain response of a viscoelastic material. It can be expressed as

$$\varepsilon(t) = K\sigma^{\beta}t^{n} \tag{1.6}$$

where K, β and n are constants at a given temperature, and β is equal to or greater than 1. While this equation models experimental data reasonably well in the linear region where β=1, however n has been observed to change over long times. A hyperbolic tangent function has been used to model the non-linear stress-strain response of a wood plastic composite by Hermanson, et. al. This can be described as

$$\sigma = a\tanh(b\varepsilon) \tag{1.7}$$

where a and b are parameters to fit the experimental data, [10] and are analogous to strength and modulus. This method is mostly empirical and does not describe time dependence. Conversely, the hyperbolic sine function has been validated by Neilsen, [11] among others. The hyperbolic sine function can be represented

$$\varepsilon(t) = K(t)\sinh\frac{\sigma}{\sigma_c} \tag{1.8}$$

where $K(t)$ defines the creep time dependence and σ_c is a critical stress. However, σ_c varies with temperature and material structure. [8] A hyperbolic sine function has also been ulitized to describe the stress dependence of the g_o and g_1g_2/a_σ terms in Eq. (1.4) by Schapery [1] and Van Holde[12].

Veazie and Gates, [13] in their study of the aging of an aerospace composite, utilized a linear viscoelastic creep compliance of the form

$$S(t) = S^0 e^{(t/\tau)^\beta} \tag{1.9}$$

where S^0,τ and β are the initial compliance, retardation time, and shape parameter respectively. While they indicate that this equation reaches its limitations at very large times, they did not approach the limits of this function in their testing to 10^8 seconds of shifted time. An additional time shift factor was used to account for aging.

1.2.3 Viscoplastic models

Other investigators have modeled the behavior of polymeric materials with viscoplastic models. Zhang and Moore [14,15], in their analysis of HDPE pipe, compared a non-linear viscoelastic model consisting of a spring and nine Kelvin elements and a viscoplastic model that assumes that both elastic and inelastic deformation occur at all stages of loading. The viscoplastic model was found to better fit rapid loading and loading rate changes.

Gates, in his work on graphite polymeric composites, utilized what may be termed a macromechanical, phenomonological, elastic/viscoplastic model to study the effects of elevated temperatures on the material. [16] Testing was conducted between 23^{o}C and 200^{o}C on various ordered laminates with the parameters of the model accounting for temperature dependence.

1.2.4 Accounting for damage

While viscoplasticity is one method to account for permanent deformation of a polymeric material, other investigators have studied the effects of damage on a composite. Typically, this occurs in the study of ordered composite laminates destined

for aerospace applications. Of primary concern is the understanding of crack propagation through composite materials, delamination, and the relation of crack density to applied load. These may be pursued in either a micromechanics fashion, where the effect of the damage is considered based on crack geometry, or a continuum mechanics fashion, where damage is defined as a continuous field, and individual crack or defect geometry is ignored. This simplifies the mathematical representation, but does not provide information on individual defects [17]. It is this latter avenue which is being pursued in this work. The purpose of this work was not to identify specific micromechanical structure developments within the composite during loading, but rather to model the observed behavior based on classical viscoelastic concepts and provide methods to predict strain response. Elahi and Weistman [5] used a continuum damage model to predict strain response by including a damage function with slowly varying and rapidly varying time dependence in their model. This was found to satisfactorily predict the strain response of a random glass/urethane composite. However, they did not incorporate temperature into their study of damage.

Rangaraj and Smith, [7] also utilized a damage model which did not identify individual cracks, crack propagation, or crack growth. In order to model the strain behavior of the material above the threshold stress where material stiffness degraded after load application, damage was modeled as a combination of instantaneous damage and time dependent damage

$$\omega(t) = 1 + (s + ct^m) < \sigma_o - \sigma_d > \tag{1.10}$$

where *s* and *c* are the instantaneous and time dependent damage parameters, *m* is an experimentally determined parameter, σ_d is the threshold stress, and σ_o is the applied creep stress.

Rangaraj and Smith defined damage as resulting in a degradation of the material's ability to carry a load which could be measured as a change in stiffness. This is consistent with work by Reifsnider [18] who has observed that stiffness changes indicate that damage has occurred in such a way that it can be related to changes in residual strength. Andersons, Limonov and Tamuzs [19] also concur stiffness changes monitored throughout a test can be used as a measure for the amount of damage which has occurred. Webb, et. al. disagree. [20] They remark that because stiffness is only measured in one direction, it does not give a full picture of the damage mechanisms which are occurring (eg. interlaminar failure, interstitial failure, matrix cracking, fiber breakage). For instance, matrix cracking in a long fiber unidirectional composite would not significantly affect the stiffness, which is primarily due to the fibers. Talreja [21] decries the use of "damage" and "change in stiffness" as synonyms, proposing that "damage" only be used to describe the actual physical changes negating confusion and discongruous results between two different researchers with different ideas of "damage." However, "damage," even with this definition, cannot be quantitatively measured, it can only be observed. Lemaitre and Chaboche [22] suggest that damage be defined based on the concept of effective stress

$$\sigma_e = \frac{\sigma}{(1-D)} \tag{1.11}$$

where σ_e is the effective stress and $D = 1 - E_d/E$ where E is the elastic modulus of an undamaged specimen and E_d is the elastic modulus of a damaged specimen and *D* is the damage. Damage may be defined as a scalar only if the orientation of microcracks and

cavities are distributed in all directions. It is this method for quantifying damage which Rangaraj and Smith [7] used for their study of their WPC. Based on its proficiency in modeling the WPC in their work, this method of quantifying damage will be continued in this research.

1.3 Time-Temperature Dependence

The behavior of polymeric materials is dependent on temperature. The time-temperature superposition principle (TTSP) proposes that temperature effects may be described by altering the time scale of the viscoelastic response. This means that the creep data recorded at a reference temperature and shifted according to

$$t^* = \frac{t}{a_T(T)} \tag{1.12}$$

where $a_T(T)$ is the time shift factor, can represent the viscoelastic creep at a temperature T, providing the data is available over a long period of time. Neilsen and Landel describe two methods of accounting for temperature effects. [9] The first was developed by Williams, Landel, and Ferry [23] for temperature dependence of the relaxation modulus of a polymer or composite and is known as the WLF equation which can be expressed as

$$\log a_T = \frac{-c_1\left(T - T_{ref}\right)}{c_2 + T - T_{ref}} \tag{1.13}$$

where c_1 and c_2 are material dependent constants, T is the temperature at which the shift factor is desired, T_{ref} is the reference temperature and $a_T(T)$ is the time shift factor, or horizontal shift factor. This was developed for amorphous polymers in the range of T_g to T_g+100^{o}C from an understanding of viscosity and free volume. Below T_g an Arrhenius relationship is typically used, which is the second model described by Neilsen and Landel. [9] This may be expressed as

$$a_T(T) = \exp\frac{E_a}{R}\left[\frac{1}{T} - \frac{1}{T_{ref}}\right] \tag{1.14}$$

where the universal gas constant R=8.31 J/molK, E_a is the activation energy, T_{ref} is the reference temperature in Kelvin, and T is the temperature at which the time shift factor is desired in Kelvin. [24]

For amorphous polymers, a horizontal shift factor as applied in Eq. (1.13) is sufficient to correctly model temperature dependent response. This can best be understood by viewing an example in **Fig. 1.3**. By applying the horizontal shift according to the curve shown in the inset, in effect shifting time, a master curve describing the behavior of the material within the tested temperature range relative to the reference temperature can be created. Upon application of the time shift factor, time becomes "reduced time," t^*, where time t in the viscoelastic model is replaced by Eq. (1.12). Materials which only require a horizontal time shift factor in the application of TTSP were termed "thermo-rheologically simple" by Schwarzl and Staverman refering to their work on linear viscoelastic behavior. [25] However the TTSP has still been used with great success for semi-crystalline polymers and crystalline polymers with the addition of an empirical vertical shift factor to create a master curve. The mechanism within these materials that results in the vertical shift factor is not completely understood although it is typically applied above the glass transition temperature. Several different theories have been provided.

1.4 Polymeric time-temperature behavior

Crissman [26] refers to the vertical shift factor as a "softening factor" in his study of semi-crystalline high-density polyethylene (HDPE) based on the instantaneous decrease in stiffness associated with polymeric materials as temperature increases. By

using a non-linear model for strain response, then subtracting out the strain due to plasticity, he was able to create a master curve, using both horizontal and vertical shift factors.

Elahi and Weitsman, [5,6] in their application of TTSP with their chopped glass/urethane composite, multiplied their instantaneous compliance term by a temperature dependent equation to account for the increase in compliance or "softening" observed as temperature increased. Penn [27] explains the need for a vertical shift factor in his examination of HDPE between –20^{o}C and 80^{o}C as softening or premelting of crystal boundaries.

Onogi, et. al., [28] utilized such methods as Differential Scanning Calorimetry, Depolarized Light Intensity, Infrared Dichroism, Nuclear Magnetic Resonance, and Dynamic Mechanical Analysis in their study of thin HDPE films 100-120μm thick. While the vertical shift factor had been thought to be a representation of the change in crystallinity, they found that crystallinity did not change with temperature until nearly 105^{o}C. Fukui et. al. [29] also did not observe crystallinity changes until around this temperature in their rheological investigation of the same material. Further investigation by Onogi et. al. found that the vertical shift factors required to construct master curves from the strain optical coefficient and the stress relaxation data obtained through rheo-optical and mechanical measurements were closely related to the rotation of the crystallites within the HDPE as temperature increases. Rotation or untwisting of the HDPE lamellae was also observed as temperature increased. However, they did not rule out Penn's conclusions, saying that softening or premelting of crystal boundaries could also play a role in the vertical shift factor.

The usage of a vertical and horizontal shift factors have also been applied to the physical aging of HDPE. Lai and Bakker [3] argued that the TTSP is generally not applicable to semi-crystalline polymers owing to the more complex mechanical behavior between the amorphous and crystalline regions. Additionally, the TTSP cannot be used to construct the short-term creep compliance master curve of HDPE, in particular, where aging of the HDPE is involved. However, Lai and Bakker applied a time-stress superposition principle and utilized a time-stress shift factor in conjunction with a stress dependent vertical shift factor to construct a master curve for HDPE based on the creep compliance of differently aged specimens, which suggested that physical aging also shifts time. This is similar to Schapery's use of a_σ in his development of the time dependent response of composites in Eq. (1.4). The creep compliance of HDPE was expressed in a non-linear fashion utilizing a Prony series with 10 terms and was able to satisfactorily predict the strain response.

In her work, Brinson [30] determined that composites are thermo-rheologically complex. This would mean that a horizontal shift factor is insufficient to account for temperature change, and a vertical shift factor would be required to describe the temperature dependent behavior.

Morgan and Ward [31] in their study of the temperature dependence of the creep and recovery response of a polypropylene mono-filament also applied a vertical shift factor to account for changes in the modulus with temperature. They noted that TTSP applied even for nonlinear materials, where Schwarzl and Staverman only investigated linear behavior. Both WLF and Arrhenius relationships for the temperature dependence of the horizontal shift factor were explored within the range of 28^{o}C to 61^{o}C.

Much research has been conducted on the time-temperature shift of HDPE due to its varied and abundant uses, its semi-crystalline morphology, and its complex viscoelastic behavior. Vertical and horizontal shift factors have been shown to be required to describe the viscoelastic behavior of HDPE. Vertical and horizontal shift factors have also been utilized to describe the behavior of other polymers such as polypropylene, and composites which are deemed thermo-rheologically complex.

1.5 Dynamic Mechanical Analysis

Dynamic Mechanical Analysis (DMA) is often used to determine the viscoelastic properties of viscoelastic materials. In this method of testing, a sample is either displaced or loaded at a given frequency in torsion, flexure, or axially. Supposing that a force is applied at frequency ω, the resulting stress in the material would be

$$\sigma = \sigma_o \cos \omega t \ . \tag{1.15}$$

Due to the inherent vibration damping of viscoelastic materials, the resulting strain would lag behind the stress by a phase angle δ, which is represented as

$$\varepsilon = \varepsilon_o \cos(\omega t - \delta) . \tag{1.16}$$

This can be seen graphically in **Fig. 1.4**. This can be represented in the complex form as

$$E^* = E' + iE'' \tag{1.17}$$

where *E'* is in phase with the strain and is known as the storage modulus for the energy stored and recovered each cycle. *E''* is 90^o out of phase and is called the loss modulus for the energy dissipated or lost as heat per cycle. This results in

$$\sigma = (E' + iE'')\varepsilon \tag{1.18}$$

or more succinctly,

$$\tan\delta = \frac{E''}{E'} \tag{1.19}$$

where tan δ is considered the dissipation factor or loss tangent. The viscoelastic data provided by DMA allows for observation of the effect of temperature on the material including morphology, relaxation processes, and the time-temperature relationship (TTSP). Additionally, the effects of frequency on the viscoelastic response of the material may be observed, as can the physical changes which occur during the curing or annealing of polymers. [32][33][9]

1.6 Fatigue of composites

The study of fatigue in composites has focussed a significant amount of time and energy in the analysis of crack growth in composite laminates and aerospace composites. This may take either a micromechanics approach where the study focuses on the geometry of the crack and the crack growth phenomenon, or a continuum damage approach which models the overall change in behavior of the material. Crack growth studies may include fiber fracture, interstitial fracture, matrix cracking, or delamination. Other significant fatigue analysis with viscoelastic composites (particularly viscoelastic polymers) has utilized DMA to record the change in the dynamic properties *E'*, *E''* and tan δ with time, or compared these parameters against frequency or temperature changes. It is rare to find measurement and modeling of the uniaxial fatigue viscoelastic strain behavior of composites, and of that, exploration of the relation of that behavior to creep behavior is minimal. These have been developed in part by Elahi and Weitsman [5,6] and Scavuzzo [34].

Study of the fatigue failure behavior in uniaxial fatigue loading of HDPE was conducted by Kaiya, et. al. [35] utilizing DMA. Determination was made of the energy

loss to heat generation relationship and the energy used to cause failure. A failure criterion was established based on the hysteresis loss energy. This was done in strain controlled tension-compression fatigue with R= -1 where ($R=\varepsilon_{min}/\varepsilon_{max}$), pure tension fatigue with R=0, and pure compression fatigue with $R=-\infty$. In tension compression, or pure compression, a kink band was formed prior to failure and the failure surface was at 45^{o} to the direction of straining in the maximum shear stress plane. In pure tension fatigue, the fracture surface was perpendicular to the axis of straining. A study was also conducted on the fatigue life relative to the strain amplitude in the three loading cases. Pure compression tests were found to have the longest life for any given strain as the cracks formed in the kink band were not expanded during loading as was found in the other cases.

Jo, et al [36] studied the effect of crystallinity compared to annealed HDPE on the strain controlled fatigue behavior of specimens, utilizing the storage modulus, E' and the dissipation factor tan δ. They also defined a "nonlinear viscoelastic parameter" which described how the stress wave differed from the fundamental stress wave based on the Fourier series expansion of the response stress. Crystalline HDPE was found to fail more suddenly without the gradual decrease in E' that was seen with annealed HDPE. A sudden increase in their non-linear viscoelastic parameter was observed at the same time as deformation of spherulites were observed via small angle light scattering, indicating that their non-linear viscoelastic parameter was a measure of structural changes within the material.

Xiao [37] studied the effect of hysteretic heating on the fatigue life of an AS-4/PEEK thermoplastic composite. He developed a way of correlating the hysteretic

heating with the thermal degradation of strength and fatigue life of this material, allowing predictions of fatigue life to be made by knowing the static strength and temperature relationship and a prediction of the temperature rise due to hysteretic heating.

O'Brien and Reifsnider [38] studied boron/epoxy laminates in strain controlled fatigue at 30Hz to predict stiffness changes based on fiber breakage or debonding, two of the several damage mechanisms which composites fail under, using a micromechanics approach. They found that matrix damage correlated well with stiffness changes in the material.

Scavuzzo [34] is one of the few researchers who has compared creep and fatigue loading of any particular material. He studied the behavior of injection molded HDPE specimens in dynamic and monotonic stress relaxation. Monotonic specimens were displaced and the stress was recorded over time. For dynamic stress relaxation, the mean of the cyclic displacement was the same as the monotonic displacement. The amplitude of the cyclic displacement was a small amount compared to the initial displacement. A more rapid time-dependent relaxation response was observed for coupons subjected to cyclic displacement than was observed in specimens subjected to a constant initial displacement.

Elahi and Weitsman [5,6] studied the response of the glass/urethane composite in uniaxial fatigue loading up to 2000 cycles utilizing a sawtooth loading function, which allowed for a summation of the strain response to each loading and unloading cycle. This greatly simplified the evaluation of the integral representation of the strain behavior in the power law form. Good results were obtained with all applied stresses except where coupon failure occurred due to lack of a failure criterion in this model. This is unique

among the literature surveyed as Elahi and Weitsman are the only researchers found which have applied classical viscoelasticity to model the strain response of a uniaxial fatigue specimen. While they had incorporated temperature dependence in creep loading of this same material, they did not examine how temperature changes affect fatigue loading.

1.7 Summary

The viscoelastic behavior of composites and polymeric materials can be modeled using significantly different approaches. These may be developed with concepts of mechanics or may be purely an empirical fit. Different studies have found different models which will satisfactorily describe the viscoelastic behavior of the same material, however, some models work better than others. HDPE is itself a unique material to model as understanding of the semi-crystalline nature is still developing, as can be seen by some of the differing opinions on the morphology occurring across temperature ranges and mechanical loading. Previous work concerning the viscoelastic behavior of the WPC studied herein considered only creep/recovery response up to 1000 minutes with a power law model. Using the TTSP, studies at elevated temperatures will increase the knowledge of the behavior by four orders of magnitude utilizing a prony series model, and will provide an understanding of the effects of temperature on the viscoelastic behavior of the material. Further, while monotonic and cyclic uniaxial loading have been studied separately, it is rare that they are studied together, and rarer yet that a cohesive model is attempted to describe both behaviors. This work will go beyond that to apply a creep model to fatigue loading, including accounting for temperature dependence and damage.

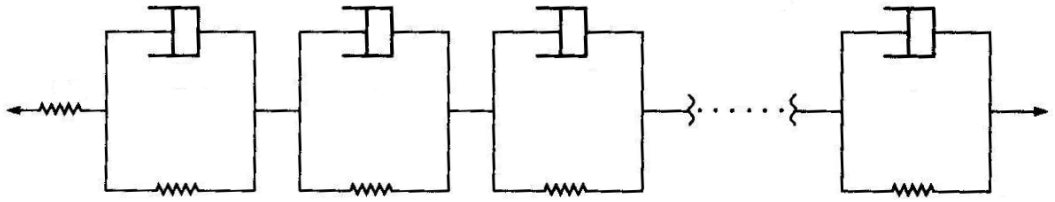

Fig. 1.1: Diagram of a Prony Series [39].

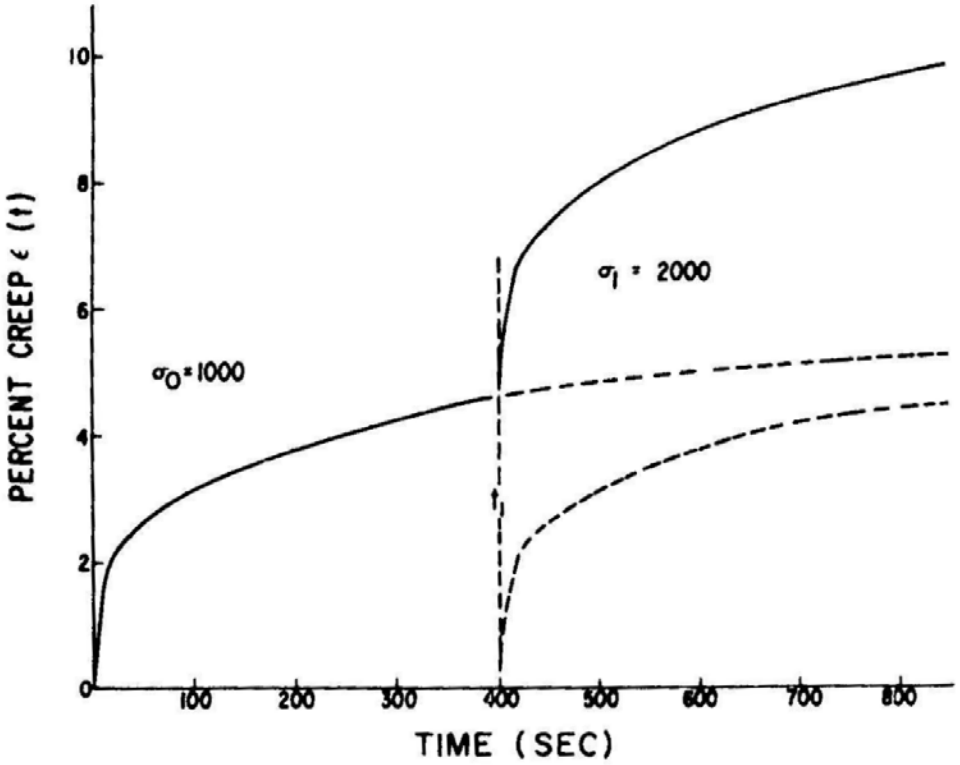

Fig 1.2: Diagram of the Boltzman Superposition Principle [9].

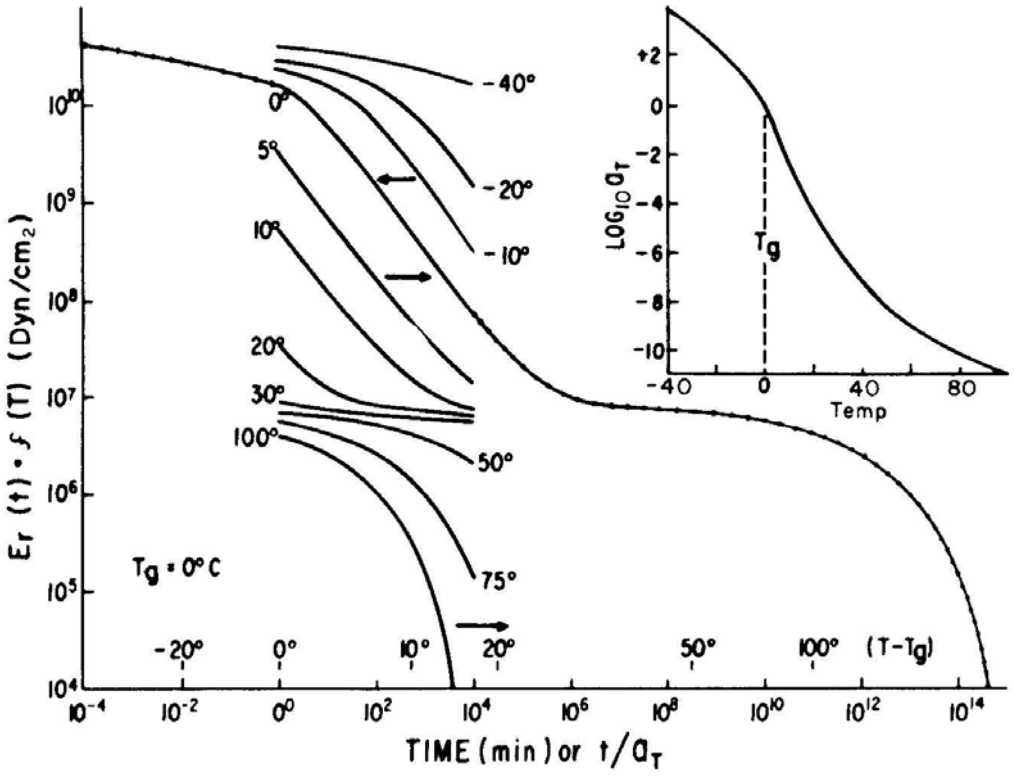

Fig. 1.3: Time-Temperature Superposition applied to the stress relaxation of a hypothetical polymer. The master curve shown is made by applying horizontal shifts in accordance with the plot of shift factors a_T against time shown in the inset. [9]

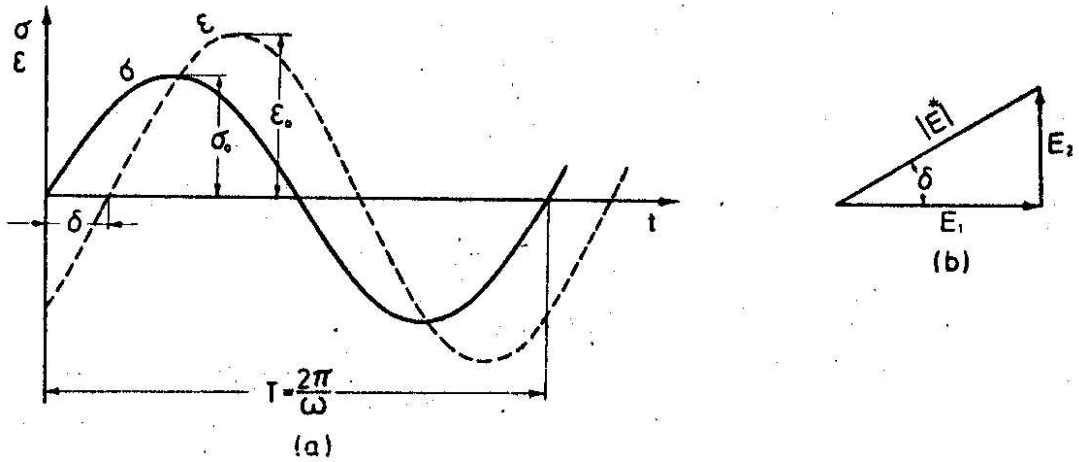

Fig 1.4: Relationships between stress, strain and resulting phase angle and storage and loss modulus and phase angle utilized during DMA analysis. [32].

REFERENCES

[1] Schapery, R.A., On the Characterization of Nonlinear Viscoelastic Materials, Polymer Engineering and Science, Vol 9:4, July 1969.

[2] Flugge Wilhelm, Viscoelasticity, Springer-Verlag, 1975.

[3] Lai, J., Bakker, A., Analysis of the non-linear creep of high density polyethylene, Polymer, Vol 36, No 1, 1995.

[4] Walrath, David E., Visceolastic Response of a Unidirectional Composite Containing Two Viscoelastic Constituents, Experimental Mechanics, June 1991.

[5] Elahi, M., and Weitsman, Y.J., On the Mechanical response of P4 Chopped Glass/Urethane Resin Composite: Data and Model, Oak Ridge National Laboratory, ORNL –6955, October, 1999.

[6] Elahi, M., and Weitsman, Y.J., Some aspects of the Deformation Response of Swirl-Mat Composites, Oak Ridge National Laboratories, ORNL/TM-13521.

[7] Rangaraj, Sudarshan V., and Smith, Lloyd V., The Nonlinear Viscoelastic Response of a Wood-Thermoplastic Composite, Mechanics of Time Dependent Materials, 3:125-139, 1999.

[8] Sain, M.M., Balatinecz, J., and Law, S., Creep Fatigue in Engineered Wood Fiber and Plastic Compositions, Journal of Applied Polymer Science, Vol. 77, pp.260-268, 2000.

[9] Nielsen, Lawrence F., Landel, Robert F., Mechanical Properties of Polymers and Composites 2nd edition, Marcel Dekker, 1994.

[10] Hermanson, John C., Adcock, Timothy, and Wolcott, Michael P., Section Design of Wood Plastic Composites, under contract No. 00014-97-C-0395, quarterly report May 27, 1999.

[11] Nielsen, Lawrence E., The Stress Dependent Creep of Polyethylenes, Journal of Applied Polymer Science, Vol. 13, pp 1800-1801, 1969.

[12] Van Holde, Kensal, A Study of the Creep of Nitrocellulose, Journal of Polymer Science, Vol. 24, pp 417-427, 1957.

[13] Veazie, David R. and Gates Thomas S., Tensile and Compressive Creep of a Thermoplastic Polymer and the Effects of Physical Aging on the Composite Time-Dependent Behavior, ASTM Special Technical Publication: Time Dependent and Nonlinear Effects in Polymers and Composites, n 1357 2000, pp160-175.

[14] Zhang, Chuntao, and Moore, Ian D., Nonlinear Mechanical Response of High Density Polyethylene. Part 1: Experimental Investigation and Model Evaluation, Polymer Engineering and Science, Vol 37 No 2, Feb 1997, pp404-413.

[15] Zhang, Chuntao, and Moore, Ian D., Nonlinear Mechanical Response of High Density Polyethylene; Part II, Uniaxial Constuitive Modeling, Polymer Engineering and Science, Vol. 37 No 2, Feb 1997, pp444-420.

[16] Gates, Thomas S., Effects of Elevated Temperature on the Viscoplastic Modeling of Graphite/Polymeric Composites, ASTM STP 1174, American Society for Testing and Materials, Philadelphia, 1993, pp201-221.

[17] Hashin, Z, Micromechanics Aspects of Damage in Composite Materials, Durability of polymer based composite systems for structural applications, London, Elsevier Applied Science, 1991.

[18] Reifsnider, Kenneth L., Damage Mechanisms in Fatigue of Composite Materials, Fatigue and Creep of Composite Materials, Proceedings of Symposium, Riso National Laboratory, 1982.

[19] Andersons, J., Limonov, V, Tamuzs, V., Fatigue of Polymer composite materials, Institute of Polymer mechanics Riga Latvia, Durability of polymer based composite systems for structural applications, Cardon A.H., and Verchery G., editors, London: Elsevier Applied Science, 1991.

[20] Webb, G.T., Breunig, T., Stock, S.R., Antolovich, S.D., Damage Accumulation in Metal Matrix Composites during fatigue with emphasis on B/Al and SiC/Al, Memoires et Etudes Scientifiques Revue de Metallurgie, October, 1990.

[21] Talreja, Ramesh, Damage mechanics of Composite materials based on Thermodynamics with internal variables, Durability of polymer based composite systems for structural applications, Cardon, A.H., and Verchey, G., editors, Elsevier Applied Science, London, 1991.

[22] Lemaitre, Jean, and Chaboche, Jean-Louis, Mechanics of Solid Materials, Cambridge University Press, 1990.

[23] Williams, M.L., Landel, R.F., and Ferry, J.D., Journal of the American Chemical Society, 77, 3701, 1955.

[24] McCrum, N.G., Buckley, C.P., Bucknall, C.B., Principles of Polymer Engineering, Oxford University Press, New York, 1988.

[25] Schwarzl, F. and Staverman, A.J., Time-Temperature Dependence of Linear Viscoelastic Behavior, Journal of Applied Physics, Vol. 23 No 8, Aug 1952.

[26] Crissman, J.M., Creep and Recovery Behavior of a Linear High Density Polyethylene and an Ethylene-Hexene Copolymer in the Region of Small Uniaxial Deformations, Polymer Engineering and Science, 26: n15, 1986.

[27] Penn, Robert W.,Dynamic Mechanical Properties of Crystalline, Linear Polyethylene, Journal of Polymer Science: Part A-2, 4: 545-557 1966.

[28] Onogi, S., Sato, T., Asada, T, and Fukui, Y., Rheo-Optical Studies of High Polymers, XVIII. Significance of the Vertical Shift in the Time Temperature Superposition of RheoOptical and Viscoelastic Properties, Journal of Polymer Science: Part A-2 Vol 8, 1211-1255, 1970.

[29] Fukui, Y., Sato, T., Ushirokawa, M., Asada, T, and Onogi, S., Rheo-Optical Studies of High Polymers. XVII. Time-Temperature Superposition of Time-Dependent Birefringence for High-Density Polyethylene, Journal of Polymer Science: Part A-2, Vol 8, 1195-1209, 1970.

[30] Brinson, L.C., Time-Temperature Response of Multi-phase Viscoelastic Solids through Numerical Analysis, PhD thesis, California Institute of Technology, Feb 1990.

[31] Morgan, C.J., Ward, I.M., The Temperature Dependence of Non-linear Creeep and Recovery in Oriented Polypropylene, Journal of the Mechanics and Physics of Solids, Vol 19, pp165-178, 1971.

[32] Findley, William N, Lai, James S., and Onaran, Kasif, Creep and Relaxation of Nonlinear Viscoelastic Materials, North Holland Publishing Company, Amsterdam , 1976.

[33] Ferry, John D., Viscoelastic Properties of Polymers, John Wiley and Sons Inc., New York, 1980.

[34] Scavuzzo, Rudolph J., Oscillating Stress on Viscoelastic Behavior of Thermoplastic Polymers, Journal of Pressure Vessel Technology, Vol. 122, August 2000.
[35] Kaiya, Norihiro, Takahara, Atsushi, Kajiyama, Fatigue Fracture Behavior of Solid-State Extruded High-Density, Polymer Journal, Vol. 21 No. 7 pp 523-531 1989.

[36] Jo, Nam-ju, Takahara, Atsushi, Kajiyama, Tisato, Analsysis of Fatigue Behavior of High-Density Polyethylene Based on Nonlinear Viscoelastic Measurement under Cyclic Fatigue, Polymer Journal, vol. 25, no. 7, pp 721-729, 1993.

[37] Xiao, X.R., Modeling of Load Frequency Effect on Fatigue Life of Thermoplastic Composites, Journal of Composite Materials, Vol. 33, No. 12/1999.

[38] O'Brien, T.K. and Reifsnider, K.L., Fatigue Damage: Stiffness/Strength Comparisons for Composite Materials, Journal of Testing and Evaluation, Vol. 5, No. 5, September 1977.

[39] Gibson, Ronald F., Principles of Composite Material Mechanics, McGraw-Hill Inc., 1994.

CHAPTER TWO

MATERIALS AND TESTING

2.1 Introduction

The material utilized in this study is not commercially available. Therefore, the method of manufacture and material constituency will be described. Further, the specimen geometry is described, as are the methods used to characterize the material. Experimental methods used for comparison with the model are also described along with material properties and descriptions of the variation within the material.

2.2 Material Processing

The wood plastic composite under investigation in this research had a composition by weight of 58% dried maple flour, 31% HDPE matrix, 8% talc, 2% zinc stearate, and 1% wax. The constituents were mixed dry in a drum blender then extruded through a twin screw counter-rotating extruder. During the extrusion process, the dry constituents were fed into the barrel where the mixture was heated with a barrel temperature of 163^{o}C (325^{o}F) and compressed while driven toward the end of the barrel and the die. Before entering the die, the melt was forced through a screen pack and the cross sectional area of the melt was reduced. The melt was then forced through the die which was maintained at 171^{o}C (340^{o}F). Upon exit from the die, the 152mm wide by 13mm thick extrusion was cooled with ~15^{o}C (50^{o}F) tap water. A schematic of the extrusion process may be seen in **Fig. 2.1** where a single screw extruder is shown.

This board was cut into 200mm (8 inch) long sections then cut into coupons 25mm (1 inch) wide or 32 mm (1-1/4 inches) wide. The 25 mm wide coupons were used

for creep and bending testing, while the 32mm wide coupons were dogboned to a 25mm wide gage section for fatigue and tensile strength testing to prevent specimen failure at the grips during testing. Coupons were marked to facilitate consistent positioning within the grips and of the extensometer. During loading of the coupons, 41 mm (1.625 inches) were clamped in each grip, and the remaining 121 mm (4.75 inches) was stressed. The extensometer was positioned directly between the grips.

2.3 Testing Methodology

2.3.1 Testing Equipment

Experiments were conducted on a 2-post servohydraulic load frame with a 45kN (10 kip) load cell. The load frame was controlled with an MTS 407 Controller. Strain was measured with an MTS 634.11E-24 extensometer with a 25 mm (1 in.) gage length. It was then conditioned with a Vishay 2120A strain conditioner and filtered through a low pass filter, which reduced extensometer noise from 70-80με to 5-7με as shown in **Fig. 2.2**. This was required due to the low magnitude of the strains considered in this research in calculating stiffnesses and verifying viscoelastic behavior. The extensometer was aligned to the edge of the coupon with an aluminum block designed to minimize experimental error due to misalignment. Also utilized for room temperature testing was a 4-post servohydraulic load frame with a 90kN (20kip) load cell. Control and strain measurement was achieved using the same equipment as for the 2-post load frame.

The 2-post load frame was equipped with an oven to facilitate measurements above room temperature. The oven was constructed of 38mm (1-1/2 inch) foil-covered foam insulation board. This was fitted around the grips to prevent significant thermal losses due to airflow through gaps. The interior dimensions were 36 cm (14 in.) in all

directions. Heating was provided by two 300-watt quartz heating elements, located across the diagonal of the oven as shown in **Fig. 2.3**. An Omega CN9000A controller was used to control oven temperature via a K-type thermocouple attached to the surface of the coupon. The thermocouple was fixed slightly below the extensometer with high temperature tape. In order to determine the soak time necessary for the temperature of the coupon to reach steady state in the oven, a blind hole was drilled in a coupon into which the thermocouple was inserted. Interior coupon temperature was found to reach equilibrium with the surface of the coupon within 15 minutes. In order to ensure that steady state was reached in the testing portion of this work, coupons were placed in the oven for several hours prior to testing, and were allowed 30 minutes to reach temperature after they had been loaded in the top grip. Data was recorded using customized Labview software.

2.3.2 Quasi-static Loading

For all loading scenarios, coupons were first placed in the top grip. The extensometer was attached and zeroed, the bottom grip was then closed. Due to coupon warpage or slight grip misalignment, initial strains were observed when the bottom grip was closed on the coupon at zero load. Therefore, the initial strain at zero load was recorded and used to adjust measured strain output during analysis of raw data. In quasi-static loading, coupons were elongated in displacement control at 1.3 mm/min (0.050 in./min). Time, load, stroke and strain data were recorded with customized Labview software. Engineering stress was calculated based on the initial cross-sectional area of the coupon. A sample stress-strain curve for a coupon at each temperature is shown in **Fig. 2.4**.

Material stiffness was measured as a chord modulus between 0.7 MPa (100psi) and 3.2 MPa (230psi or 30% Sut) at room temperature. This stress was below what is termed the "threshold stress" above which permanent deformation and stiffness change occurred. Use of this range allowed for a consistent zone of measurement regardless of the stress level the coupon was being loaded to. This is similar to the range used by Rangaraj [1] in his measurement of elastic modulus for his WPC. Rangaraj had used a chord modulus during the unloading portion of the creep/recovery test over the same stress range at which initial stiffness was measured during loading to determine changes in the stiffness of the coupon during the creep test. Experimental application of this method proved inconsistent in practice. For this reason, the elastic modulus was measured well after recovery, (approximately $30t_o$) during a ramp load and immediate unload at room temperature over the same range as initial stiffness was measured to determine stiffness change.

2.3.3 Creep Loading

A schematic of a typical creep test is shown in **Fig. 2.5**. A creep load is applied at $t=0$ for a time $t=t_o$ at which time the load is instantaneously removed. Ideally, creep coupons would be loaded and unloaded instantaneously. However, this cannot be achieved in practice. Coupons were therefore loaded at a ramp rate of 200N/sec (45 lb/sec) then held at a load for a determined amount of time, 0, 10, or 1000min. For recovery, load on the coupon was removed at the same rate at which it was applied. When near zero load was reached, the bottom grip was opened, completely unloading the coupon. The coupon was then allowed to recover for three times the creep duration ($3t_o$) during which strain was recorded. Loading was accomplished in 4-17 seconds depending

on the creep load level. This was found to be a favorable load application rate in work by Rangaraj [1], being rapid enough to have negligible effect on the creep outcome, and not being too rapid so as to damage the coupon by imparting inertia effects to the specimen.[2] LabView software was utilized to record load, stroke and strain data at user controlled periods. A test matrix for creep loading may be seen in **Table 2.1**.

Table 2.1: Test matrix for creep and recovery tests. Entries in the table indicate the number of test replicates.

Sut	30%			50%			70%			90%		
Creep Duration (min)	0	10	1000	0	10	1000	0	10	1000	0	10	1000
23°C	5	5	3	5	5	3	5	5	3	5	2	0
45°C	0	5	1	0	3	1	5	5	3	0	2	0
65°C	0	3	1	0	3	1	5	5	3	0	4	0

The strain during the unloading phase was not adjusted as described in the previous section as the grip-induced strain was nonexistent as the bottom grip was open during recovery.

2.3.4 Fatigue Loading

Fatigue loading was likewise accomplished in load control. Coupons were loaded with R=.1 ($R=\sigma_{min}/\sigma_{max}$) in all stress levels tested. Experimental strain measurements recorded with the extensometer over the range from 0.1Hz to 30Hz were found to be the most accurate at lower frequencies where extensometer slip was less likely to occur. Fatigue life and hysteretic heating were observed to decrease with load frequency (to be discussed in section **2.4.2**). A frequency of 0.5Hz was therefore chosen for subsequent fatigue tests reported in this work. Experimental peak cyclic strain was recorded at

intervals throughout the tests utilizing customized LabView software. To evaluate the viscoelastic response of the WPC at various temperatures and stresses, three coupons were tested at each stress level and temperature: 30% and 70%Sut at 23^{o}C, 45^{o}C, and 65^{o}C for 100 minutes. Several coupons were also tested for longer durations at 30% and 70% to better evaluate the model over long times. Initial and final elastic moduli were recorded to determine the fatigue induced damage.

2.3.5 Dynamic Mechanical Analysis

Dynamic Mechanical Analysis (DMA) was utilized to determine time temperature shift factors. Analysis was conducted on a Rheometrics Solid Analyzer (RSA II). Specimens were machined from the center of straight coupons to eliminate edge effects, saw marks, and possible damage due to the circular saw cutting of the coupons. Specimens were machined on a Bridgeport milling machine using a fly cutter and an endmill for finish cuts to achieve good surface finish on the specimen, minimizing surface imperfections which could have caused stress concentrations affecting the results. Specimen dimensions were 45 mm long, 6 mm wide, and 2 mm thick. These were loaded into a dual cantilever fixture. A flexural strain of 3.0×10^{-5} was applied at frequencies between .01Hz and 10 Hz in a frequency sweep at each temperature. Data was recorded at 5 frequencies within each decade. A frequency sweep was conducted every 2^{o}C from –30^{o}C to 65^{o}C. Initial soak time to reach –30^{o}C was 10 minutes. Soak time associated with each 2^{o}C temperature jump was 1 minute.

2.4 Results

2.4.1 Material Characterization

Quasi-static tests were conducted to determine baseline material properties for the formulation. The dependence of material properties on the location across the width and along the length of the extruded board was also investigated. No location dependence was discovered in the coupons along the length of the boards. However, variations in stiffness and ultimate strength were discovered across the width of the board as shown in **Fig. 2.6**. Strength was on the order of 10% higher in the coupons taken from the outside edge of the board than in the coupons cut from the interior of the board. Stiffness was nearly 20% higher at the outside of the board. These increases were expected given the 3-dimensional cone-shaped reduction of the die area as the material was extruded, which resulted in greater compression of the extruded material near the edges of the die. In order to minimize variation in the properties of dogboned and straight coupons used for the other experiments covered in this work, the outer 20mm were discarded from each edge of the board prior to cutting the coupons. The effect of coupon geometry can also be observed in **Fig. 2.6**. Dogboning of coupons had a negligible effect on the measured stiffness, and a beneficial effect on measured strength.

To consider the effect of temperature on coupon strength, seven coupons were loaded at 23^{o}C, 45^{o}C, and 65.5^{o}C (73, 110, and 150^{o}F). The strength and elastic modulus were recorded and plotted. Both strength and elastic modulus decreased in a nearly linear fashion with temperature as can be seen from **Fig. 2.7**. Strength at 65.5^{o}C was nearly half that at 23^{o}C. Normalization of the strength and elastic modulus with the reference strength and elastic modulus at 23^{o}C is shown in **Fig. 2.8**. Note that the rates of change

of strength and elastic modulus are not identical but are similar. Further, material toughness increased by a factor of three at 65°C relative to material toughness at 23°C. A comparison of the stress-strain response of the WPC at 23, 45 and 65°C is shown in **Fig. 2.4**.

In order to compare the responses of coupons loaded at different temperatures in creep and fatigue, the percentages of ultimate strength used to denote the loading of the coupon were normalized with the ultimate strength at each temperature as shown in **Table 2.2**. Thus, for example, a coupon loaded in creep at 30% Sut at 23°C was loaded to 3.2MPa, while a coupon loaded at 30% Sut at 65°C was loaded to 1.7MPa.

Table 2.2: Normalization with respect to temperature dependent ultimate strength (Sut).

Temp (°C)	30% Sut (MPa)	50% Sut (MPa)	70% Sut (MPa)	90% Sut (MPa)	100% Sut (MPa)
23	3.2	5.4	7.5	9.7	10.7
45	2.4	4.0	5.6	7.3	8.1
65	1.7	2.8	3.9	5.0	5.5

2.4.2 Fatigue

It is known that HDPE is rate dependent; therefore, initial trials were conducted to determine the effects of loading frequency on the fatigue life of the coupons. The coupons were loaded with σ_{max} = 80% Sut of the wood-plastic material. A thermocouple was attached to the coupon in order to monitor temperature change during the test. Testing was conducted at frequencies of 0.09 Hz, 0.5 Hz, 5Hz, and 30 Hz. Five coupons were tested at each frequency. As can be seen in **Fig 2.9**, fatigue life increased with loading frequency. This is consistent with work published by Xiao [3] who noted that when the rise in temperature due to hysteretic heating is not significant, fatigue life will

increase with load frequency. This has been found to be true with graphite/epoxy and boron/epoxy composites. However, with composites such as glass/epoxy and an AS4-PEEK thermoplastic composite, which are known to exhibit high hysteretic heating, the opposite occurred. Temperature rise was observed in AS4-PEEK in all load frequencies from 1Hz to 10Hz and increased as frequency increased. In the WPC studied here, hysteretic heating was only measurable at 30Hz where the temperature increased 15^{o}C prior to failure. Hysteretic heating was not observed at other frequencies tested. By contrast, according to Hertzberg and Manson, virgin polyethylene fails in fatigue primarily by thermal melting, rather than mechanical processes. [4] Other factors not mentioned by these authors which may also effect the fatigue life could include the increased duration of load application as frequency decreases, and the stiffness and strength of the polymer increasing with load rate.

2.4.3 DMA

Analysis of the data by RSA proprietary "Orchestrator" software calculated specific time shift factors which would result in superposition of the individual relaxation curves taken at each temperature with respect to the reference temperature of 23^{o}C. (The relaxation curves showed the variation of E' vs. frequency (Hz) across a frequency sweep from 0.1 Hz to 10Hz.) This was done within the software by determining the factor required to minimize the difference between the reference curve (in this case 23^{o}C) and the curves from each of the other temperatures numerically. The software then was able to calculate the constants, c_1 and c_2, based on the slope and intercept of the plot of $(T-T_{ref})/\log a_T$ versus $(T-T_{ref})$. Vertical shift factors were excluded in this analysis of the data. The Arrhenius relationship was determined by solving the Arrhenius equation for the

activation energy in terms of the reference temperature, the current temperature, the shift factor, and the known universal gas constant. The average of the activation energies over the range from –31°C to 0°C was used since the Arrhenius equation typically describes the temperature dependence near or below the T_g. A plot showing the shift factors produced by the DMA analysis, the WLF equation, and the Arrhenius equation for a representative coupon is shown in **Fig. 2.10**. As can be seen, the Arrhenius relationship better describes the shift factors in the lower temperatures than does the WLF equation. A representative master curve created with the WLF equation for a specimen is shown in **Fig. 2.11**.

2.5 Summary

The material properties of the extruded WPC were shown to exhibit some location dependence across the width of the board. Material property variation was minimized through selection of coupon location across the board width. Extensometer noise, which would have been a significant percentage of the strain response in some test cases, was minimized through electronic filtering. Mechanical testing methods and procedures were described as well as the procedures used to minimize factors such as ramp loading speed which could effect experimental results. Further, description was given of the DMA test equipment utilized for determination of the horizontal shift factor for the WPC.

Frequency effects on fatigue life were observed. As ultimate failure is not an aim of this work, a relatively low frequency of 0.5 Hz was selected out of experimental convenience. The material at hand exhibits a strong temperature dependence in stiffness, strength, and time dependence. The latter appears to be adequately described by TTSP while the former may be accommodated through concepts of continuum damage.

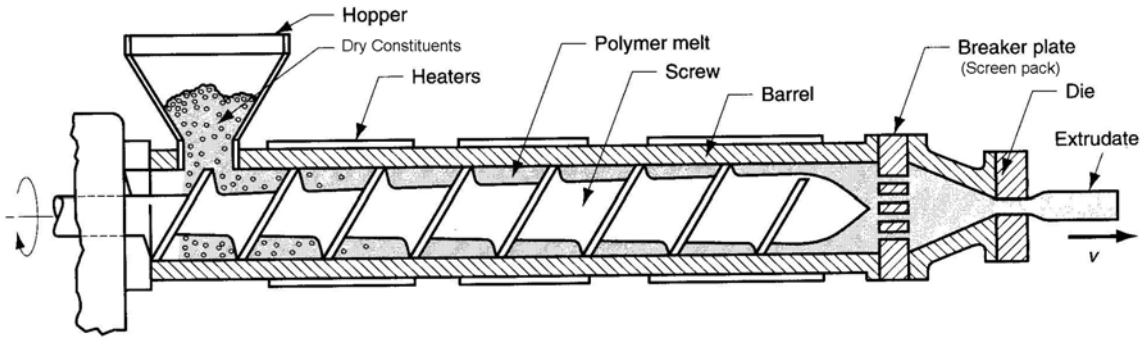

Fig 2.1: Schematic of extrusion process showing a single screw extruder. [5]

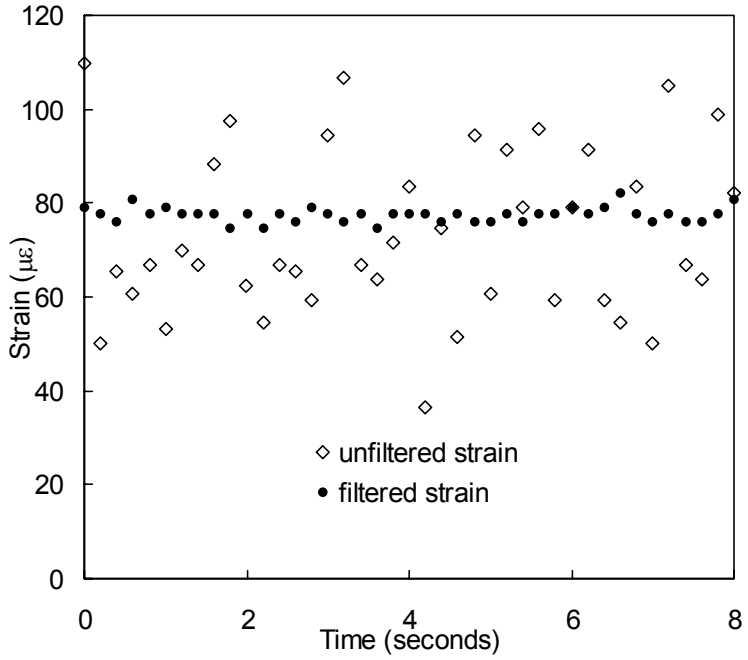

Fig. 2.2: Filtered strain response vs. unfiltered strain response.

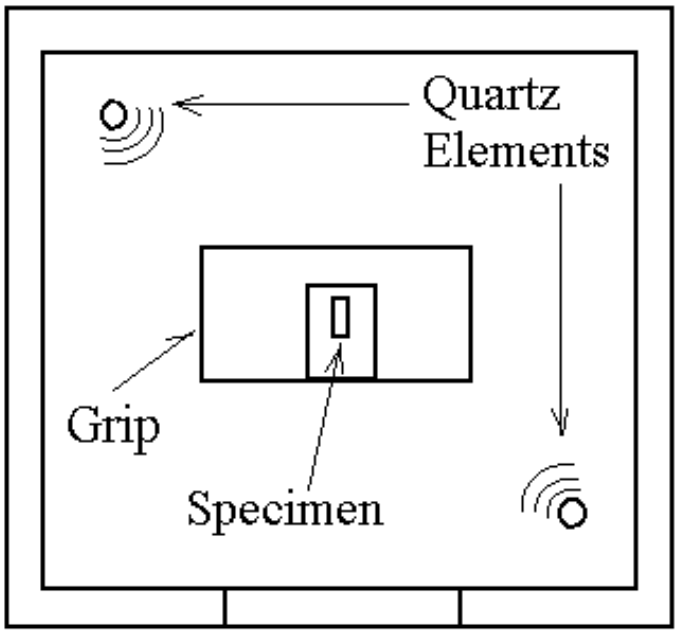

Fig. 2.3: Top view of oven showing placement of heating elements.

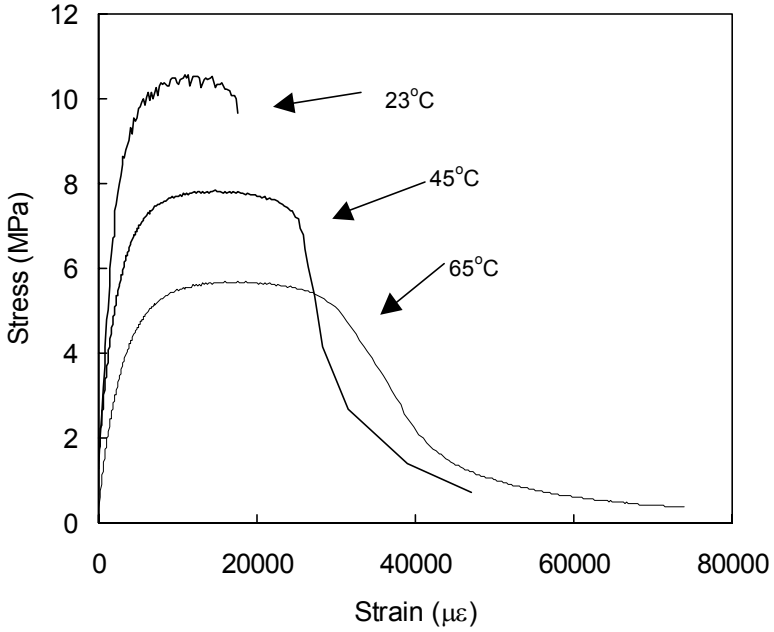

Fig. 2.4: Representative stress-strain curves for coupons at 23°C, 45°C, and 65°C.

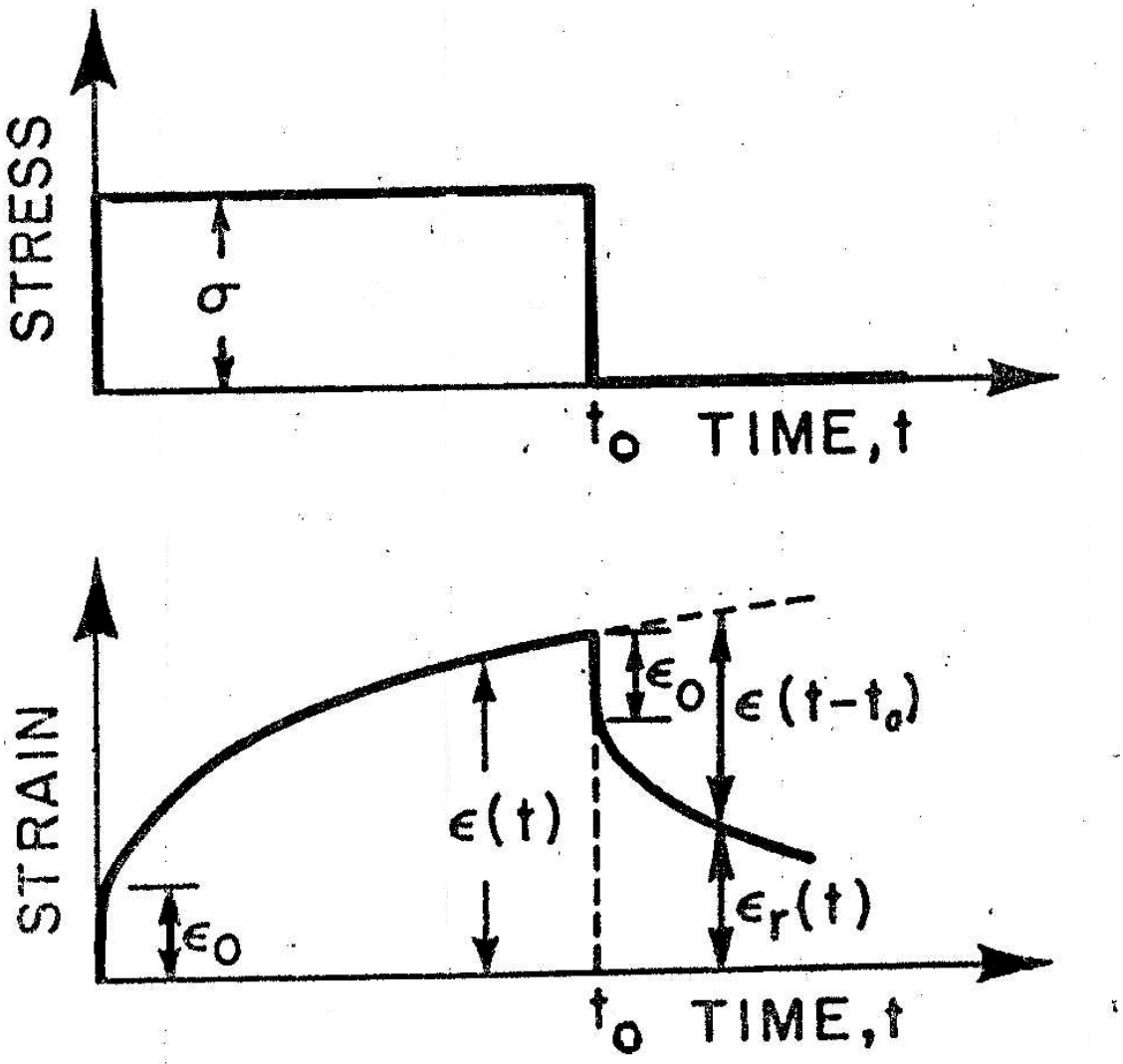

Fig. 2.5: Schematic of creep recovery test. [6]

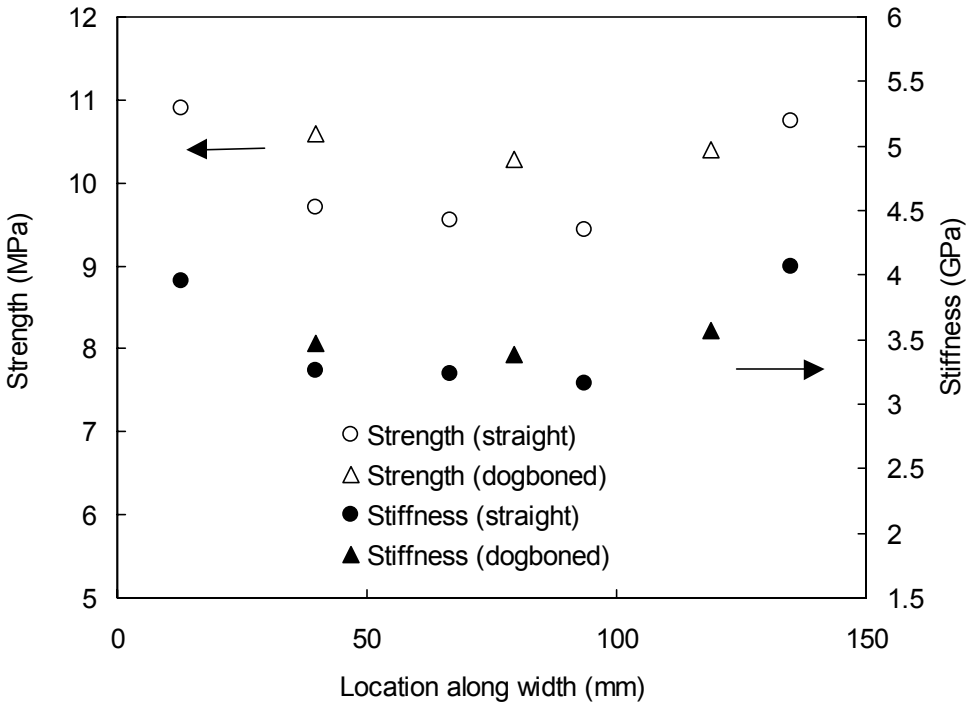

Fig. 2.6: Location dependence of strength and modulus across width of board.

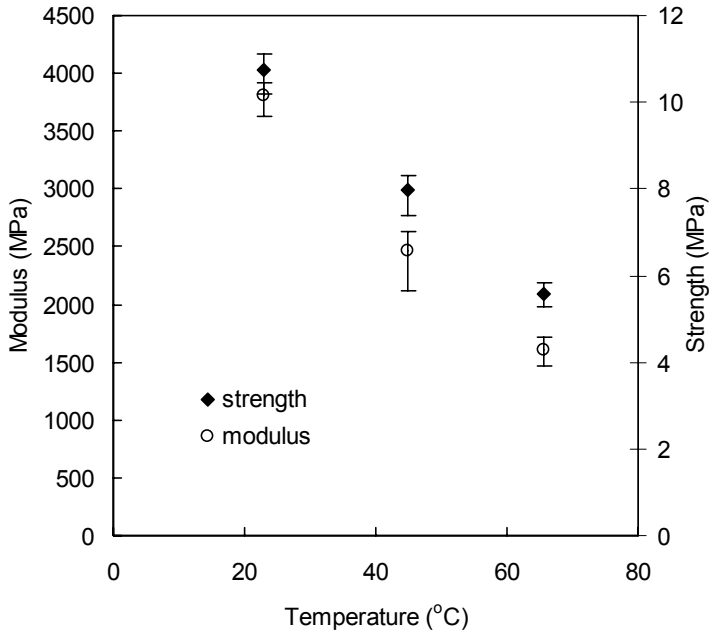

Fig. 2.7: Temperature dependent strength and elastic modulus.

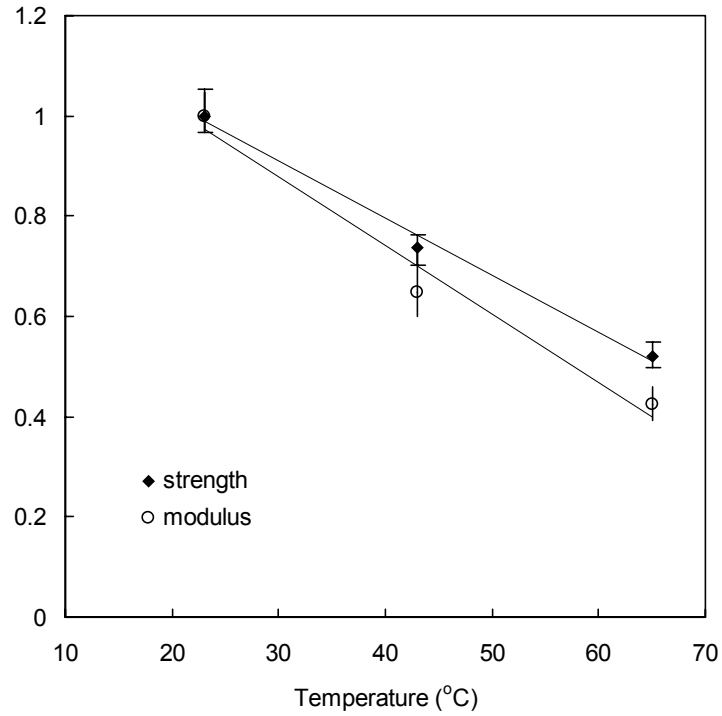

Fig. 2.8: Normalized strength and elastic modulus with strength and elastic modulus at 23°C.

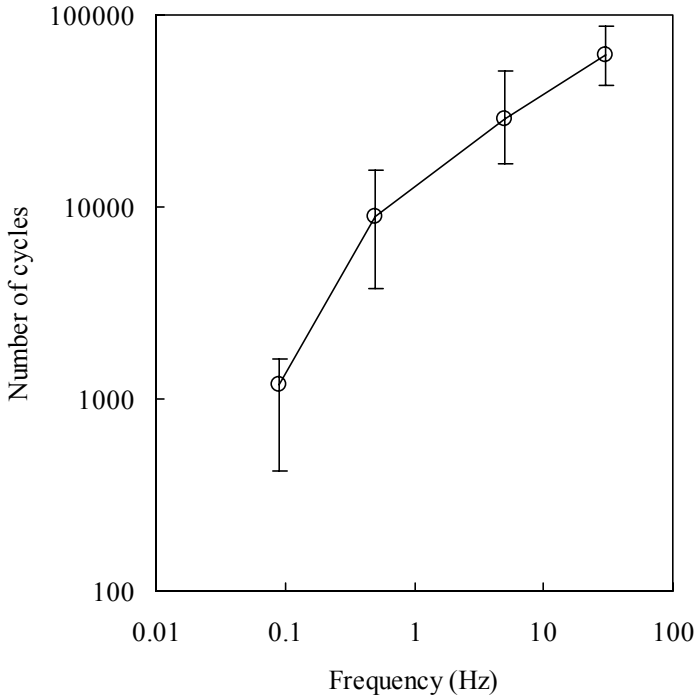

Fig. 2.9: Dependence of fatigue life on fatigue frequency; R=.1, σ_{max}=80%Sut at 23°C.

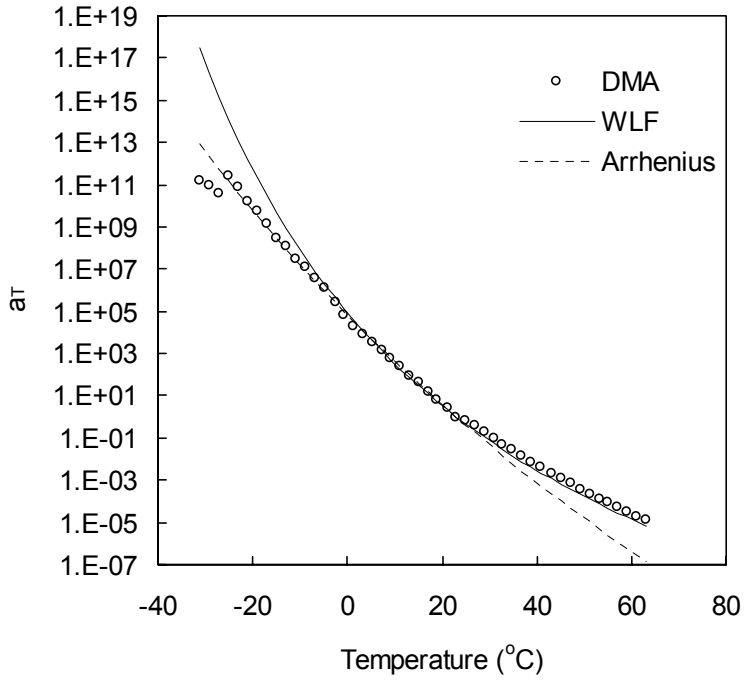

Fig. 2.10: Comparison of experimental DMA, Arrhenius, and WLF time shift factors.

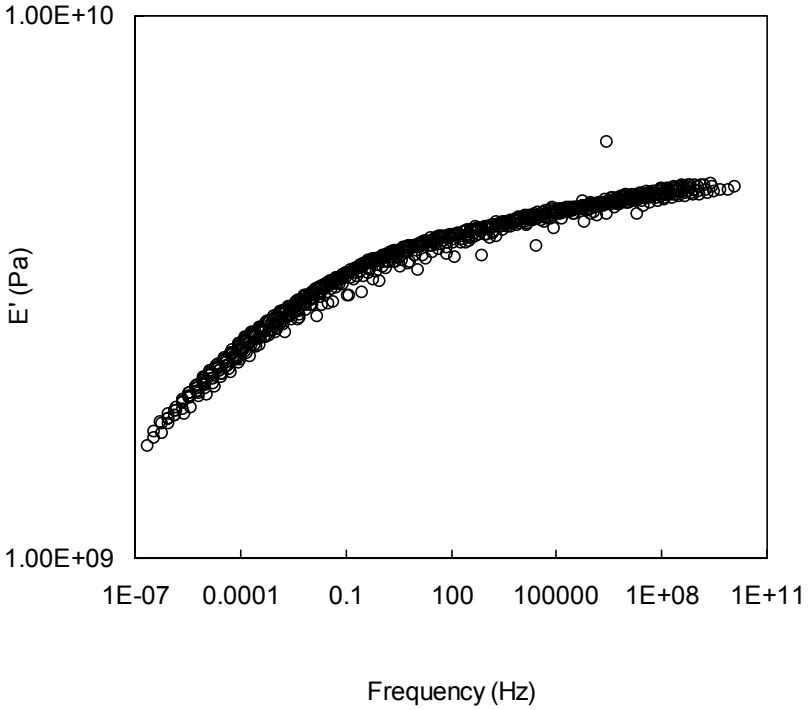

Fig. 2.11: DMA master curve created with WLF shift factors for representative specimen.

REFERENCES

[1] Rangaraj, Sudarshan V., Durability Assessment and Modeling of Wood Thermoplastic Composites, Master's Thesis, Washington State University, August 1999.

[2] Lockett, F.J., Nonlinear Viscoelastic Solids, Academic Press, London, 1972.

[3] Xiao, X.R., Modeling of Load Frequency Effect on Fatigue Life of Thermoplastic Composites, Journal of Composite Materials, Vol. 33 No. 12, 1999.

[4] Hertzberg, Richard W., and Manson, John A., Fatigue of Engineering Plastics, Academic Press, New York, 1980.

[5] Groover, Mikell P., Fundamentals of Modern Manufacturing: Materials, Processes, and Systems, John Wiley and Sons, Inc., New York, 1999.

[6] Schapery, R.A., On the Characterization of Nonlinear Viscoelastic Materials, Polymer Engineering and Science, Vol. 9:4, July 1969.

CHAPTER THREE

TEMPERATURE DEPENDENT VISCOELASTIC CREEP

3.1 Introduction

Creep and recovery tests were performed according to the methods described in the previous chapter. This data was then used to develop and evaluate a viscoelastic model which would describe the behavior of the material at temperatures above room temperature utilizing the time-temperature superposition principle.

3.2 Power Law Model

3.2.1 Development of power law model

Previous work by Rangaraj [1] and Rangaraj and Smith [2] on the viscoelastic response of wood-plastic composites utilized Schapery's convolution integral Eq. (1.1), to describe the coupon time dependent strain response, repeated here for convenience,

$$\varepsilon(t) = \int_{-\infty}^{t} D(t-\tau)\frac{d\sigma(\tau)}{d\tau}d\tau \tag{3.1}$$

where *D(t)* is the time-dependent compliance of the material, and where

$$\sigma(\tau) = \sigma_o H(\tau) \tag{3.2}$$

is the applied stress for idealized creep loading with *H(t)* being the Heaviside step function. This function controls the instantaneous application of a constant load σ_o. Rangaraj utilized a linear power law compliance to model the viscoelastic strain response below a threshold stress. This can be expressed as

$$D(t) = D_o + D_1 t^n \tag{3.3}$$

where D_o is the time independent or instantaneous compliance, D_1 is the time dependent compliance, and *n* is an empirically determined material parameter. Values for these

parameters were reported by Rangaraj as $0.22 < D_o < .28$ GPa^{-1} ($1.51 < D_o < 1.95$ Msi^{-1}), D_1=0.045 Gpa^{-1}min^{-n} (0.31 Msi^{-1}min^{-n}) and n=0.39. Ranges for parameters were due to slight material inconsistencies. Evaluation of Eq. (3.1) with (3.2) and (3.3) results in a predicted strain response of the material in creep loading as

$$\varepsilon(t) = (D_o + D_1 t^n)\sigma_o \tag{3.4}$$

Creep recovery may be modeled by letting the stress function in Eq. (3.2) equal

$$\sigma_r(\tau) = \sigma_o H(\tau) - \sigma_o H(\tau - t_o) \tag{3.5}$$

where t_o is the elapsed time when the creep load was removed. Evaluation of Eq. (3.1) for the recovery strain, ε_r, results in the following equation for the strain response in recovery

$$\varepsilon_r(t) = D_1[t^n - (t - t_o)^n]\sigma_o . \tag{3.6}$$

Rangaraj and Smith [2] found that the linear viscoelastic models shown in Eq. (3.4) and (3.6) adequately described the time dependence of their wood-plastic composite in creep and recovery as well as in ramp loading scenarios below the threshold stress. Application of their model to the specimens used in this research required some slight modifications in the values of the constants to properly model the data. Values for D_o were found to be between 0.23 and 0.33 GPa^{-1} (1.6 and 2.3 Msi^{-1}) while values for D_1 were found to vary between 0.026 and 0.047GPa^{-1}min^{-n} (0.18 and 0.32 Msi^{-1}min^{-n}). Variation in material parameters was due to inherent material variation and location dependence of the material properties across the width of the board. Comparisons of the power law model and experimental data for a representative coupon is provided in **Fig. 3.1**.

3.2.2 Development of non-linear viscoelastic power law model

In order to model the viscoelastic response above the threshold stress, Rangaraj [1] utilized a continuum damage model to account for the observed stiffness loss and permanent deformation observed. Damage, recalling the discussion in Chapter 1, can have a rather ambiguous definition and may be defined differently depending on the researcher. Lemaitre and Chaboche [3] suggest that damage be defined based on the concept of effective stress

$$\sigma_e = \frac{\sigma}{(1-D)} \tag{3.7}$$

where σ_e is the effective stress and $D = 1 - E_d/E$ where E is the elastic modulus of an undamaged specimen and E_d is the elastic modulus of a damaged specimen. It is this method for quantifying damage which Rangaraj and Smith [2] used for their study of their WPC. They reported damage occurring at approximately 5 MPa, or around 45% of the ultimate strength (Sut) of their WPC. Applying the concept of effective stress to Eq. (3.1) results in

$$\varepsilon(t) = \int_{-\infty}^{t} D(t-\tau)\frac{d\sigma_e(\tau)}{d\tau}d\tau \tag{3.8}$$

where the effective stress can be expressed as

$$\sigma_e(t) = \sigma_o(t)\cdot\omega(\sigma_o,t)\cdot H(t) \tag{3.9}$$

where σ_o is the applied stress and $\omega(\sigma_o,\tau)$ is the damage function. The damage function has components of instantaneous damage and time dependent damage, represented by s and c respectively and can be described as

$$\omega(\sigma_o,t) = 1 + (s + ct^m) < \sigma_o - \sigma_d > \tag{3.10}$$

where σ_d is the threshold stress above which damage occurs and *m* is a material dependent constant. Rangaraj and Smith determined the values *c*=0.14 $Mpa^{-1}min^{-m}$ and *s*=0.056Mpa^{-1}. Rangaraj and Smith had developed a stress dependent function for *m*. In the stress ranges utilized in this research, *m* could be closely approximated by *m*=0.15. Combining Eq. (3.8), (3.9), and (3.10), the creep strain response may be approximated by

$$\varepsilon(t) = \left[(D_o + D_1 t^n)K_{T1} + D_o C t^m + D_1 CmMt^{n+m}\right]\sigma_o \tag{3.11}$$

where

$$K_{T1} = 1 + s(\sigma_o - \sigma_d)\cdot H(\sigma_o - \sigma_d) \tag{3.12}$$

and

$$M = \frac{1}{m} - \frac{n}{m+1} - \frac{n(1-n)}{2(m+2)} \tag{3.13}$$

is a binomial series expansion as there is not a closed form solution to the integration of the convolution integral incorporating damage when *m* is not an integer. Calculation of the recovery strain must take into account permanent deformation. Using procedures from Smith and Weitsman, [4] Rangaraj and Smith found that the recovery strains could be represented by

$$\varepsilon_r(t) = \varepsilon_v(t) - \varepsilon_v(t - t_o) + \varepsilon_p(t_o) \tag{3.14}$$

for $t > t_o$ where the viscoelastic strain are

$$\varepsilon_v(t) = (1 - K_p)[(D_o + D_1 t^n)K_{T1} + D_o C t^m + D_1 CmMt^{n+m}]\sigma_o + K_p \varepsilon_d \tag{3.15}$$

and where K_p=.249 is the empirically determined rate of growth of the permanent strain relative to the maximum creep strain, and ε_d=800με is the threshold strain, below which permanent deformation was negligible. [2] The permanent component of strain $\varepsilon_p(t)$ was found to be

$$\varepsilon_p(t) = K_p[(D_o + D_1 t^n)K_{T1} + D_o C t^m + D_1 CmMt^{n+m}]\sigma_o \tag{3.16}$$

Correlation between this model and a representative coupon loaded for 10 minutes at 70% Sut at 23°C can be seen in **Fig 3.2.**

3.3 Time-Temperature Superposition

3.3.1 Shifting Time

The time-temperature superposition principle (TTSP) proposes that time and temperature affect the viscoelastic response of a material in similar ways, and temperature effects may be described by altering the time scale. This means that the creep data recorded at a temperature higher than the reference temperature and shifted using the appropriate shift factor,

$$t^* = \frac{t}{a_T(T)} \tag{3.17}$$

will represent the viscoelastic creep at the reference temperature where $a_T(T)$=1 at an extended period of time. Time scaling is presented visually in **Fig. 1.3** which shows the application of the time shift factor to experimental stress relaxation data. This shift factor is called the horizontal shift factor or time shift factor because it shifts the creep curve or stress relaxation curve horizontally with time. The materials for which the TTSP applies are termed "thermo-rheologically simple"[5]. While Neilsen and Landel have written that TTSP is typically limited to amorphous polymers, it can also be applied to semi-crystalline polymers, such as HDPE, if a "vertical shift factor" is also utilized.[6] This can be expressed as

$$\varepsilon(t) = \sigma_o pD\left(\frac{t}{a_T(T)}\right) \tag{3.18}$$

where p is the vertical shift factor and $a_T(T)$ is the horizontal shift factor. This is in keeping with work by several other authors in both polymers and composites [7, 8, 9, 10, 11,12]. As was mentioned in Chapter One, these materials where a vertical shift factor is required are termed "thermo-rheologically complex." [13]

Two methods are typically used to provide the horizontal or time shift factor for shifting viscoelastic models. Williams, Landel, and Ferry developed an equation for temperature dependence of the relaxation modulus of a polymer or composite in what is known as the WLF equation. [14] This was developed for amorphous polymers in the range of T_g to T_g+100°C from an understanding of viscosity and free volume. Below T_g an Arrhenius relationship is typically used, [6] although an Arrhenius relationship can also be used in regions where the WLF equation would typically apply as an empirical fit to the shift factor or above where the WLF equation applies.

Penn [9] and Morgan and Ward [12] in their studies of HDPE found that within temperature ranges that included that studied in this work, there was insufficient information to determine whether an Arrhenius relationship or a WLF equation was a better fit. With this in mind, both methods to determine a_T were evaluated.

3.3.2 Application to WPC

The WLF equation can be represented as

$$\log a_T = \frac{-c_{1g}\left(T - T_g\right)}{c_{2g} + T - T_g} \tag{3.19}$$

where a_T is the time shift factor, T_g is the glass transition temperature in Kelvin, and T is the temperature in Kelvin at which the shift factor is desired. The constants c_{1g} and c_{2g} are material dependent and have been found experimentally for many polymers. The average

values for c_{1g} and c_{2g} for all polymers were determined to be 17.4 and 51.6 respectively. [15]

The WLF equation (3.19) was developed with T_g as the reference temperature. In the current work, a reference temperature of 23°C was used. It was therefore necessary to convert the constants c_{1g} and c_{2g} to reflect a reference temperature of 23°C. Neilsen and Landel [6] describe the method for adjusting the constants to use a reference temperature other than the glass transition temperature in the equation. The constants are modified in the following manner:

$$c_1 = \frac{c_{1g} c_{2g}}{c_{1g} + T_{ref} - T_g} \tag{3.20}$$

$$c_2 = c_{2g} + T_{ref} - T_g \tag{3.21}$$

such that the WLF equation becomes

$$\log \tilde{a}_T = \frac{-\tilde{c}_1 \left(T - T_{ref}\right)}{\tilde{c}_2 + T - T_{ref}} \tag{3.22}$$

Because the T_g of the WPC was not known, the T_g for HDPE was an appropriate place to start. However, uncertainties exist over the glass transition temperature for HDPE. While values of T_g for HDPE have been reported between –133°C and 67°C in various sources [16, 17, 18, 19] Sperling reports that the greatest support among investigators are for T_g's in three regions: -30°C, -80°C, and -128°C [19]. A T_g of -90°C was selected as reported by Callister. [16] The constants c_{1g} and c_{2g} for HDPE likewise are not available in the literature as they are dependent on the elusive T_g, so the "universal constants" were used. Tabulated values for individual polymers vary only slightly from the universal constants, so the values used are expected to approximate the appropriate constants for HDPE. From Eq. (3.20) and (3.21), the constants for a

reference temperature of 23°C were found to be $\tilde{c}_1$ = 6.885 and $\tilde{c}_2$ = 164.6°K. Shift factors determined from Eq. (3.22) will be referred to as "preliminary" since they were obtained from the universal constants and an observed value of T_g, and will be denoted with a "~".

The Arrhenius relationship used to describe the shift factors can be expressed as

$$\ddot{a}_T(T) = \exp\frac{\tilde{E}_a}{R}\left[\frac{1}{T} - \frac{1}{T_{ref}}\right] \tag{3.23}$$

where the universal gas constant R=8.31 J/molK, $\tilde{E}_a$ is the preliminary activation energy determined from published values, T_{ref} is the reference temperature in Kelvin, and T is the temperature at which the time shift factor is desired in Kelvin. [20] Published values for the activation energy for HDPE found to best fit experimental data from thin HDPE films (100-120μm) and small cylindrical HDPE specimens studied with DMA are between 20.7kcal/mol and 25.2kcal/mol (87kJ/mol and 106kJ/mol). [9,10,11] The average, $\tilde{E}_a$ =96.5kJ/mol, was therefore used, and compared with subsequent experimental data. The shift factors obtained from published values of the activation energy will also be referred to as preliminary but will be denoted $\ddot{a}_T$ to differentiate it from the shift factors obtained from the WLF equation. Preliminary activation energies will be denoted with a "~".

Elahi and Weitsman, who utilized a power law compliance in their study of glass fiber/urethane composite, showed that the time shift factor a_T can be determined empirically. The log of the time shift factor found experimentally was plotted with respect to temperature and a polynomial curve fit was used to find an equation describing a_T over the temperature range desired. In order to account for matrix softening, they also

plotted the change in the instantaneous compliance D_o and using a polynomial fit, found an equation for $F(T)=D_o(T)/D_o$, the instantaneous temperature shift factor (ie. vertical shift). [7] These shift factors were incorporated into the viscoelastic model used for the WPC at 23°C given by Eq. (3.4) and Eq. (3.6) which, when evaluated, produced

$$\varepsilon(t,T) = [D_o F(T) + D_1\left(\frac{t}{\widetilde{a}_T(T)}\right)^n]\sigma_o \tag{3.24}$$

and

$$\varepsilon_r(t,T) = D_1[\left(\frac{t}{\widetilde{a}_T(T)}\right)^n - \left(\frac{t-t_o}{\widetilde{a}_T(T)}\right)^n]\sigma_o . \tag{3.25}$$

This model appeared to be an appropriate model, as previous research by Brinson had concluded that all composites behave as thermo-rheologically complex materials, therefore required both a horizontal and vertical shift factors.[13] Experimental verification of this model was therefore attempted.

3.3.3 Vertical and horizontal shifting

To empirically determine the time shift factor for this material, four coupons were loaded in creep to 2.03 MPa (300psi) at 23°C (20% Sut), 43°C (26% Sut), and 65°C (37% Sut) for 10 minutes and allowed to recover. A stress of 2.03 MPa was used because it did not produce an appreciable change in the measured stiffness in any of the temperature ranges. The time shift factor a_T, and the instantaneous compliance shift factor $F(T)$ were empirically chosen to fit Eq. (3.24) and Eq. (3.25) to the strain response of each coupon [7]. The values of $\widetilde{a}_T$ found experimentally are compared with the horizontal shift factors calculated using $\widetilde{c}_1$ and $\widetilde{c}_2$ in Eq. (3.22) and with $\widetilde{E}_a$ from Eq. (3.23), as is shown in **Fig. 3.3**. Given the preliminary $\widetilde{a}_T$ from experimental data, as well as knowing T_{ref}, T, and R,

a value for $\widetilde{E}_a$ was calculated to best fit the experimental data. This resulted in $\widetilde{E}_a$ =64.2kJ/mol which fit the data well. Very good correlation between the empirical data and the predictions from the WLF equation were obtained.

The values of the instantaneous shift factor *F(T)* are shown in **Fig. 3.4**, which suggested a linear dependence with temperature. A linear relationship was also consistent with the nearly linear dependence of stiffness on temperature, as shown in **Fig. 2.8**. The linear equation for the instantaneous stiffness shift factor as a function of temperature *T* was found to be

$$F(T) = .0041T - 12.050 \tag{3.26}$$

Using the WLF equation described above, a comparison between a representative coupon and the predicted strain response from Eq. (3.24) and Eq. (3.25), at σ_o=37% Sut and T= 65^{o}C is shown in **Fig. 3.5**. The model appears to capture the creep and recovery response of the coupon reasonably well. While the prediction of Eq. (3.24) is slightly above the experiment in this case, it was within the observed experimental scatter of the WPC.

3.4 DMA

3.4.1 DMA shift factor development

In order to verify the shift factors found from creep testing, five randomly selected samples machined from untested coupons were analyzed using Dynamic Mechanical Analysis (DMA). It was found that a master curve could be developed for each specimen tested utilizing only a horizontal shift factor as can be seen in **Fig. 3.6.** This implied that the WPC is "thermo-rheologically simple" instead of "thermo-rheologically complex" as had been presumed in the development of Eq. (3.24) and

(3.25). The constants of the WLF equation were calculated by the RSA II software as a best fit over the range of –31°C to 65°C for each specimen tested as was described in section **2.4.3**. Averages were taken of the WLF constants c_1 and c_2 of the 5 specimens to determine the WLF equation governing this material. The average values of c_1 and c_2 were 20.534 and 128.78°K respectively. The WLF equation with the DMA developed constants was a good fit to the experimental data over -10°C-65°C.

The activation energy (E_a) for the Arrhenius equation was calculated by solving Eq. (3.23) for E_a then calculating E_a from the a_T calculated by the DMA software for each temperature and the known values of T, T_{ref} (23°C), and R. An average of the experimental shift factors for the four coupons tested between -31°C and 0°C was calculated as 325kJ/mol and was found to represent well the experimental determined shift factors in this region. This can be seen in **Fig. 2.11.** A comparison of the WLF equation to the DMA determined shift factors in the range of 23°C to 65°C which is considered in this work can be seen in **Fig. 3.7**. The Arrhenius equation is also shown in this figure.

DMA demonstrated that the WPC could be modeled as a thermo-rheologically simple material. This more generalized approach to expressing temperature dependence was therefore pursued.

3.4.2 DMA shift factor verification

While the shifts produced from the DMA analysis resulted in a master curve for the specimens tested, verification of its applicability to the full size coupons under uniaxial creep loading was necessary. To accomplish this, these shift factors were applied to the compliance curves developed from creep strain response of four coupons

tested at 23, 45 and 65°C. They were found to form approximately continuous curves, or master curves. (Time shifting alone used in Eq. (3.24) did not produce a smooth curve.) The creep compliance master curve created from the average WLF equation from DMA can be seen in **Fig. 3.8** for a representative coupon. A creep compliance master curve was also attempted using the preliminary horizontal and vertical shifts utilized in Eq. (3.24). The preliminary shifts are compared with the DMA shift in **Fig. 3.8**. While Eq. (3.24) was shown to be a satisfactory preliminary model, it is evident that these shifts do not conform to the TTSP, otherwise a master curve could have been created.

The time shift factor developed from DMA analysis was applied to the power law model instead of the preliminary horizontal and vertical shifts applied in Eq. (3.24) and (3.25). The DMA shifts should provide accurate modeling of the viscoelastic behavior of the material if the power law model can express creep response for long durations, as the horizontal shift factor based in TTSP is independent of the viscoelastic model. However, results from the power law model for a coupon at 65°C using the DMA developed horizontal shift factor did not correlate with experimental observations, as shown in **Fig. 3.9**. It is obvious that the time dependence and magnitude of the model do not match the experimental results.

Calculation of T_g from the WLF equation developed by DMA was undertaken by working backwards using Eq. (3.20) and (3.21). Because there were three unknowns: c_{1g}, c_{2g}, and T_g, and only two equations, one constant was approximated. Aklonis and MacKnight [15] show a table of WLF parameters for various polymers. While c_{1g} and c_{2g} vary only slightly with temperature, c_{1g} was shown to vary less. For this reason, the value of c_{1g} was selected as the universal constant for polymers, 17.4. Solving for c_{2g} and

T_g produced 79.13°K and 246.3°K (–26.7°C) respectively. This value of T_g was near one of the accepted glass transition temperatures for HDPE of –30°C.

The WLF equation developed with DMA appears to be a more suitable approach to describing temperature effects than was the combination of vertical and horizontal shift factors used initially. Apparently the power law, while adequate for short times at 23°C up to around 1000 minutes, does not describe the viscoelastic response at extended times or temperatures using only a horizontal shift. Thus the benefit of using only a horizontal shift is discounted by the need for a more complicated expression of compliance.

3.5 Prony Series Model

3.5.1 Constant stress

The power law will only describe one mode of viscoelastic behavior. Its inability to predict the viscoelastic behavior of the WPC at longer times through application of verified shift factors indicated that there were several modes of time dependent behavior which occur in the WPC. Lai and Bakker utilized a Prony Series model with great success in modeling the effects of aging on the viscoelastic behavior of HDPE. [21] A Prony Series models the viscoelastic behavior as a series of springs and dashpots in parallel, with a lone spring in series with the parallel combinations of springs and dashpots (Kelvin elements) as represented in **Fig. 3.10.** The time dependent compliance of this model can be represented as

$$D(t) = D_o + \sum_{r=1}^{N} D_r \left[1 - e^{\frac{-t}{\tau_r}} \right] \tag{3.27}$$

where D_o and D_r are positive constants, and where τ_r is the retardation time. Applying this compliance model to the convolution integral to evaluate the strain response results in

$$\varepsilon(t) = \left[D_o + \sum_{r=1}^{N} D_r \left(1 - e^{\frac{-t}{\tau_r}} \right) \right] \sigma_o \tag{3.28}$$

for the strain response in creep and

$$\varepsilon_r(t) = \left[\sum_{r=1}^{N} D_r \left(e^{\frac{-(t-t_o)}{\tau_r}} - e^{\frac{-t}{\tau_r}} \right) \right] \sigma_o \tag{3.29}$$

for the strain response in recovery.

In order to create the Prony Series model for this material, the compliance curves developed from creep strain response data at 23, 45 and 65^{o}C were plotted against shifted time using the respective horizontal shift factor described by the WLF equation for each temperature. A master curve was thus formed for each coupon. Mathcad 7 Professional (Mathsoft Inc.) utilizing error minimization, was used to produce a least squares fit to the compliance (i.e. Eq. (3.28) divided by σ_o) with five Kelvin elements. The resulting equation was then evaluated through the convolution integral to predict strain response and applied to other coupons which had undergone various creep loads to verify the model. Some slight modifications were made to the constants in order to provide a smooth, best-fit curve. The resulting compliance master curve model is plotted against the compliance master curves created by the four coupons in **Fig. 3.11**. The values for D_o, D_r, and τ_r are shown in **Table 3.1**.

Table 3.1: Coefficients for Prony Series model.

r	D_r Gpa^{-1} (Msi^{-1})	τ_r min
0	13.4 (1.94)	∞
1	4.48 (.65)	20
2	6.21(.9)	1000
3	5.52 (.8)	12000
4	7.77 (1.126)	148641
5	12.9 (1.8748)	3000000

It may be observed from **Fig. 3.11** that the Prony Series model departs from the creep response of the material below approximately 5 minutes, and above 10^7 minutes at 23^oC, (which is the equivalent of 10^4 minutes at 45^oC or about 15 minutes at 65^oC). However, the ability of the Prony Series to satisfactorily represent the behavior of the material for the equivalent of a creep test for 10^7minutes at 23^oC (nearly 7000 days or 19 years) is very significant. The model could readily be extended to consider longer durations as well as better model the initial 5 minutes if more terms were included in the series and compared to longer duration tests at elevated temperatures.

3.5.2 Non-linear effects

It was noted that the material exhibited stress dependent behavior, even with the power law, which was overlooked during previous analysis of this material in which a linear viscoelastic model was used. The stress dependence of D_o and D_1 are shown in **Fig 3.12.** It was apparent that a non-linear viscoelastic model must be used for the Prony Series. Schapery [22] represents the time-dependent, non-linear compliance as

$$D(t) = \frac{\varepsilon(t)}{\sigma_o} = g_o D_o + g_1 g_2 \Delta D\left(\frac{t}{a_\sigma}\right) \tag{3.30}$$

where D_o is the instantaneous compliance, and $\Delta D(t/a_\sigma)$ is the time dependent compliance. It should be noted that application of the non-linear parameters can occur after the time dependent compliance has been integrated through the convolution integral since they are constant in time. The non-linear parameters g_o, g_1, g_2 and a_σ are stress dependent.

Due to the observed non-linearity in the creep response at all stresses, it was determined that two of the stress dependent parameters utilized in Schapery's non-linear compliance model Eq. (3.30) could account for the non-linearity observed with this material. This can be applied to the strain response in creep as

$$\varepsilon(t) = \left[g_o D_o + \sum_{r=1}^{5} D_r \left(1 - e^{\frac{-t}{\tau_r a_\sigma}} \right) \right] \sigma_o \tag{3.31}$$

where g_o and a_σ are stress dependent parameters. These parameters were empirically fit to the strain response curves from experimental data in the range of 20% Sut to 43% Sut at 23°C. **Fig. 3.13** shows the dependence of g_o and a_σ on the applied stress and can be described by

$$g_o(\sigma) = .0816\sigma_o + .8225 \tag{3.32}$$

$$a_\sigma(\sigma) = -.248\sigma_o + 1.8555 \tag{3.33}$$

where σ_o is in MPa. While some material scatter is apparent in **Fig. 3.13**, a linear stress dependence was found to satisfactorily model the non-linear behavior utilizing Eq. (3.31). (Eq. (3.32) and (3.33) had r^2 values of .78 and .56 respectively. Above 43% Sut, the relationships between stress and the values of g_o and a_σ changed significantly. This is

likely a result of damage formation as observed from Eq. (3.10). This will be discussed further in the following section.

Observation of the effects of damage discussed in section 3.2.2 indicates that the threshold stress for this material was between 43% and 50% Sut. The non-linear model, Eq. (3.31), was therefore not used above 43% Sut. **Fig. 3.14, 3.15**, and **3.16** compare the model to the experimental strain response for representative coupons at various stress levels and temperatures. As the lower grip is released during the unloading of the coupons, an impulse can be caused in the coupon. This impulse caused extensometer slippage, resulting in the recovery offset seen in **Fig 3.14** and **3.16.** Other deviation from the model seen in these figures is within the observed inherent variability of the material.

The failure to capture the initial 5 minutes or so of the creep model in **Fig. 3.14** is due to limitations of the Prony Series developed from the master curve. This can be seen in **Fig. 3.12** and was discussed previously. However, the model quickly matches the time dependent portion of the curve after the initial 5 minutes. Similarly, the initial portion of the unloading strain response is not predicted during the recovery portion of the model. However, at temperatures above 23^{o}C, due to the shifted time, the model does describe the initial strains well. Long-term creep tests of 1000 minutes at room temperature are also well modeled, as shown in **Fig 3.17.**

3.5.3 Threshold stress

Previous work by Rangaraj and Smith with their WPC had shown that above a threshold stress of 5Mpa, roughly 45% Sut, damage had occurred at 23^{o}C. A study was therefore undertaken of the stress at which the onset of damage occurred at each temperature range. Coupon stiffness was measured as a chord modulus at room

temperature prior to testing. Coupons were allowed time to recover after initial loading before testing occurred. A 10-minute creep and recovery test was then performed according to the test matrix shown in **Table 3.2**. Coupon stiffness was then measured again after sufficient time ($30t_o$) had elapsed. Stiffness loss is shown as a percentage of initial stiffness in **Fig. 3.18** at the three temperatures tested.

The threshold stress appears to be between 43% and 50% at all three temperatures. This is consistent with the findings of Rangaraj at room temperature. It is interesting that threshold stress appears to scale with temperature and was a little less than half of the ultimate strength at each temperature. Damage, manifesting itself as stiffness loss, appears to have non-trivial temperature dependence, however. At 90%Sut,

Table 3.2: Test matrix showing number of coupons tested to determine threshold stress.

%Sut	23°C	45°C	65°C
23%	0	0	3
30%	3	3	3
37%	3	3	3
43%	3	3	3
50%	3	3	3
70%	3	3	3
90%	3	3	3

the stiffness loss at other temperatures is constant. While damage at 45°C is higher than the ambient condition, it decreases at 65°C. This may be related to a phase change in the material, possibly involving annealing effects of the matrix for which the current model is

not suited. Crissman [8] had heat treated his specimens at 75°C for 72 hours prior to testing, and Lai and Bakker found that heating HDPE specimens for 18 hours in an oven at 90°C rid the HDPE specimens of residual processing stresses. [22] It is likely with this WPC that some relaxation of the material occurred. Crystallinity of the HDPE, as reported by Fukui et al, and Onogi et al [10,11] was not affected by temperature until nearly 105°C and should not affect the current work. The melt temperature of HDPE is near 140°C [19].

Of interest also is the consistent loss in stiffness of approximately 3-4% observed at 45°C and 65°C below the threshold stress. This could be due to damage in the interfacial region between the wood and the matrix due to differences in the thermal expansion coefficients of wood and HDPE. The thermal expansion coefficients of both HDPE and wood were investigated.

It is known that HDPE has a linear thermal coefficient of expansion of 90με/°C.[20] The volumetric coefficient of expansion can be calculated by multiplying the linear coefficient by a factor of 3, equaling 270με/°C [17]. Wood has orthotropic coefficients of thermal expansion, but is very dependent on the specific gravity and the moisture content. Wood can have a thermal expansion coefficient between 31 and 4.5με/°C along the grain direction in the ovendry condition. (Ovendry refers to the condition of the wood after having been in a well ventilated oven at 102-105°C for as long as necessary so that the weight of the wood is no longer changing due to moisture loss.) Perpendicular to the grain in the ovendry condition, it is possible to have thermal expansion coefficients 5 to 10 times the parallel-to-grain expansion. However, if moisture content in the wood is low, near 3-4%, moisture loss due to heating will cause

shrinkage of the wood particle. To further complicate analysis, wood with moisture content of 8-20% will initially expand, then over time will shrink as moisture leaves the wood. [23] As specific data is not available for the WPC, data for solid wood was utilized to approximate the moisture dependent behavior for the WPC. Relative humidity was known to vary between 25-35% during WPC testing. The steady state moisture content of wood at this humidity is 6.9% at 23°C and 5.5% at 65°C. Based on the relationship for percent shrinkage S_m, [23]

$$S_m = S_o\left(\frac{M_{ref} - M}{M_{ref}}\right) \tag{3.34}$$

where M_{ref} is the reference moisture content, M is the moisture content at which the percent shrinkage from M_{ref} is desired, and S_o is a species dependent material parameter, the volumetric shrinkage from 6.9% to 5.5% moisture content is 2.56%, based on the data for red maple. The expansion of the HDPE coupled with the shrinkage of the wood particles is likely the cause of the stiffness loss beneath the threshold stress at 45°C and 65°C.

3.5.4 Development of damage model for Prony Series

In order to develop the a model to predict the behavior above 43%Sut, the concepts of damage developed for the power law model by Rangaraj and Smith [2] was used as a guide. Eq. (3.9) and (3.10), repeated for convenience, were utilized to fit the data at room temperature.

$$\sigma_e(t) = \sigma_o(t) \cdot \omega(\sigma_o, t) \cdot H(t) \tag{3.9}$$

$$\omega(\sigma_o, t) = 1 + (s + ct^m) < \sigma_o - \sigma_d > \tag{3.10}$$

where *s*, *c*, and *m* are material dependent constants. As before, the effective stress and time dependent compliance were evaluated using the convolution integral. Integration produced

$$\varepsilon_c(t) = \left[\left[g_o D_o + \sum_{r=1}^{5} D_r \left(1 - e^{\frac{t}{\tau_r a_\sigma}} \right) \right] [1 + s\langle \sigma_o - \sigma_d \rangle] + F_c(t) \right] \sigma_o \tag{3.35}$$

where

$$F_c(t) = \int_0^t \left(g_o D_o + \sum_{r=1}^{5} D_r \left(1 - e^{\frac{t-\tau}{\tau_r}} \right) \right) mc\,\tau^{m-1} \langle \sigma_o - \sigma_d \rangle d\tau \tag{3.36}$$

which does not have a closed form solution when m is not an integer. Therefore, numerical integration in the form of Simpson's rule was utilized such that

$$F_c(t) \approx \sum_{i=1}^{N} \frac{t}{6N} \left[G\left(t, t\frac{i-.5}{N} \right) + 4G\left(t, t\frac{i}{N} \right) + G\left(t, t\frac{i+.5}{N} \right) \right] \tag{3.37}$$

where $G(t, \tau)$ is the integrand of Eq. (3.36), and N is the number of iterations. A convergence study was completed to determine how many iterations were required for convergence. Convergence was determined to occur after 3000 iterations or $300t_o$. This was within 5% of the strain value produced at 100,000 iterations. A plot of the convergence study is shown in **Fig. 3.19**. The number of iterations was increased by the factor $a_\sigma^{-1} a_T(T)^{-1}$ to maintain the same number of iterations per minute of data as time was affected by the stress and time-temperature shift factors. The number of iterations did not increase by that exact amount as N was required to be an integer, so the closest value which would allow N to remain an integer was used, erring on the side of increasing the number if iterations slightly if necessary.

Earlier work with the power law model had shown m=0.15 modeled time dependent damage well. The equations for non-linear stress dependence (g_o and a_σ) were held constant at the threshold stress for $\sigma_o < \sigma_d$. Empirically fitting the model to the data at 23°C, resulted in s=0 and c=0.160MPa^{-1}min^{-m}. This adequately modeled the time dependent strain response of the WPC at 50% and 70%, as can be seen in **Fig. 3.20** and **Fig. 3.21**, although some overprediction of the initial 5 minutes is observed in **Fig. 3.21**. Although not explicitly apparent in these plots, greater variation was observed in the experimental strain response as the stress level exceeded the threshold stress. This may be due to stress localization, where the effects of imperfections in the composite are magnified. Accordingly, the model, did not describe the increased time dependence seen at 90% Sut at 23°C shown in **Fig. 3.22**. This indicates, as Rangaraj found, that at 90% the material is entering the tertiary creep phase, the model of which was not an aim of this study. Recovery in the region where damage occurred was not modeled.

3.5.5 Application of damage model to coupons at 45°C and 65°C

Application of this model to coupons tested at elevated temperatures was attempted. The shift factor $a_T(T)$ developed from DMA experimental data was applied to Eq. (3.35) and (3.36) according to Eq. (3.17). Strain response was over-predicted at both 45°C and 65°C, and at both stress levels as seen in **Fig. 3.23** and **Fig. 3.24**. This suggests that the damage and viscoelastic response may scale differently with temperature. As observed in **Fig. 3.18**, while temperature accelerates strain response, it tends to have a benevolent effect on damage. This indicates that in this material temperature affects damage differently than it does strength. This may be due to the reduction of brittle failure as the matrix softens, the blunting of microcracks, increased matrix toughness

associated with higher temperatures as seen in **Fig. 2.9**, or a combination of these factors. The greater mobility of the polymer chains relative to each other as indicated by the increased compliance at higher temperatures may also be a factor.

3.6 Summary

The behavior of HDPE has been difficult to describe due in part to its semi-crystalline nature and unresolved glass transition temperature. The behavior of the WPC is likewise not definable by simple means, but has changing characteristics depending on the length of time the material is loaded, the stress level, and the temperature. A linear viscoelastic power law model was shown to be insufficient for modeling the WPC at extended times due to changes in its time dependence. The non-linear Prony Series was seen to provide a better description of the viscoelastic behavior of the WPC both at room temperature and at temperatures up to 65^{o}C and below 43% Sut. The WPC was found to be thermo-rheologically simple, and both a WLF and Arrhenius model for temperature dependence described the temperature dependence well in the temperature range studied. The addition of a continuum damage model to predict behavior above 43% at 23^{o}C was successful under ambient conditions. Damage was found to depend on temperature; however, it decreased relative to the ultimate strength as temperature increased. Accordingly the non-temperature dependent damage model consistently overpredicted the strain response.

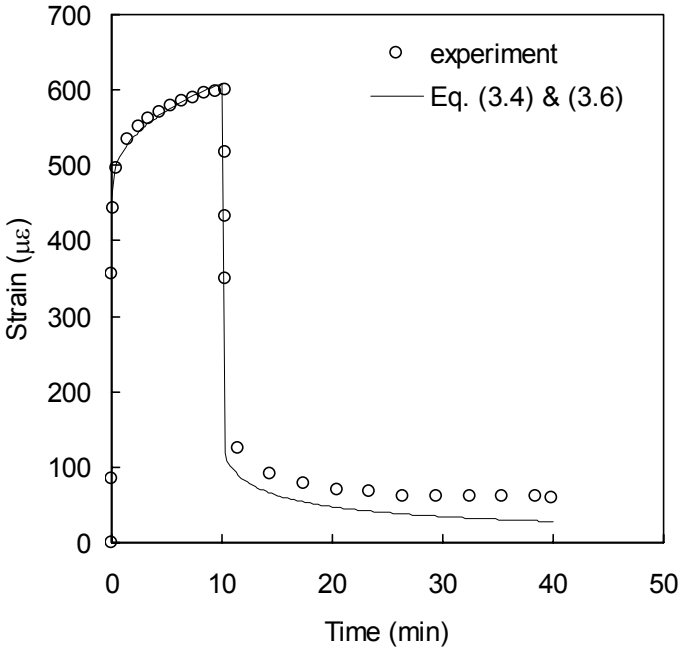

Fig. 3.1: Comparison of power law model with experimental data, σ_o=20%Sut at 23°C.

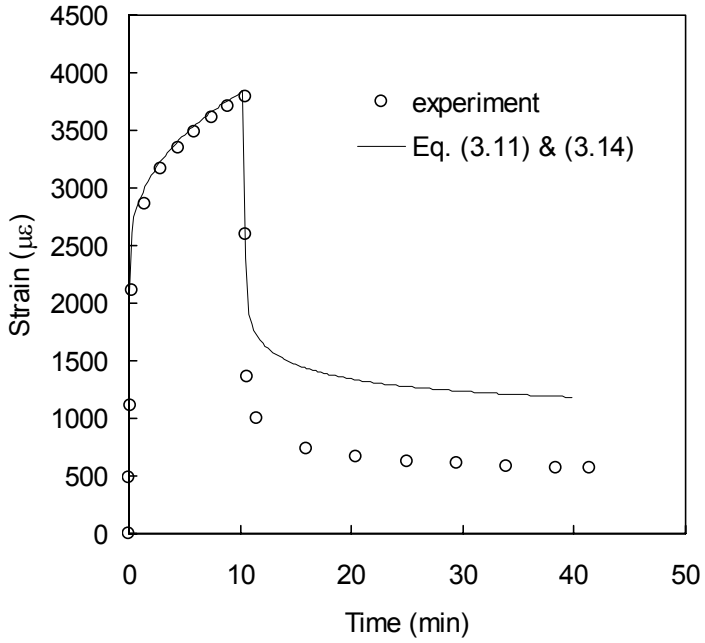

Fig 3.2: Comparison of power law model with damage with experimental data for representative coupon with σ_o=70%Sut at 23°C.

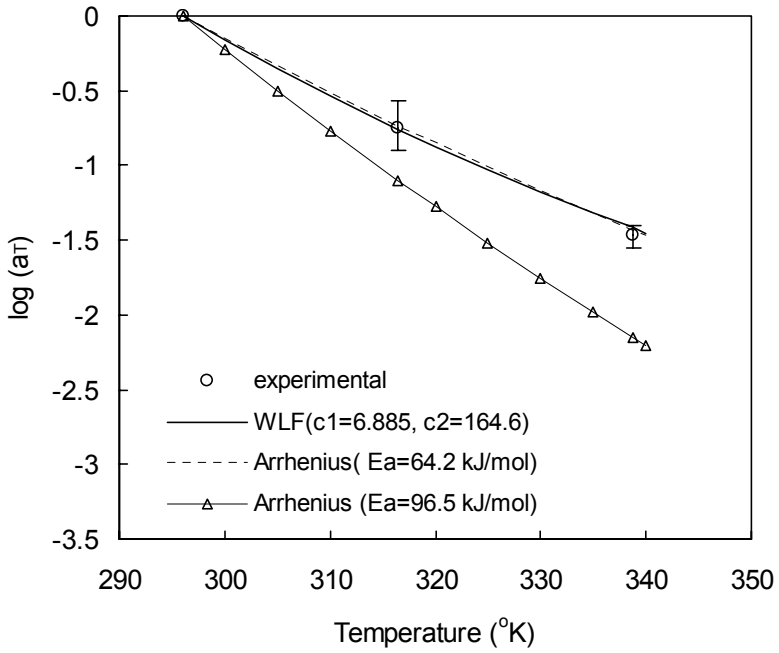

Fig 3.3: Comparison of preliminary shift factors obtained from creep testing with the WLF and Arrhenius relations, where the existence of a vertical shift factor is presumed.

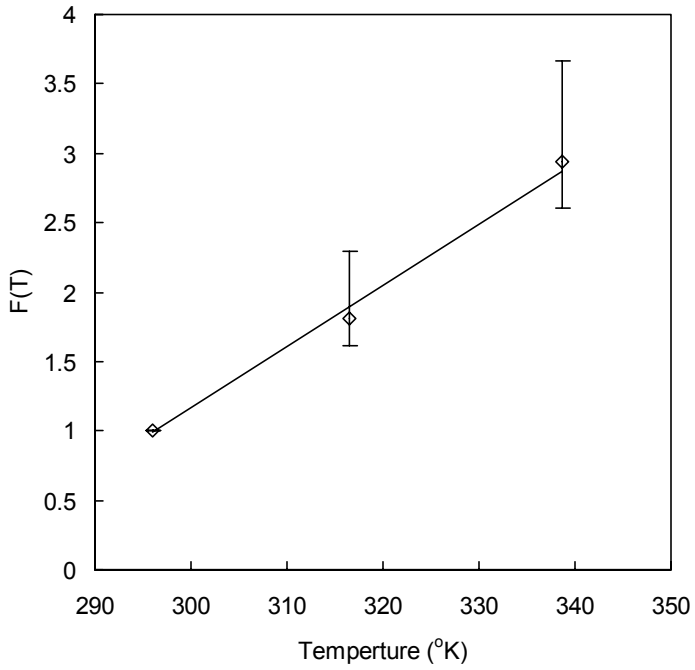

Fig. 3.4: Comparison of vertical shift factor *F(T)* to experimental data.

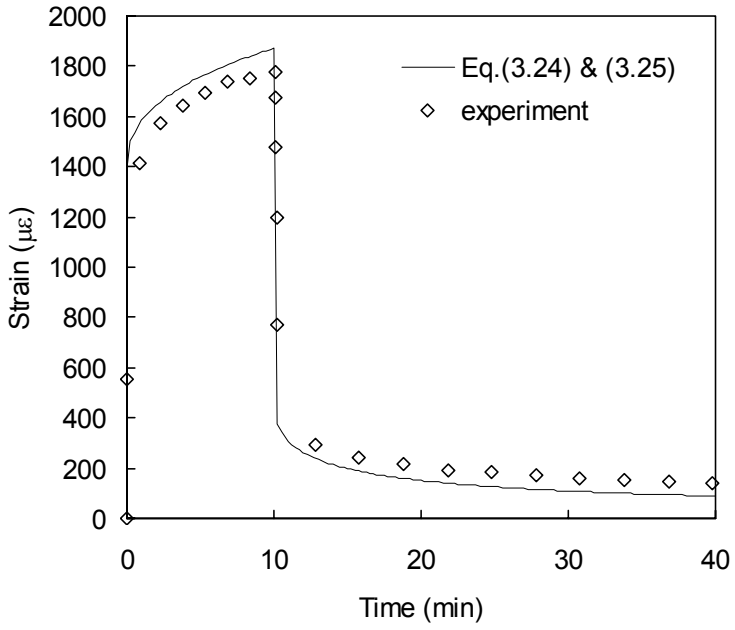

Fig. 3.5: Comparison of Eq. 3.24 and 3.25 with representative coupon with σ_o=37% Sut and T= 65°C.

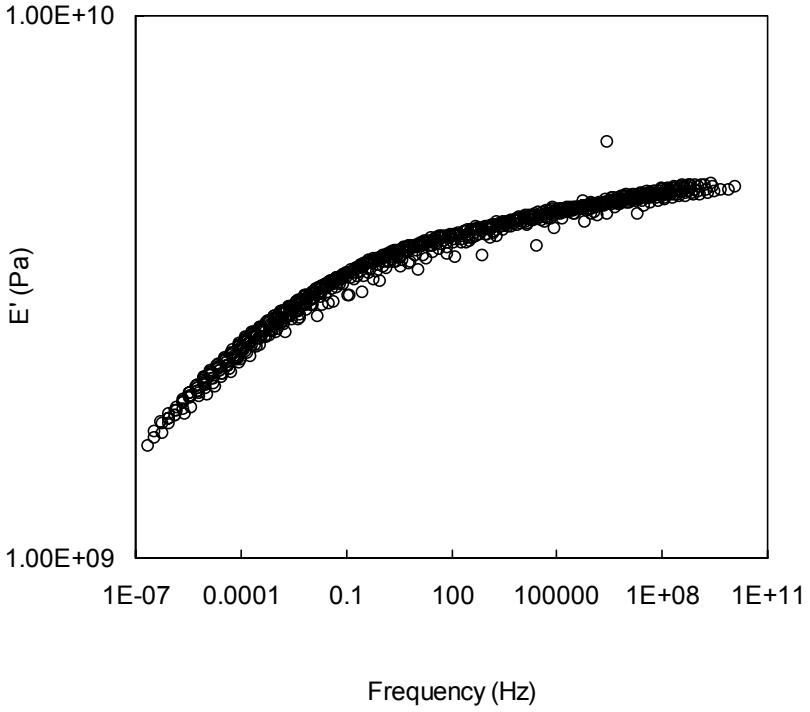

Fig. 3.6: Master curve created using experimentally developed shift factors from DMA.

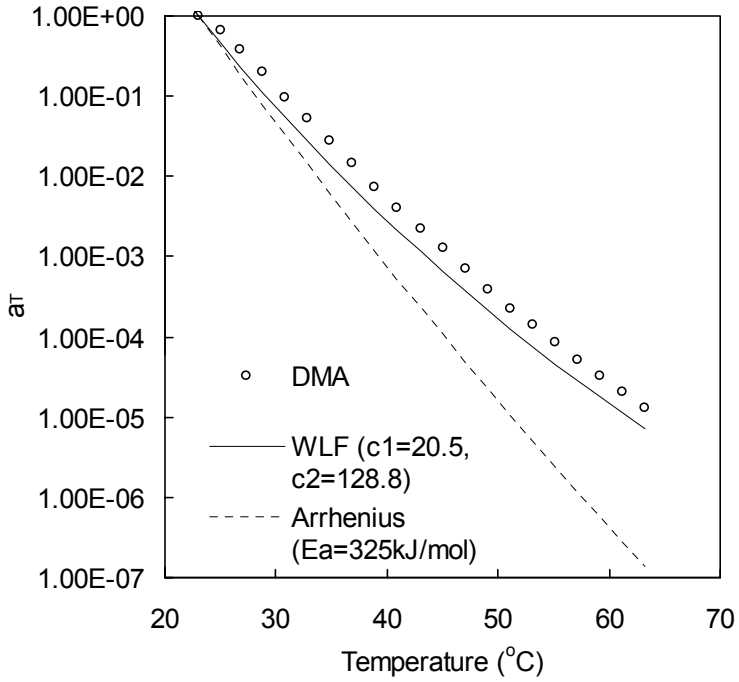

Fig 3.7: Comparison of the shift factor found from DMA with the Arrhenius and WLF equations.

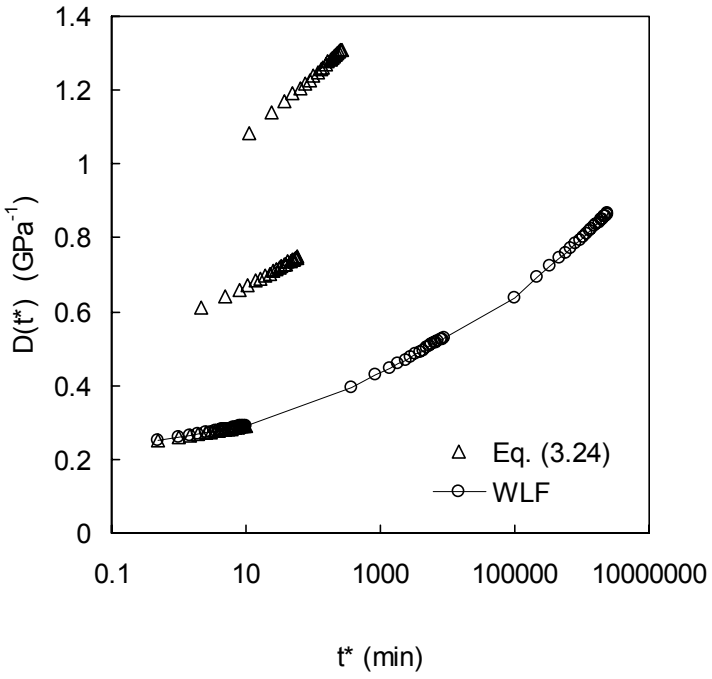

Fig. 3.8: Comparison of representative coupon master curve fit with preliminary horizontal and vertical shift factors used in Eq. (3.24) and a WLF horizontal shift determined by DMA.

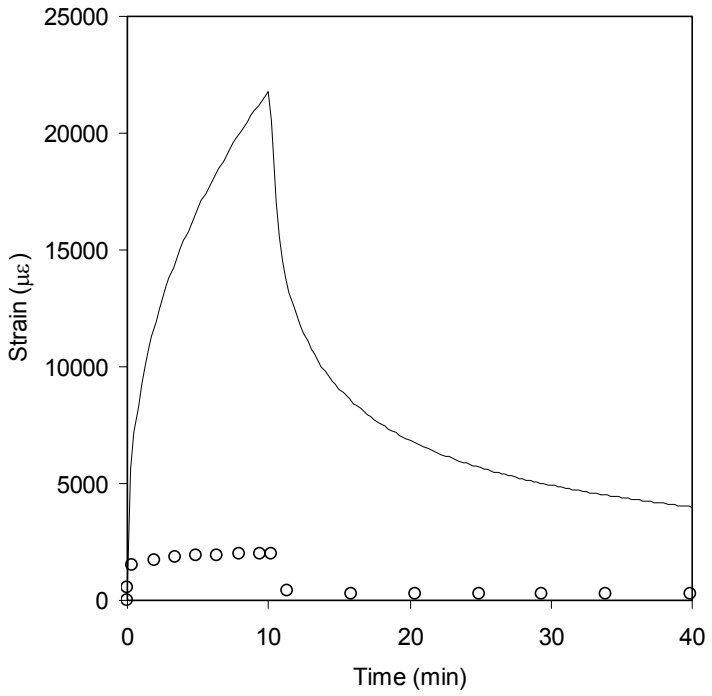

Fig. 3.9: Comparison of representative coupon with DMA time shift factor applied to power law with σ_o=43% Sut at 65°C.

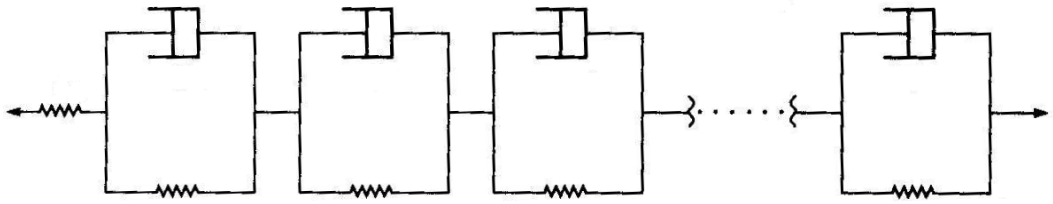

Fig 3.10: Graphic reprensentation of the Prony Series model, taken from [24].

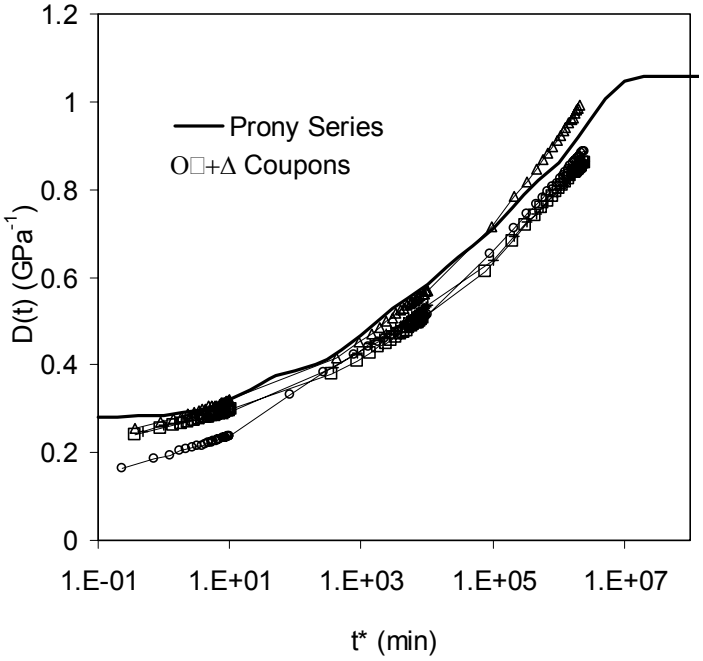

Fig. 3.11: Prony Series comparison with master curves for four coupons at σ_o=2.07 MPa. Inherent coupon to coupon variation is evident.

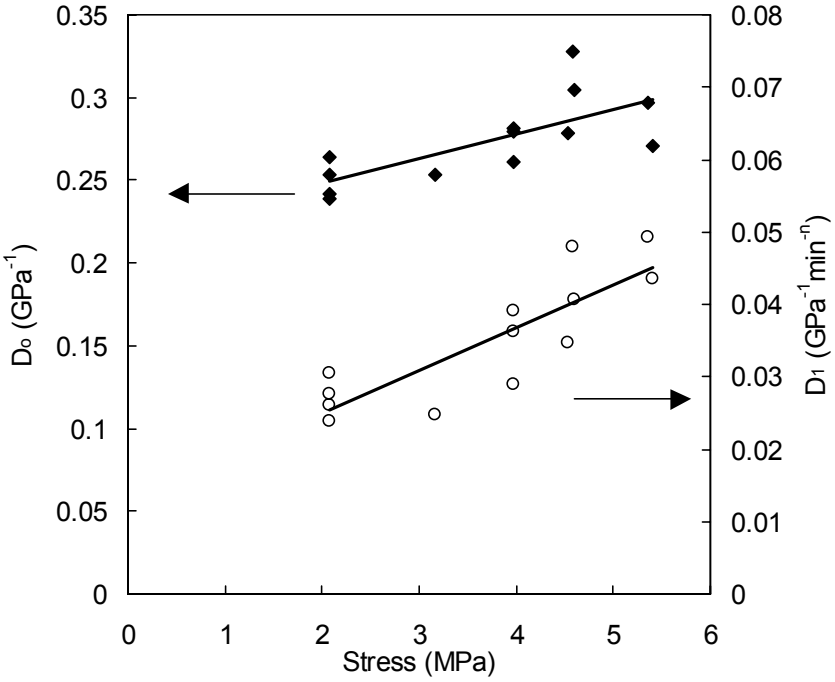

Fig. 3.12: Stress dependence of power law parameters D_o and D_1.

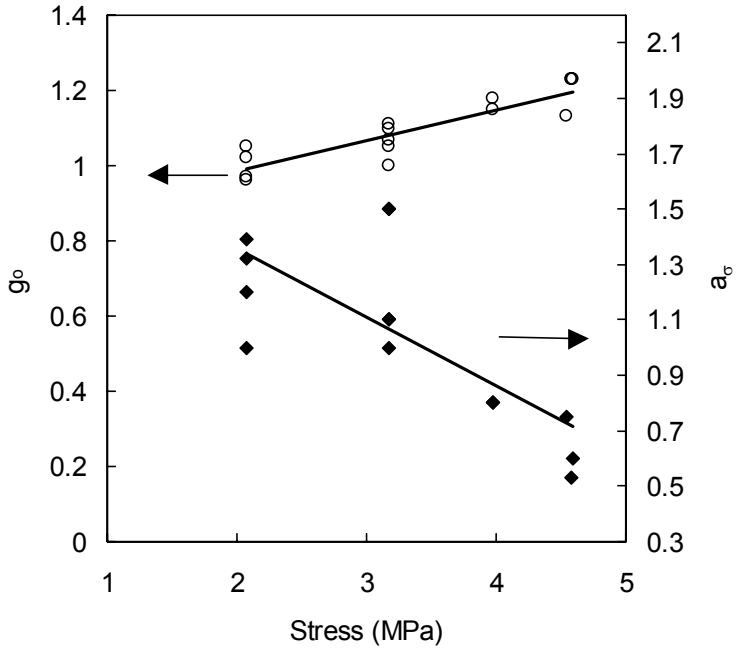

Fig 3.13: Stress dependent parameters for non-linear Prony Series model.

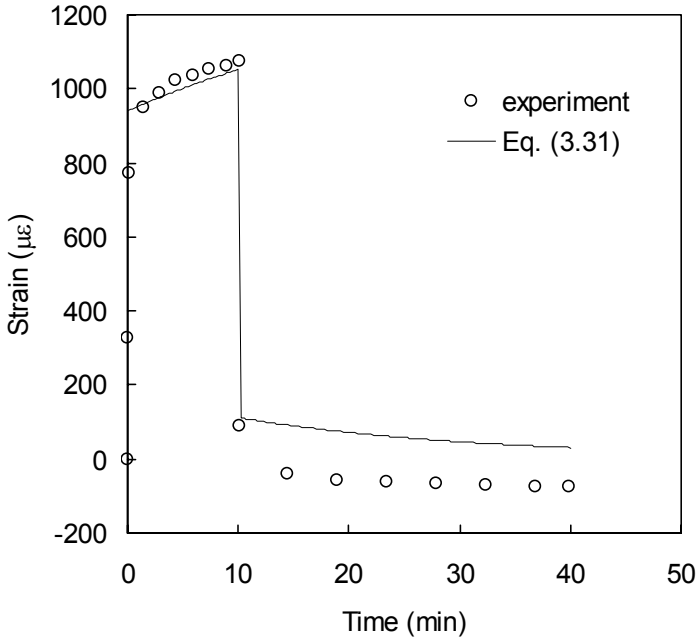

Fig 3.14: Comparison of Prony Series model with representative coupon at 30% Sut at 23°C.

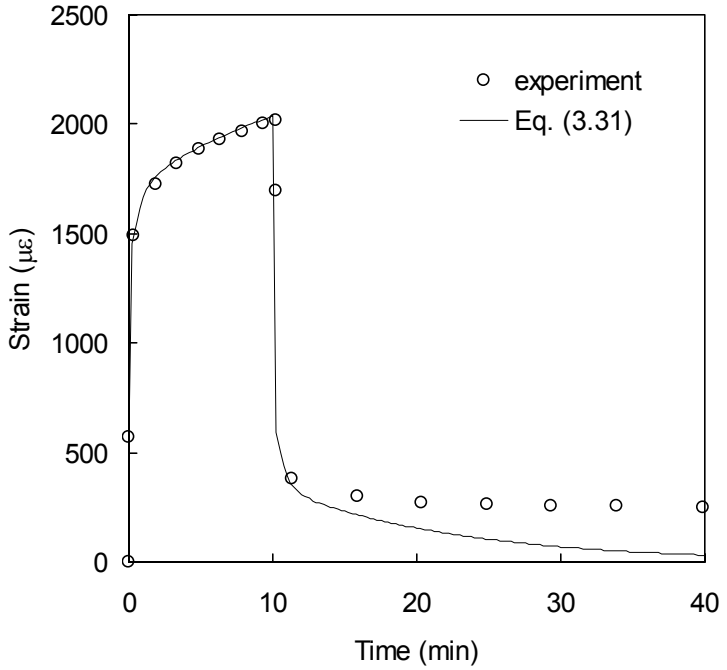

Fig 3.15: Comparison of Prony Series model with representative coupon with σ_o=43% Sut at 65°C.

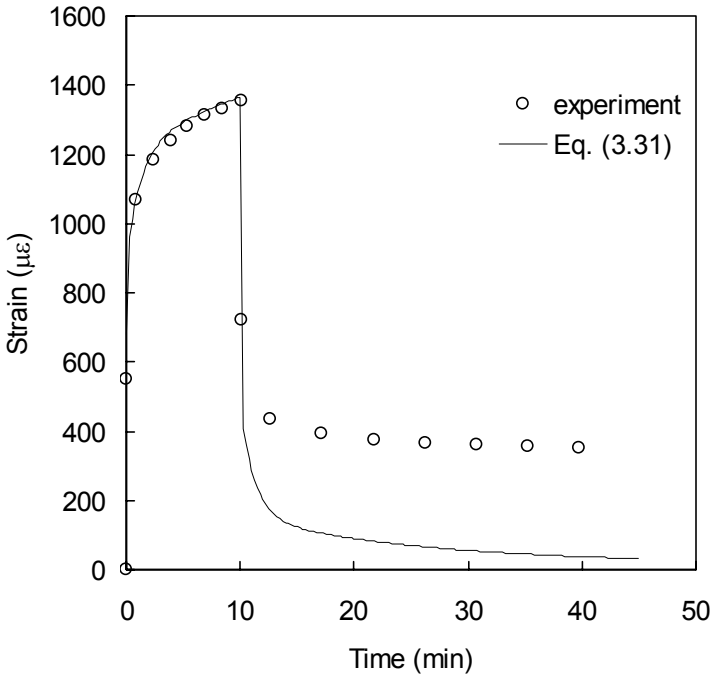

Fig 3.16: Comparison of representative coupon with Prony Series model at σ_o=30% Sut at 45°C. Extensometer slippage is seen in recovery.

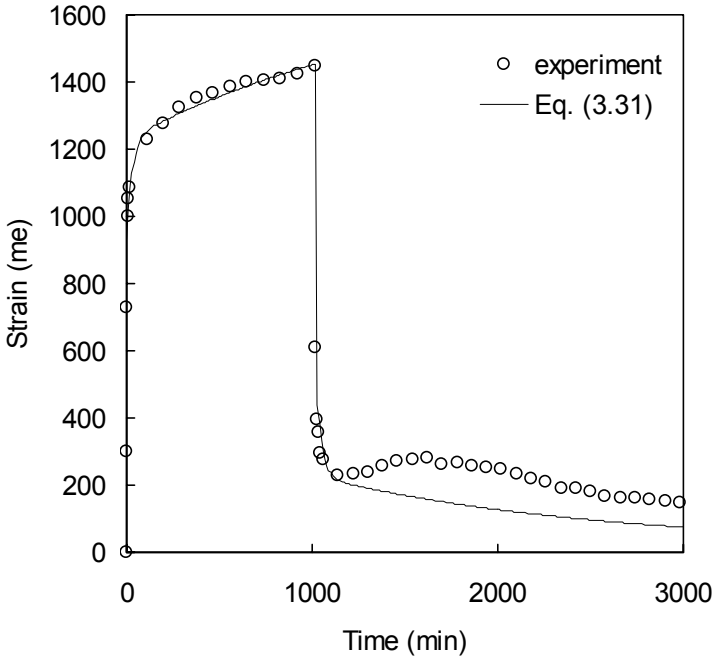

Fig 3.17: Comparison of representative coupon with Prony Series model with σ_o=30% Sut at 23°C. Recovery strain response phenomenon due to lab temperature fluctuation.

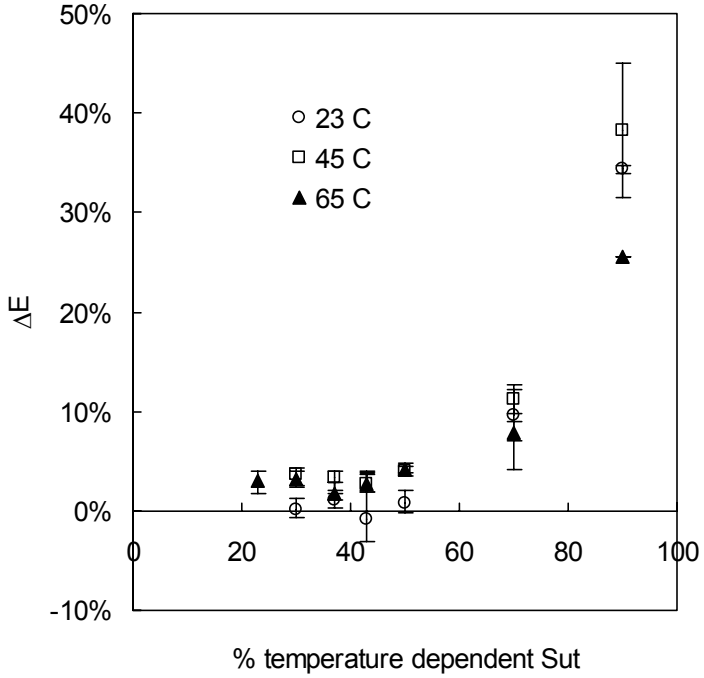

Fig 3.18: Threshold stress determination. ΔE=1-E_i/E_f where E_f is the final stiffness and E_i is the initial stiffness

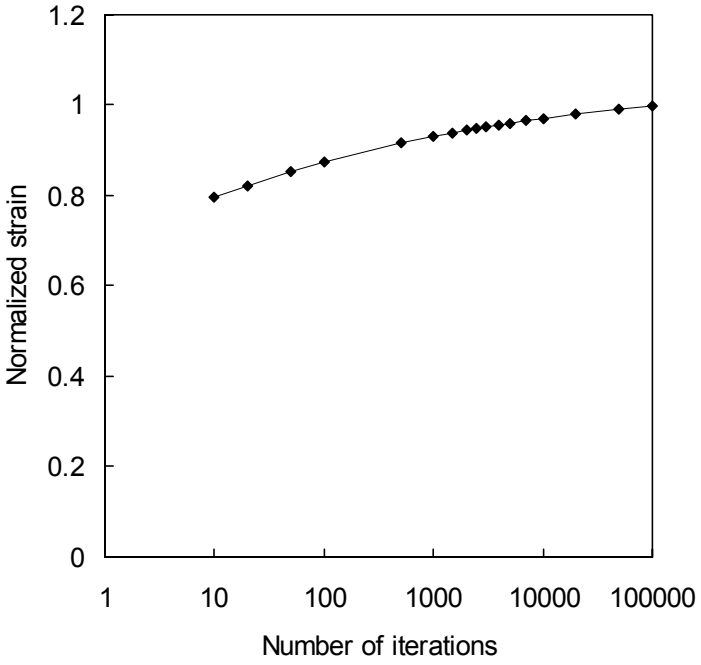

Fig 3.19: Convergence of Simpson's rule for evaluation of Prony Series model incorporating damage.

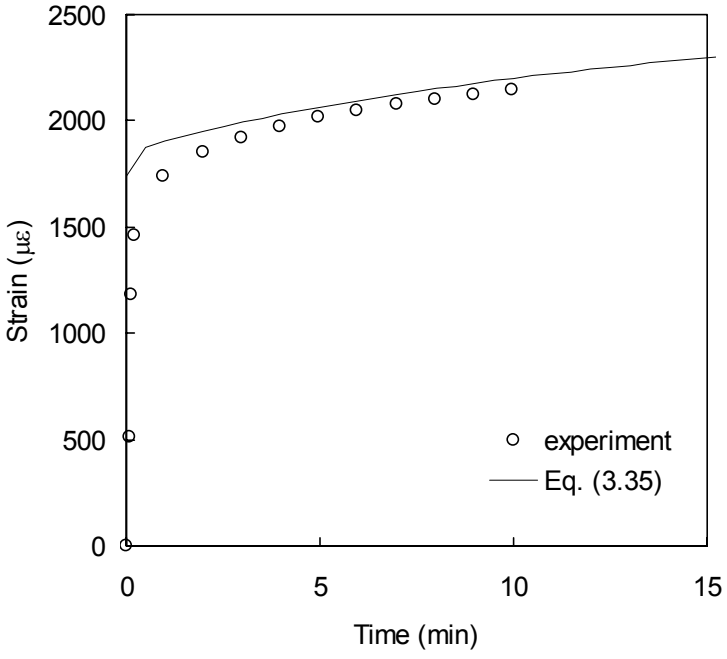

Fig 3.20: Comparison of Prony Series model with representative coupon in creep at σ_o=50% Sut at 23^{o}C.

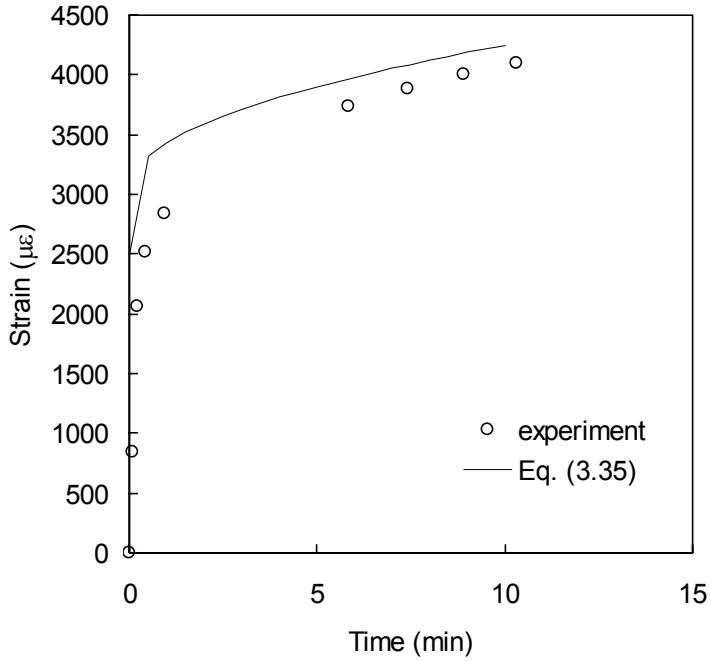

Fig 3.21: Comparison of Prony Series model with representative coupon in creep at σ_o=70% Sut at 23°C.

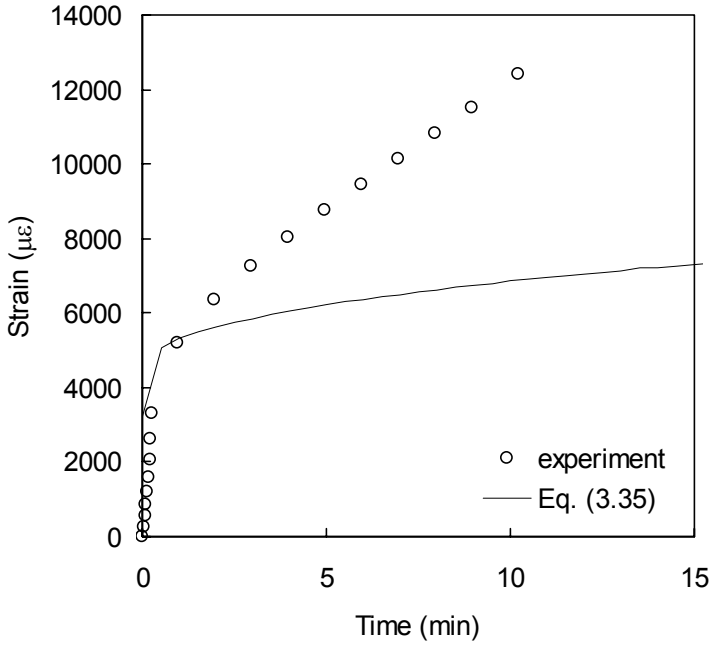

Fig 3.22: Comparison of Prony Series model with representative coupon at σ_o=90% Sut at 23°C.

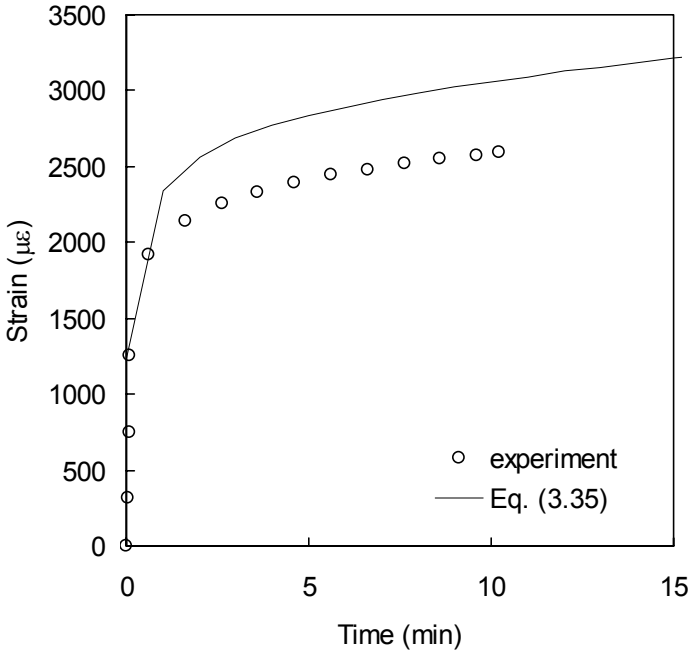

Fig 3.23: Comparison of Prony Series model with representative coupon in creep at σ_o=50% Sut at 45°C.

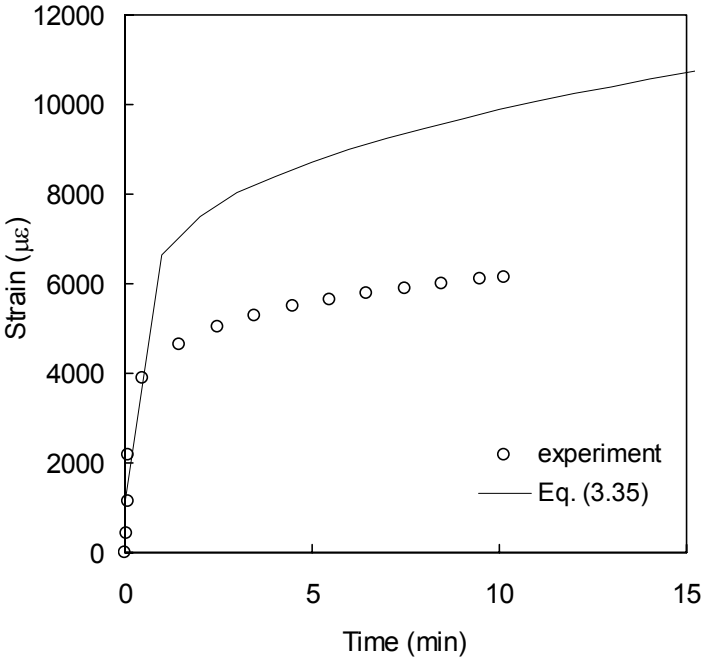

Fig 3.24: Comparison of Prony Series model with representative coupon in creep at σ_o=70% Sut at 65°C.

REFERENCES

[1] Rangaraj, Sudarshan V., Durability Assessment and Modeling of Wood-Thermoplastic Composites, Master's Thesis, Washington State University, August 1999.

[2] Rangaraj, Sudarshan V., and Smith, Lloyd V., The Non-linear Viscoelastic Response of a Wood-Thermoplastic Composite, Mechanics of Time-Dependent Materials, 3:125-139, 1999.

[3] Lemaitre, Jean, and Chaboche, Jean-Loius, Mechanics of Solid Materials, Cambridge University Press, UK, 1990.

[4] Smith, L.V., and Weitsman, Y.J., The visco-damage mechanical response of swirl mat composities, International Journal of Fracture, 92(3) 1999, 201-220.

[5] Schwarzl, F. and Staverman, A.J., Time-Temperature Dependence of Linear Viscoelastic Behavior, Journal of Applied Physics, Vol 23 No 8, Aug 1952.

[6] Nielsen, Lawrence F., and Landel, Robert F., Mechanical Properties of Polymers and Composites 2nd edition, Marcel Dekker, 1994.

[7] Elahi, M., and Weitsman, Y.J., On the Mechanical response of P4 Chopped Glass/Urethane Resin Composite: Data and Model, Oak Ridge National Laboratory, ORNL –6955, October, 1999.

[8] Crissman, J.M., Creep and Recovery Behavior of a Linear High Density Polyethylene and an Ethylene-Hexene Copolymer in the Region of Small Uniaxial Deformations, Polymer Engineering and Science, 26: n15, 1986

[9] Penn, Robert W.,Dynamic Mechanical Properties of Crystalline, Linear Polyethylene, Journal of Polymer Science: Part A-2, 4: 545-557 1966.

[10] Fukui, Y., Sato, T., Ushirokawa, M., Asada, T, and Onogi, S., Rheo-Optical Studies of High Polymers. XVII. Time-Temperature Superposition of Time-Dependent Birefringence for High-Density Polyethylene, Journal of Polymer Science: Part A-2, Vol 8, 1195-1209, 1970.

[11] Onogi, S, Sato, T., Asada, T, and Fukui, Y., Rheo-Optical Studies of Hight Polymers, XVIII. Significance of the Vertical Shift in the Time Temperature Superposition of RheoOptical and Viscoelastic Properties, Journal of Polymer Science: Part A-2 Vol 8, 1211-1255, 1970.

[12] Morgan, C.J., Ward, I.M., The Temperature Dependence of Non-linear Creeep and Recovery in Oriented Polypropylene, Journal of the Mechanics and Physics of Solids, Vol. 19, pp165-178, 1971

[13] Brinson, L.C., Time-Temperature Response of Multi-phase Viscoelastic Solids through Numerical Analysis, PhD Thesis, California Institute of Technology, Feb 1990.

[14] Williams, M.L., Landel, R.F., and Ferry, J.D., Journal of the American Chemical Society, 77, 3701, 1955.

[15] Alkonis, John. J., and MacKnight, William J., Introduction to Polymer Viscoelasticity, 2nd edition, John Wiley and Sons, New York, 1983.

[16] Callister, William D., Materials Science and Engineering: an Introduction, 3rd edition, John Wiley and Sons, 1994.

[17] Van Krevelen, D.W., Properties of Polymers, Elsevier Scientific Publishing Company, Amsterdam, 1976.

[18] Mark, James E., Physical Properties of Polymers Handbook, American Chemical Society, Washington D.C., 1993.

[19] Sperling, L.H., Introduction to Physical Polymer Science, 2nd edition, John Wiley and Sons, 1992.

[20] McCrum, N.G., Buckley, C.P., Bucknall, C.B., Principles of Polymer Engineering, Oxford University Press, New York, 1988.

[21] Lai, J., and Bakker, A., Analysis of the non-linear creep of high-density polyethylene, Polymer, 36:1, 1995.

[22] Schapery, R.A., ON the Characterization of Nonlinear Viscoelastic Materials, Polymer Engineering and Science, Vol. 9:4, July 1969.

[23] Wood Handbook: Wood as an Engineering Material, Reprinted from the Forest Products Laboratory General Technical Report FPL-GTR-113 with the consent of the USDA Forest Service, Forest Products Society, 1999.

[24] Gibson, Ronald F., Principles of Composite Material Mechanics, McGraw-Hill Inc., 1994.

CHAPTER FOUR

VISCOELASTIC FATIGUE RESPONSE OF WPC

4.1 Introduction

Much of the study on fatigue undertaken for viscoelastic materials has been in the areas of predicting fatigue life and crack growth. Further, study of the effects of fatigue on the viscoelastic properties E', E" and tan δ has also been undertaken. However, little has been done with predicting the strain response of a viscoelastic material in cyclic loading. After the successful application of the Prony Series viscoelastic model to a step stress input at various temperatures, the competence of the model to predict the strain response of the WPC when subjected to a cyclic loading scenario was investigated. Previous work in the viscoelastic modeling of fatigue loading conducted by Elahi and Weitsman [1] utilized a cyclic ramp loading function on a glass/urethane composite. Temperature dependence was not incorporated into their model. Some comparison between creep behavior and fatigue behavior of HDPE to a cyclic displacement has also been studied by Scavuzzo [2] and He [3] at room temperature, but a model was not developed to describe the behavior.

The present work will develop a model to describe the viscoelastic behavior of the WPC in fatigue loading. This will be accomplished by applying a sinusoidal stress function to the creep models developed in Chapter Three. The temperature dependence, stress dependence, and damage developed for creep loading will also be utilized in the viscoelastic fatigue model presented herein.

4.2 Power Law Model

4.2.1 Development of power law fatigue model

The power law established by Rangaraj and Smith [4] was utilized to describe the viscoelastic fatigue response. This model, while found not to adhere to the strict application of the TTSP provided a convenient expression for cyclic response. The application of a cyclic load to the viscoelastic model can be modeled by replacing the step stress function in the convolution integral Eq. (3.1) with the an equation for cyclic stress

$$\sigma_f(t) = \left(\sigma_m + \sigma_a \sin(ft)\right)H(t) \tag{4.1}$$

where f is the frequency of the oscillation in minutes, σ_m is the mean cyclic stress, and σ_a is the stress amplitude. Again, $H(t)$ is the Heaviside step function which controls the onset of the cyclic stress. Evaluating this stress function with the power law compliance in the convolution integral produces

$$\varepsilon(t) = D(t)\cdot\sigma_m + \int_0^t \left[D_o + D_1\cdot(t-\tau)^n\right]\cdot\left[f\sigma_a \cos(f\tau)\right]d\tau \tag{4.2}$$

which does not have a closed form solution as n is not an integer. Simpson's rule was chosen to numerically integrate this equation. In order to efficiently calculate the strain response due to fatigue loading, a Fortran program was written to perform this integration and record the peak strain response of the first cycle of every minute. This program is attached in Appendix 1. The frequency f in cycles per minute was calculated as $2\pi(\gamma)60$ where γ is the frequency in Hertz. The time at which the first peak strain occurred immediately after each minute was calculated as $(4(60)(\gamma))^{-1}\text{min}^{-1}$.

A convergence study was completed to determine the number of iterations required for convergence at 100 minutes, 500 minutes and 10,000 minutes. It was found

that the strain response converged at a variable number of iterations equal to *5,000t,* where *t* is the time at which the peak strain is being evaluated. Also, the value of the strain response predicted by the Fortran model at *5,000t* was within 2% of the response predicted at twice the number of iterations at each of the times studied, as can be seen in **Fig. 4.1**.

4.2.2 Experimental verification

In order to minimize the inherent scatter observed between coupons, prior to fatigue testing, a 10-minute creep and recovery test to 30% Sut at 23°C was conducted. This allowed the values for the parameters D_o and D_1 to be determined for each coupon, removing some of the variability which would have resulted had average values of D_o and D_1 been used. A comparison of the power law model to the creep recovery for a representative coupon is shown in **Fig. 4.2**. The parameters from this comparison were found to be D_o= .273 Gpa^{-1} (1.88 Msi^{-1}), D_1=.032 $Gpa^{-1}min^{-n}$ (0.22 Msi^{-1}/min^{-n}). As was discussed in Chapter Two, a frequency of 0.5Hz was used for fatigue testing due to the reduced slippage of the extensometer and the absence of detectable temperature effects. Specimens were loaded in fatigue at 23°C with σ_{max}=30%Sut and R=0.1 as described in Chapter Two. A comparison of the peak cyclic strain from Eq. (4.2) with a representative coupon is shown in **Fig 4.3**. **Fig 4.4** compares the strain response of the model with that same coupon for times greater than 100 minutes. This indicates that while the first five minutes appear to have about the same time dependence, and strain response, the time dependence of the viscoelastic model is greater than that observed experimentally. By viewing the behavior at times nearing 1000 minutes, it is easy to see that the WPC initially has a rapid strain response initially, but soon the strain response nearly flattens

out. The viscoelastic model developed with the power law, conversely, continues to climb as time increases, and does not appear to nearly flatten out, even after 1000 minutes.

4.2.3 Time-temperature superposition of power law model

The preliminary vertical and horizontal temperature shift factors utilized in Eq. (3.24) were applied to the model to predict temperature dependence of the fatigue response as

$$\varepsilon(t) = \left(D_o F(T) + D_1 (\frac{t}{\widetilde{a}_T(T)}) \right) \cdot \sigma_m + \int_0^{\frac{t}{\widetilde{a}_T(T)}} \left[D_o F(T) + D_1 \cdot (t-\tau)^n \right] \cdot \left[f\sigma_a \cos(f\tau) \right] d\tau \quad (4.3)$$

where *F(T)* is the instantaneous shift factor and $\widetilde{a}_T(T)$ is the preliminary time dependent shift factor. Coupons were loaded to 30% Sut at 45°C and 65°C. The Fortran model predicted the strain response at a temperature by evaluating the model at the applied stress levels at shifted time. In order to compare the experimental results and the power law model on the same time scale, the time data given by the model was multiplied by the time shift factor for the temperature. A representative coupon at 65°C with R=0.1 is shown in **Fig. 4.5**. The comparison shows that time dependence is over-predicted by the model. Likewise, the magnitude of the predicted behavior is approximately twice that of the experimental response.

4.2.4 Power law viscoelastic behavior of other polymeric materials

Due to the inability of the power law viscoelastic model to predict the behavior of the WPC in fatigue at any temperature, questions were raised as to whether this was a phenemonon of the fatigue responses of HDPE, or whether this was a shortcoming of the viscoelastic fatigue model. Specimens of virgin HDPE, a polypropylene (PP) based

WPC, and a poly-vinyl chloride (PVC) based WPC were acquired. Several coupons of the PP WPC and virgin HDPE were dogboned to the same dimensions as the HDPE based WPC studied in this work for quasi-static testing to determine strength and elastic modulus. The PVC was not dogboned, due to dimensional limitations of the source material. This resulted in a lower measured Sut as failure in quasi-static testing occurred at the stress concentration at the grips. These coupons were also 7.6 mm thick instead of 12.7mm, as were the other coupons. **Table 4.1** lists the results of this testing. Values for the HDPE WPC studied in this work are also listed for comparison.

Table 4.1 Comparison of strength and elastic modulus for viscoelastic materials tested.

Material	Strength (MPa)	Elastic Modulus (GPa)	D_o (GPa^{-1})	D_1 (GPa^{-1})	n
Virgin HDPE	19.8	1020	.783	.333	.3
PP-WPC	11.6	4040	.174	.015	.3
PVC-WPC	22.5	6840	.13	.013	.19
HDPE WPC	10.7	3800	~.27	~.033	.39

As observed in **Table 4.1**, the primary benefit of the wood component is to increase stiffness and reduce time dependence. Straight coupons were cut to the same dimensions as those described in Chapter Two for the WPC used in this work, excluding the thickness of the PVC specimens. These coupons were loaded in creep to approximately 30% of their ultimate strength at 23°C, as found by the quasi-static loading, for 10 minutes and allowed to recover. The values of D_o, D_1, and n were chosen to obtain a best fit with the power law for each coupon. These coupons were then loaded in fatigue to approximately 30% of the experimentally determined ultimate strength at

23^{o}C for between 90 and 600 minutes. The viscoelastic fatigue model was applied using the parameters obtained from Table 4.1 for each material.

Fig. 4.6-4.11 show a comparison for a representative coupon of each material compared to the power law model for creep and recovery then the corresponding fatigue experimental and predicted response. In **Fig. 4.7**, the viscoelastic fatigue model developed for the virgin HDPE coupon continues to indicate a greater time dependence than is observed in the experimental fatigue response, in the same way as it did for the HDPE WPC under investigation. In comparison, while the initial offset doesn't quite match, the time dependence of the strain response of the PP-WPC and PVC-WPC appears to closely match the experimental data as can be seen in **Fig. 4.9** and **Fig 4.11**. This indicates further that the power law viscoelastic model does not describe well the behavior of HDPE, as was seen in the previous chapter.

In their study of the continuous and dynamic stress relaxation of HDPE, Scavuzzo[2] and Fe[3] observed different time dependent relaxations. In their testing, HDPE coupons were displaced a specified amount. Some were allowed to relax under monotonic displacement, while others were given a cyclic displacement oscillating around the constant displacement applied to the monotonic coupons. A summary of their results is shown in **Fig 4.12**. Note that rapid relaxation is observed initially in fatigue loading, which then levels out as time increases. In monotonic displacement, however, a slower initial relaxation with a greater time dependence is observed. This is similar to the results shown in **Fig 4.3**, and **4.4** where the coupons exhibit an immediate strain response, then the strain response tends to flatten out.

4.3 Prony Series Model

4.3.1 Development of the Prony Series fatigue model

In spite of the apparent contradictions between the creep and fatigue response of the WPC observed with the power law, the Prony Series compliance was applied to fluctuating stress. The development of the Prony Series fatigue model was very similar to the power law development. Eq. (4.2) was applied to the convolution integral with the Prony Series compliance. This resulted in a time, stress, and temperature dependent strain as

$$\varepsilon(t,\sigma,T)=\left[g_o D_o+\sum_{n=1}^{5} D_n\left(1-e^{\frac{-t}{\tau_n a_T(T)}}\right)\right]\sigma_o+\int_0^{\frac{t}{a_\sigma a_T(T)}}\left[g_o D_o+\sum_{n=1}^{5} D_n\left(1-e^{\frac{-t+\tau}{\tau_n}}\right)\right]\left[f\sigma_a\sin(f\tau)\right]d\tau \tag{4.4}$$

where the integrand, denoted G(t,τ) must be approximated with Simpson's rule, as was described above. This can be represented as

$$\int G(t-\tau)d\tau=\sum_{i=1}^{N}\frac{t}{6N}\left[G\left(t,t\frac{i-1}{N}\right)+4G\left(t,t\frac{i-.5}{N}\right)+G\left(t,t\frac{i}{N}\right)\right] \tag{4.5}$$

where N is the number of iterations. The same number of iterations per minute (*5,000t*) used for the power law model was found to be sufficient in evaluating the prony series, as can be seen in the convergence study in **Fig 4.13**. For times of 100 and 1000 minutes of fatigue, the strain response at *5,000t* iterations was found to be within 2% of the response found with a number of iterations an order of magnitude higher. This study was performed with σ_m=1.35MPa and σ_a=1.10MPa. A copy of the prony series viscoelastic fatigue Fortran model is attached in Appendix 2. The stress dependence observed in the creep modeling of the WPC was also utilized in modeling the fatigue behavior. The

stress dependence was calculated at the peak stress, $\sigma_m+\sigma_a$, where the strain response was evaluated.

4.3.2: Experimental verification of Prony Series model

As can be seen from **Fig. 4.14** and **Fig 4.15,** the time dependence predicted by the Prony Series model is very similar to that exhibited by the material. The difference in the instantaneous magnitude of the model and the experiment is due to coupon stiffness variation. **Fig. 4.15** shows a comparison of the power law model, the Prony Series model, and the experimental data utilizing the same coupon as shown in **Fig. 4.3** and **Fig. 4.4**. While also indicating the inherent variability between coupons, it also shows that the Prony Series model predicts the time dependence of the material in fatigue quite well at 23^{o}C.

4.3.3 Time-temperature superposition in Prony Series model

The temperature shift factor was accounted for in the same way as was used for the power law. The number of iterations was increased to *15,000t*. The time data from the Prony Series model was multiplied by the shifted time to enable comparison with experimental data. As can be seen from **Fig. 4.16**, predicted strain response was very similar in magnitude to the experimental strain at σ_{max}=30% at 45^{o}C. The time dependence was greater than experimentally observed. The magnitude of the experimental strain response was seen to vary between coupons. While the predicted viscoelastic behavior is much closer to experimental behavior than was observed for the power law model, it appears that the Prony Series viscoelastic fatigue model does not describe the mechanisms involved in fatigue of the WPC at elevated temperatures.

4.4 Damage Applied to Models

4.4.1 Power law fatigue model with damage

In order to account for fatigue loading where specimens were subjected to stresses above their threshold stress, a fatigue model for damage was developed. The damage function utilized for the creep models was also utilized for fatigue. For the power law model, damage was described as

$$\omega(\sigma_f, t) = 1 + (s + ct^m) < \sigma_f - \sigma_d > \tag{4.6}$$

where σ_f is given by Eq. (4.1). The function inside the McCauly brackets may be represented as

$$< \sigma_f - \sigma_d >= (\sigma_f(t) - \sigma_d) H(\sigma_f(t) - \sigma_d) \tag{4.7}$$

where H is the Heaviside step function. Subsequent differentiation of the effective stress

$$\sigma_e(t) = \sigma_f(t) \cdot \omega(\sigma_f, t) \cdot H(t) \tag{4.8}$$

which is evaluated together with the time dependent compliance in the convolution integral produces the viscoelastic response of the WPC to fatigue as

$$\varepsilon(t) = D(t)\sigma_m \langle \sigma_m - \sigma_d \rangle + \int_0^t D(t-\tau) \begin{bmatrix} f\sigma_a \cos(f\tau)\omega(\sigma_f, \tau) + \sigma_f(t) mc\tau^{m-1} \langle \sigma_f(t) - \sigma_d \rangle + \\ \sigma_f(t)\left(s + c\tau^m\right)\left(f\sigma_a \cos(f\tau) H(\sigma_f(t) - \sigma_d)\right) \end{bmatrix} d\tau \tag{4.9}$$

where the integrand must be numerically integrated and where *D(t)* is given by Eq. (3.3) in the previous chapter and the damage parameters are the same as given in Chapter Three. Simpson's rule was chosen to evaluate the integral. Many more integrations per time step were required for adequate modeling of the fatigue response. This can be seen

from **Fig. 4.17** where *15,000t* iterations were required for convergence. This is due to the sudden vertical jump in strain response that occurs as the applied stress passes through the threshold stress and discontinuities result in the model as strain suddenly increases with the application of damage. The program used to evaluate Eq. (4.9) (included in Appendix 3) was verified by comparison of its results with the linear fatigue model. A comparison of the model for a representative coupon at R=0.1, σ_{max}=70% Sut at 23^{o}C is shown in **Fig. 4.18**. The power law does not match the experimentally observed time dependence when damage is present.

4.4.2 Prony Series fatigue model with damage

To account for damage in the non-linear Prony Series, the same damage model utilized for the power law model, Eq. (4.6), was used. This was developed in the same way as the power law damage model, where the Prony Series was used for the compliance in Eq. (4.9). As found previously for the Prony Series, s=0, and c=.160GPa^{-1}min^{-m}. The program used to evaluate Eq. (4.9) (included in Appendix 4) was verified by comparison of its results with the linear fatigue model. Above 43% Sut, the non-linear terms were evaluated at the threshold stress as was determined for creep loading. A comparison with experimental strain response and the power law model is shown in **Fig. 4.18**. The Prony Series model does not model the behavior of the WPC above the threshold stress well in either time dependence or magnitude. Damage is overpredicted in this model.

4.4.3 Fatigue damage discussion

While the damage model utilized worked well in creep loading, it did not characterize the damage occuring in fatigue. The continuum damage function, Eq. (4.6),

presumes that there is an instantaneous (*s*) and time dependent (*c*) portion of damage that increases with time above the threshold stress. No instantaneous damage was found during creep loading with the Prony Series model. From **Fig. 4.18**, it appears that the time dependent damage is too great, as this is the only damage affecting the model. As damage is applied in the model, it accrues as long as the stress is above the threshold stress. This apparently is not what occurs in the actual fatigue of the WPC at hand. Likely, after the initial damage accumulation during the first few cycles, material damage only occurs at the peaks of the stress cycle, imparting a much smaller amount of damage per cycle than is predicted by the current damage model. It would appear from the experimental data, that crazing occurs or microcracks form during the initial few cycles of the fatigue loading. These cracks are then prevented from propagating by the wood particles or by blunting and softening of the crack tips due to hysteretic heating.

However, X-ray computed Tomography (CT) performed on a sample of the WPC loaded to 70% Sut in fatigue did not discern the formation of microcracks on the mesoscopic scale. The spatial resolution of the CT scanner was 0.27mm, which may be greater than the size of the microcracks if present. Damage, presenting itself through a change in density of the material, however, was observed to occur though CT analysis in the specimens previously loaded in creep and fatigue although the nature of the damage was not evident from the analysis. Temperature dependent damage was also observed in CT scanning.[5] While not indicating how the damage model was inadequate for fatigue loading, CT analysis does indicate the presence of damage and appeared to show quantitative differences in damage between creep and fatigue loading. The damage

function used to describe the creep behavior is insufficient for modeling the behavior of the WPC in fatigue loading.

A comparison of the percent reduction in elastic modulus is given in **Fig. 4.19** for fatigue loading. This indicates the relative damage occurring between coupons loaded in fatigue for 100 minutes with σ_{max}=30% and 70% of the temperature dependent Sut. A qualitative comparison with creep data can be made using **Fig. 3.18**, which indicates the reduction in elastic modulus after a 10 minute creep test as a function of applied load. Note that at 70% Sut, the change in modulus after 100 minutes of fatigue is slightly lower than was observed after 10 minutes of creep. This supports the peak strain comparisons, which also indicate slower damage growth in fatigue. Interestingly, temperature induced damage below the threshold stress observed for creep in **Fig. 3.18** are not as apparent in **Fig. 4.19**.

Due to the inability of the Prony Series model to describe the strain response of the WPC at temperatures above 23^{o}C in creep above the threshold stress, modeling of the fatigue response above the threshold stress at temperatures above 23^{o}C was not attempted.

4.4 Summary

The power law models appears to be insufficient for modeling the viscoelastic response in fatigue loading for the WPC at hand at room temperature at room temperature, and at the other temperatures tested. However, it does appear to describe the viscoelastic fatigue response of other polymeric materials at room temperature, indicating that the power law may be a better fit for those other materials than it is for the WPC under investigation. The viscoelastic response predicted by the Prony Series

model, while slightly above the experimental response, showed the same time dependence as the experimental response at room temperature. At elevated temperatures, it appeared that the Prony Series model was no longer describing the behavior of the material.

Neither the Prony Series nor the power law model were sufficient to describe the behavior of the WPC when the fatigue cycle included some of the region above the threshold strength. While the damage model utilized in creep worked well in creep loading, it does not characterize the damage occurring in fatigue loading.

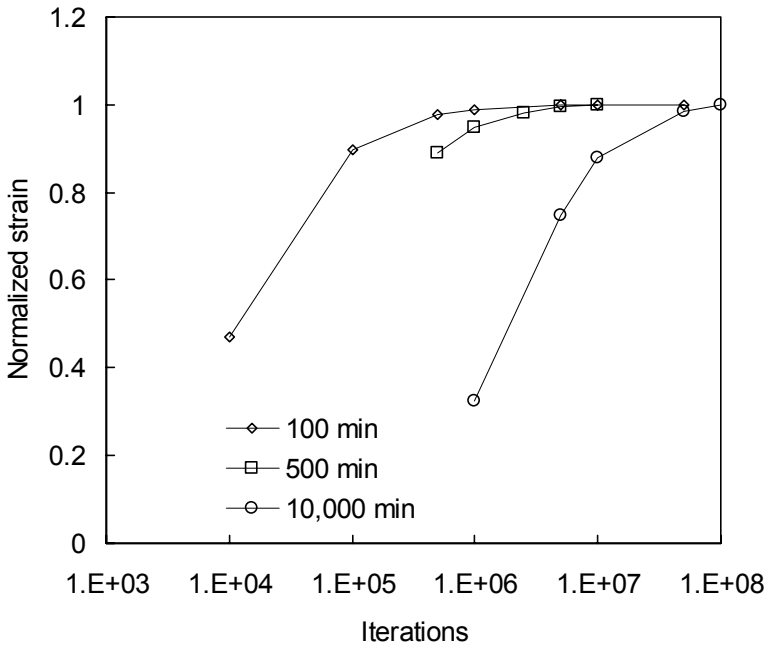

Fig 4.1: Convergence study for Fortran fatigue model using Simpson's rule.

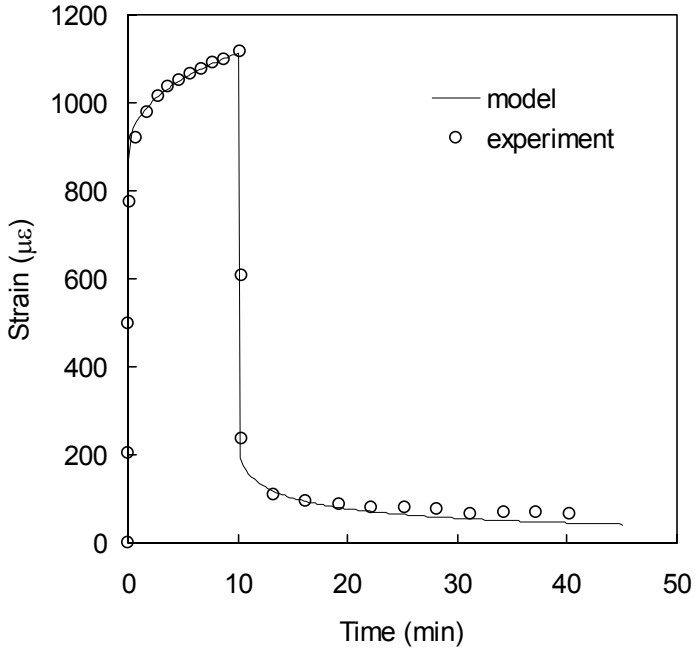

Fig 4.2 Comparison of power law model to 10 minute creep/recovery data at 30%Sut, 23°C.

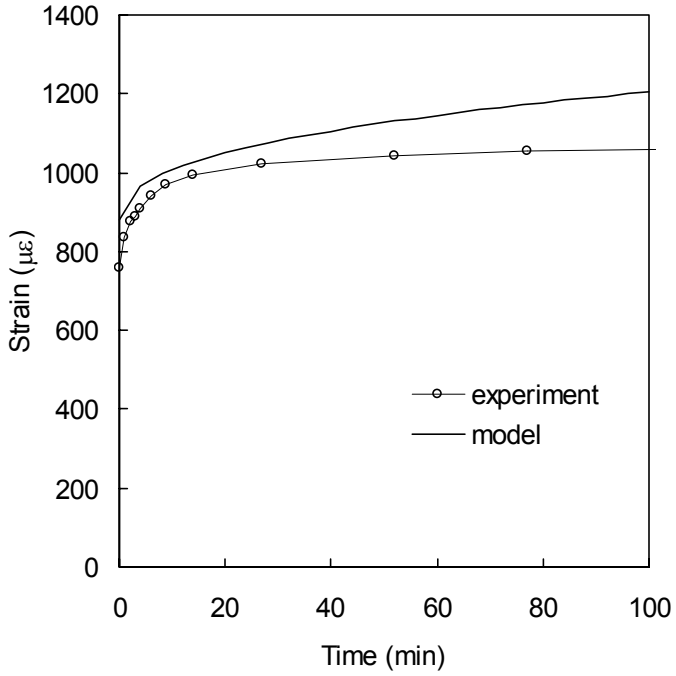

Fig 4.3: Comparison of peak cyclic strains of fatigue model using coupon dependent parameters with experimental data, R=0.1, σ_{max}=30% Sut at 23°C.

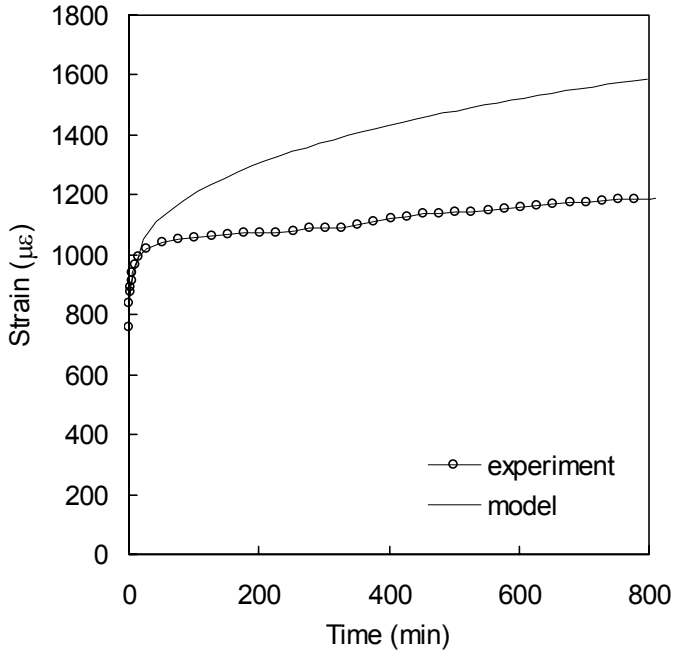

Fig 4.4: Same coupon as **Fig. 4.3** showing 800 minutes of data for comparison.

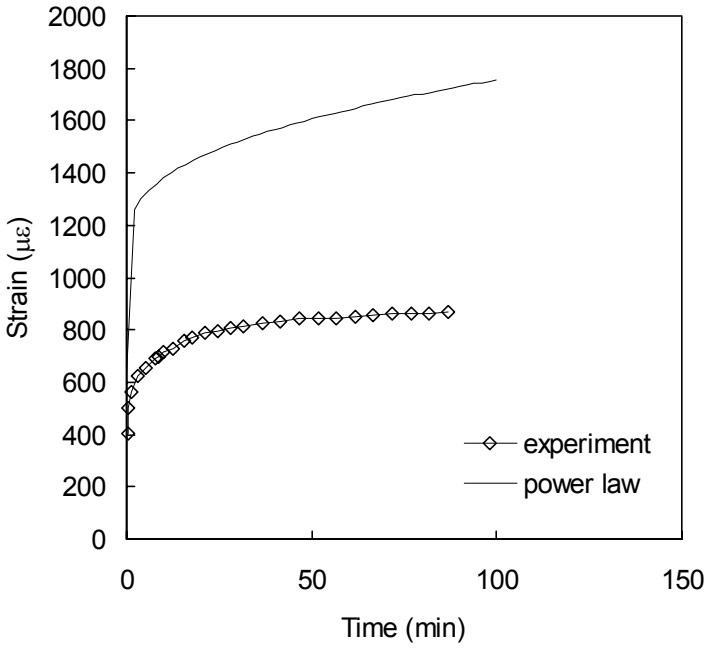

Fig 4.5: Comparison of viscoelastic power law model and representative coupon at 65°C and σ_{max}=30%Sut with R=0.1. Power law model time is multiplied by $a_T(T)$ according to the time shift factor of Eq. (3.24), for comparison with experimental data.

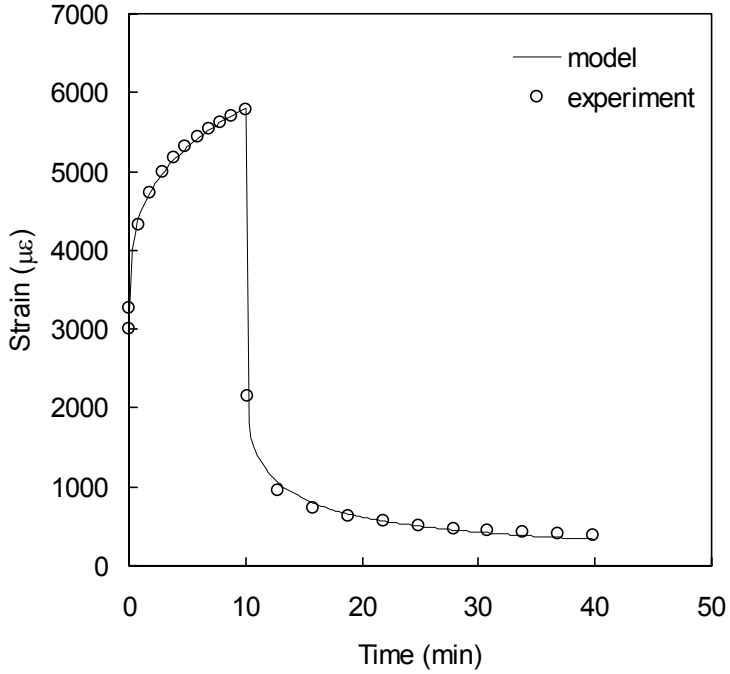

Fig 4.6: Comparison between power law model for HDPE and representative coupon. D_o=.783 Gpa^{-1} (5.4 Msi^{-1}) D_1=.333 Gpa^{-1}min^{-n} (2.3 Msi^{-1}min^{-n}) n=0.30, σ_o=3.17MPa.

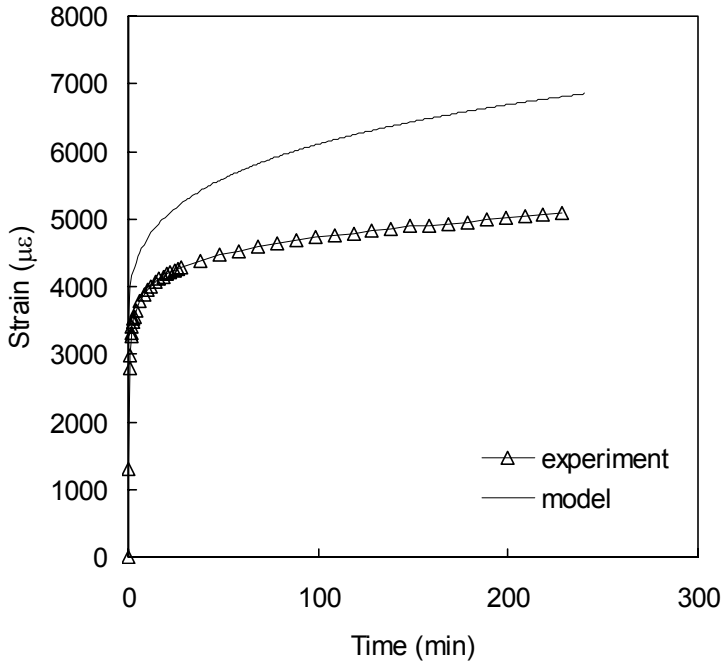

Fig 4.7: Comparison of HDPE power law fatigue model and representative coupon, σ_{max}=4.1 MPa with R=0.1, f=0.5 Hz.

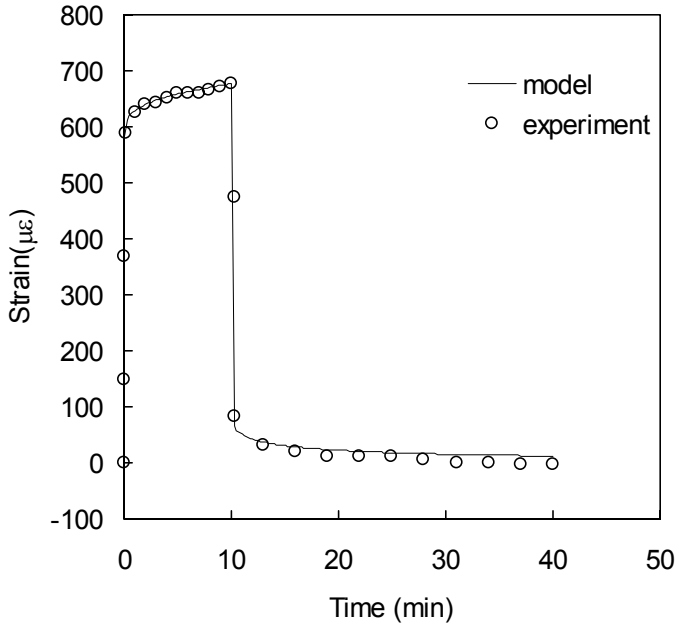

Fig 4.8: Comparison between power law model for PP WPC and representative coupon. D_o=.174 Gpa^{-1} (1.205 Msi^{-1}) D_1=.015 Gpa^{-1}min^{-n} (.10 Msi^{-1}min^{-n}) n=0.30, σ_o=3.17MPa.

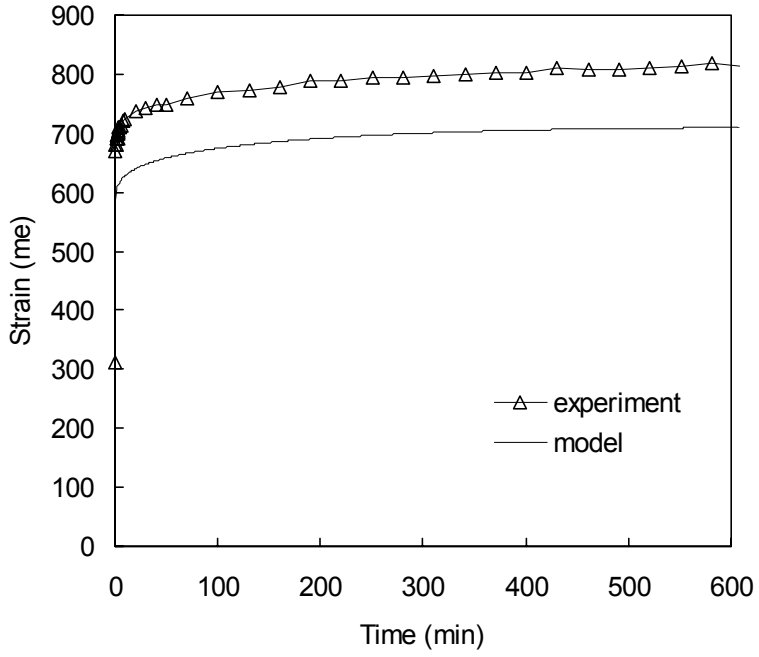

Fig 4.9: Comparison of PP WPC power law fatigue model and representative coupon, σ_{max}=3.17MPa with R=0.1, f=0.5 Hz.

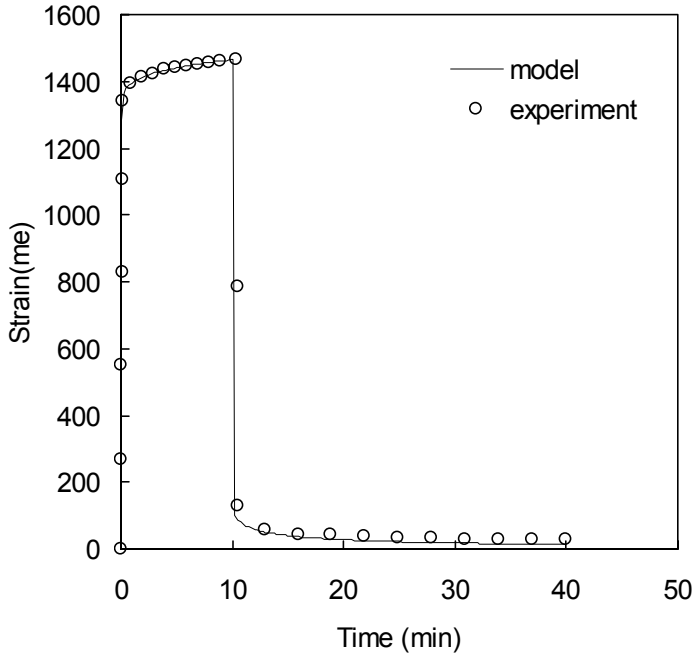

Fig 4.10: Comparison between power law model for PVC WPC and representative coupon. D_o=.13 Gpa^{-1} (0.9Msi^{-1}) D_1=.013 Gpa^{-1}min^{-n} (.09 Msi^{-1}min^{-n}) n=0.19, σ_o=9.72MPa.

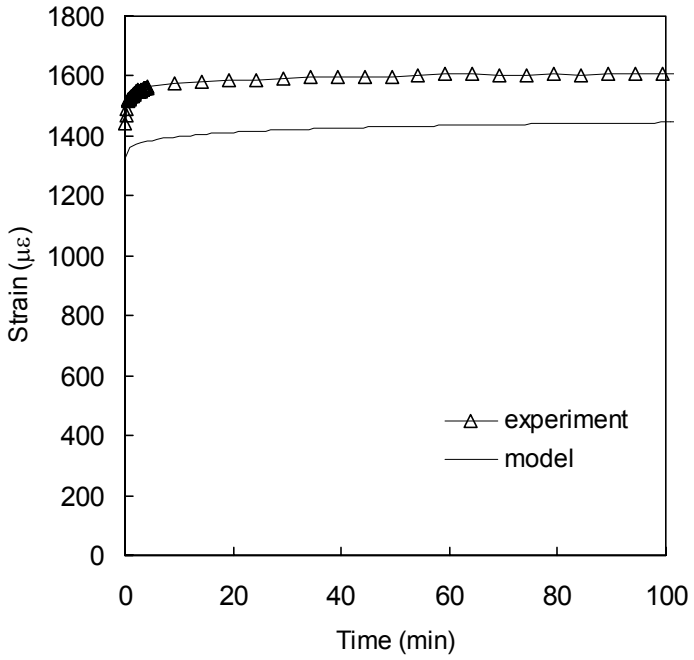

Fig 4.11: Comparison of PVC WPC power law fatigue model and representative coupon, σ_{max}=9.72MPa with R=0.1, f=0.5 Hz.

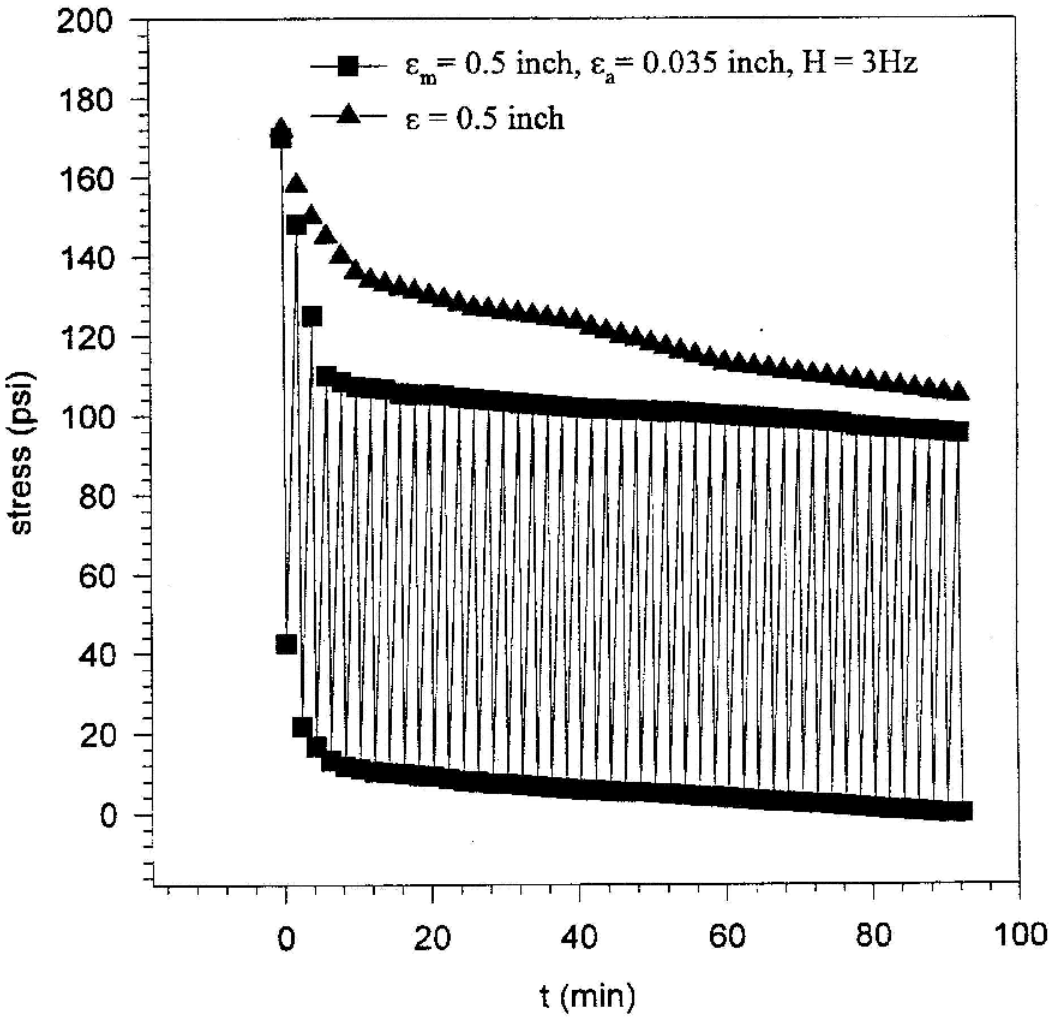

Fig 4.12: Dynamic relaxation compared to relaxation from monatonic displacement. Taken from thesis of Fang He [3].

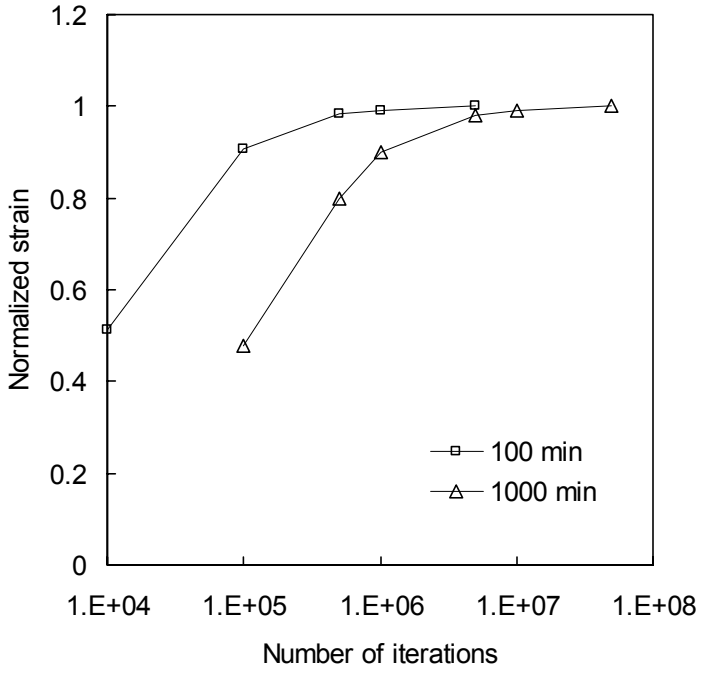

Fig 4.13: Convergence study for Prony Series fatigue model.

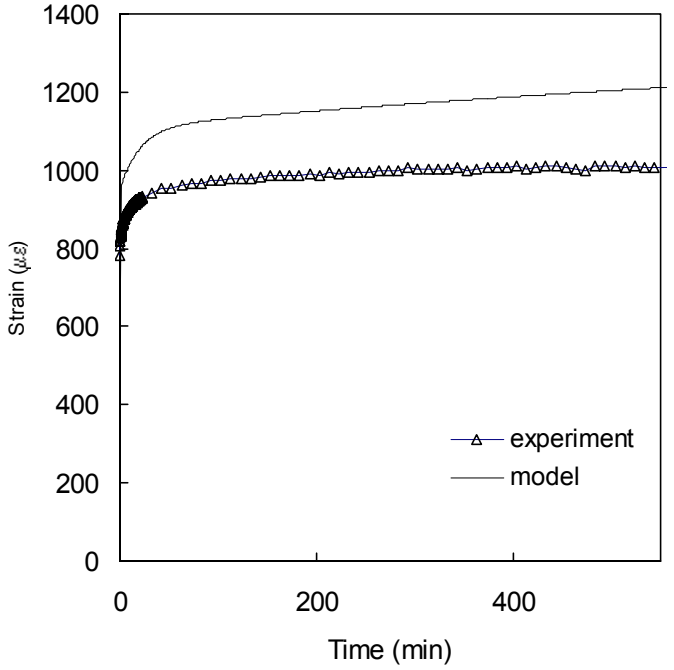

Fig 4.14: Comparison of Prony Series model with experimental data at 23°C and σ_{max}=30%Sut with R=.1.

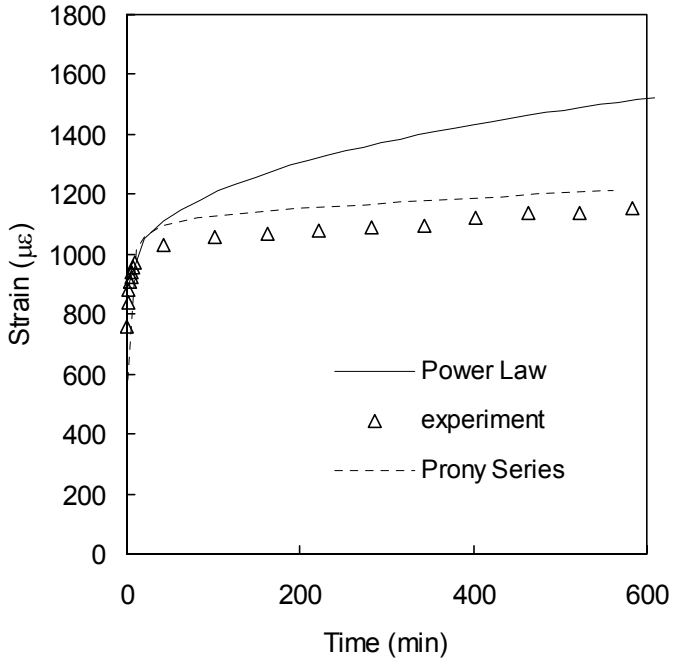

Fig 4.15: Comparison of Prony Series model with power law and experimental data for the coupon shown in **Fig 4.3** and **4.4**.

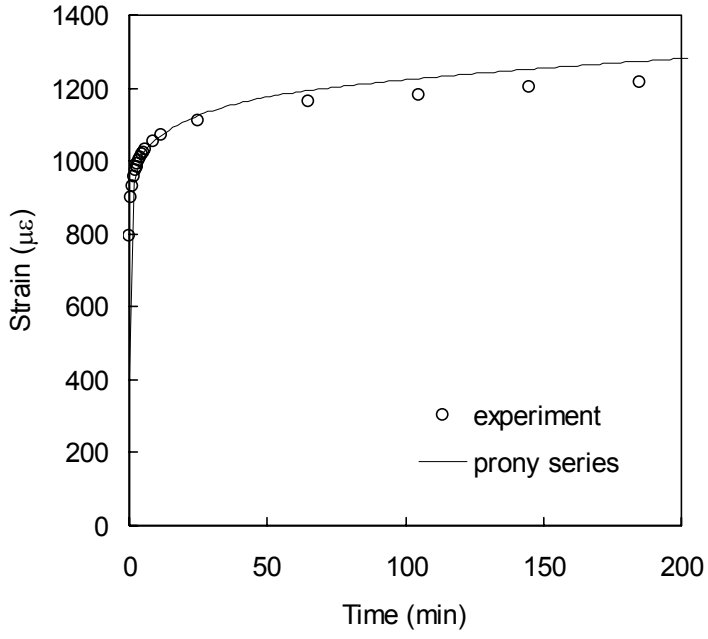

Fig. 4.16: Comparison of representative coupon and Prony Series model at 45°C and σ_{max}=30%Sut with R=0.1. Shifted time from Fortran model is multiplied by a_T to compare with real time measured experimentally.

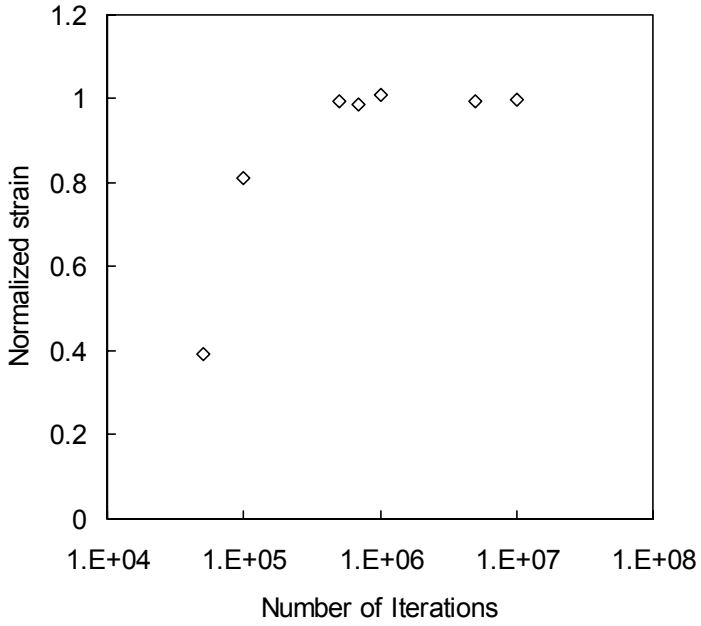

Fig 4.17: Convergence of the power law damage model at 100 minutes. *15,000t* iterations required.

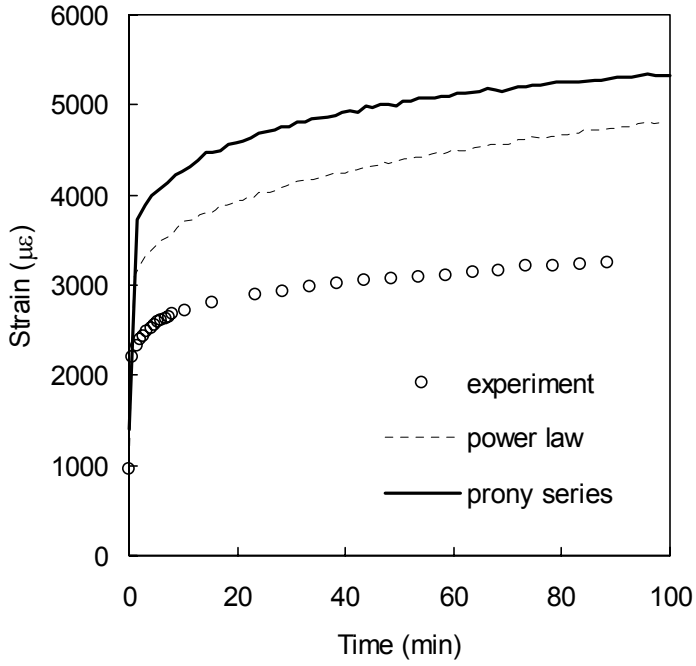

Fig 4.18: Comparison of power law model an Prony Series model to representative coupon at 23°C and σ_{max}=70%Sut with R=0.1.

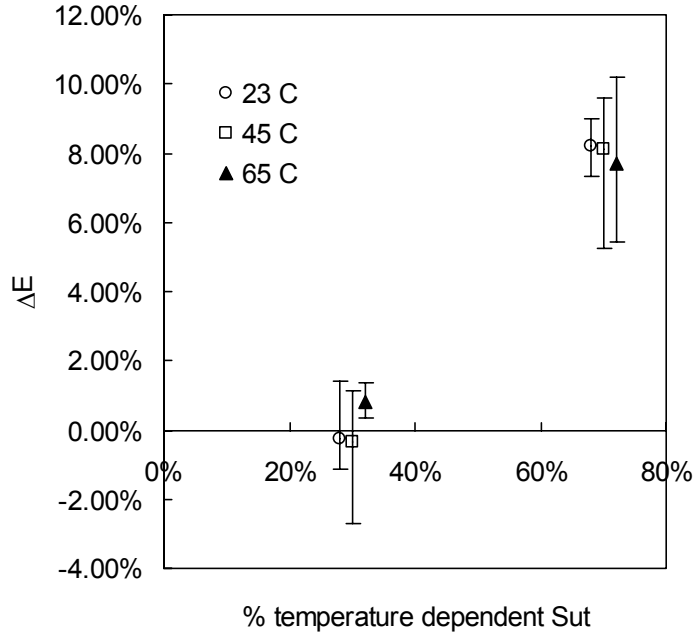

Fig. 4.19: Percent reduction in elastic modulus ΔE=1-E_i/E_f in fatigue loading where E_f is the final stiffness and E_i is the initial stiffness.

REFERENCES

[1] Elahi, M., and Weitsman, Y.J., On the Mechanical response of P4 Chopped Glass/Urethane Resin Composite: Data and Model, Oak Ridge National Laboratory, ORNL –6955, October, 1999.

[2] Scavuzzo, Rudolph J., Oscillating Stress on Viscoelastic Behavior of Thermoplastic Polymers, Journal of Pressure Vessel Technology, Vol. 122, August 2000.

[3] He, Fang, Fatigue and Stress Relaxation Behavior of High-Density Polyethylene, Master's Thesis, University of Akron, December, 1997.

[4] Rangaraj, Sudarshan V., and Smith, Lloyd V., The Non-linear Viscoelastic Response of a Wood-Thermoplastic Composite, Mechanics of Time-Dependent Materials, 3:125-139, 1999.

[5] Shi, Q., and Bathias, C., Analytical results from X-ray computed Tomography on wood plastic composite, ITMA/CNAM, Paris, March 2001.

CHAPTER FIVE

CONCLUSIONS AND RECOMMENDATIONS

5.1 Conclusions

The power law and Prony Series viscoelastic models were evaluated in their ability to describe the time dependent behavior of the wood-plastic composite in creep and fatigue loading. The WPC was found to be thermo-rheologically simple according tests conducted with DMA. The horizontal shift factor was described satisfactorily by the WLF equation. While the power law was adequate for describing the behavior at short times and an equation with preliminary shift factors was readily obtainable for describing the temperature dependence of the WPC for short times, it was not found to describe well the behavior of the WPC when the TTSP was applied using the DMA shift factor. A Prony Series model was developed, which, while more complex, was able to describe the creep response for up to 10^7 minutes (in shifted time) based on the TTSP. Good correlation was obtained between experimental data and the Prony Series model at 23^{o}C, 45^{o}C, and 65^{o}C. The threshold stress was found to scale with the temperature dependent ultimate strength. A continuum damage model was developed to describe the strain response for the WPC at 23^{o}C but overpredicted the strain response at elevated temperatures above the threshold stress indicating that the magnitude of damage was temperature dependent.

Application of the creep viscoelastic model to predict the peak cyclic strain during fatigue loading was undertaken. Good correlation between the Prony Series and the experimental data at 23^{o}C was obtained. Temperature was found to affect the cyclic strain response for the WPC, such that the model did not satisfactorily predict the strain

response. Likewise, above the threshold stress, the damage model did not predict the strain response, indicating that the time dependence damage as accounted for by the creep model does not match the behavior of the WPC in cyclic loading.

The viscoelastic behavior of the WPC is not described by a simple model. Rather, it must be described by a non-linear Prony Series model that allows for modeling of the several time dependent viscoelastic behaviors of the material. Additionally, the material behaves non-linearly, requiring stress dependent terms. A threshold stress is also observed, requiring a damage model to represent behavior above the threshold stress. The damage was found to be dependent on temperature, and on the loading function.

5.2 Recommendations:

Further creep tests performed for longer durations at the three temperatures tested would increase the time period that could be described by the Prony Series model at various temperatures. Further, if creep tests were performed at more frequent temperature intervals, perhaps every 5^{o}C, superposition of the creep curves could be conducted, producing a more complete compliance master curve without gaps. This could be used to develop a master curve and time shift factor $a_T(T)$ without using DMA. This would further the predictive ability of the model over a wide range of elevated temperatures below the melting point.

Further investigation of the viscoelastic behavior at temperatures below 23^{o}C would provide a complete understanding of the temperature dependent behavior of this material.

Use of a technique such as computed Tomography scanning of the WPC to compare the structure before and after creep, cyclic, and temperature loading at a greater

variety of loading scenarios would provide information on the changing nature of the damage mechanism with temperature and loading. This may provide directions as to the type of damage model required to predict the behavior of the WPC under cyclic loading, however, the inclusion of these findings may further convolute the already complex model.

APPENDIX ONE

Power law fatigue model below threshold strength

```
      implicit double precision (a-h,o-z)
      integer i,j,k,N
c
c-----define functions
c       FT=stiffness shift factor
c        aT=time shift factor
c       f(x,y)=function being integrated
c        g(z) is function before integral
      g(z)=d0*FT+done*(z)**dn
      f(x,y)=(d0*FT+done*(((x-y))**dn))*(w)*sigamp*cos(w*y)
c
      k=50
c
c        define realn as real number for use in equation
c       realn=N
c
c-----defining constants
c
      pi=3.14159265358979323846
      sigamp=207
      sigmean=253
c       temp in kelvin
      temp=296
      tref=296.
      d0=1.6
      FT=.0441*temp-12.05
      done=.22
      dn=.39
      freq=.5
      offset1=1./(4.*60.*freq)
      w=2.*pi*60.*freq
      aT=10.**((-6.885*(temp-tref))/(164.6+temp-tref))
c
c       write format for output file
c
      iin=10
      iout=11
      open (unit=11,status='unknown',file='23C30%pwl',form='formatted')
c
c       evaluate integral using simpson's rule
c
      do 100 j=0,k
        realj=(1.+16.*j)*offset1
        Sn=0.
        sum=g(realj/aT)*sigmean
```

```
                N=j*5000
                realn=N
c
        do 200 i=2,N
                reali=i
c               realn=N
c       continuing with simpson's rule
c
c               sum=sum+(realj/(6.*realn))*(f(realj,realj*(reali-1.)/realn)+
c       .       4.*f(realj,realj*(reali-.5)/realn)+f(realj,realj*reali/realn))
c
c
c---- loop for calculating max strain for first cycle of each minute
c
c
        sum1=f(realj,realj*(reali-1.)/realn)
c
        sum2=f(realj,realj*(reali-.5)/realn)
c
        sum3=f(realj,realj*(reali)/realn)

        Sn=(realj/(6.*realn))*(sum1+4.*sum2+sum3)+Sn
c
        200   end do
         Sn=Sn+sum
c
c        create output file
c
         write(11,1000) realj/aT,Sn
c
        1000      format(e25.14,e25.14)
        100 end do
        end
```

APPENDIX TWO

Prony series fatigue model below threshold stress

```
      implicit double precision (a-h,o-z)
      integer i,j,k,N
c
c-----define functions
c       aT=time shift factor
c       f(x,y)=function being integrated
c       g(z) is function before integral
      h(u)=sigmean+sigamp*sin(w*u)
      diff(t)=(h(t)-thresh)*step
      g(z)=d0*b+d1*(1-exp(-z/tau1))+
     .d2*(1-exp(-z/tau2))+d3*(1-exp(-z/tau3))
     .+d4*(1-exp(-z/tau4))+d5*(1-exp(-z/tau5))
c
      f(x,y)=g(x-y)*w*sigamp*cos(w*y)*(1+(s+dc*y**dm)*diff(y))
     .+g(x-y)*h(y)*(dm*dc*y**(dm-1)*diff(y)+
     .(s+dc*y**dm)*w*sigamp*cos(w*y)*step)
c
      k=100
c
c-----defining constants
c
      pi=3.14159265358979323846
      sigamp=490.
      sigmean=600.
c       temp in kelvin
      temp=296.
      tref=296.
      d0=1.94
      d1=.65
      tau1=20.
      d2=.9
      tau2=1000
      d3=.8
      tau3=12000
      d4=1.126
      tau4=148641
      d5=1.8748
      tau5=3000000
      freq=.5
      offset1=1./(4.*60.*freq)
      w=2.*pi*60.*freq
      dm=0.15
      s=.00
      dc=.0011
```

```
c       threshold stress of .43% Sut
        thresh=670.
        aT=10.**((-20.534*(temp-tref))/(128.78+temp-tref))
c
        if (sigamp+sigmean.gt.thresh) then
        b=.000563*(thresh)+.8225
        c=-.00171*(thresh)+1.8555
        else
        b=.000563*(sigamp+sigmean)+.8225
        c=-.00171*(sigamp+sigmean)+1.8555
        end if
c
c       write format for output file
c
        iin=10
        iout=11
        open (unit=11,status='unknown',file='23C70%62',form='formatted')
c
c       evaluate integral using simpson's rule
c
        do 100 j=0,k
          realj=(j+offset1)
          Sn=0.
          sum=g(realj/(c*aT))*sigmean
                N=j*50000
                realn=N
c
        do 200 i=2,N
                reali=i
c               realn=N
c       continuing with simpson's rule
c
c               sum=sum+(realj/(6.*realn))*(f(realj,realj*(reali-1.)/realn)+
c       .       4.*f(realj,realj*(reali-.5)/realn)+f(realj,realj*reali/realn))
c
c
c---- loop for calculating max strain for first cycle of each minute
c
        if (h(realj*(reali-1.)/realn) .le. thresh) then
                step=0.
        else
                step=1.
        end if
        sum1=f(realj,realj*(reali-1.)/realn)
c
        if (h(realj*(reali-.5)/realn) .le. thresh) then
```

```
            step=0.
        else
            step=1.
        end if
        sum2=f(realj,realj*(reali-.5)/realn)
c
        if (h(realj*(reali)/realn) .le. thresh) then
            step=0.
        else
            step=1.
        end if
        sum3=f(realj,realj*(reali)/realn)

        Sn=(realj/(6.*realn))*(sum1+4.*sum2+sum3)+Sn
c
c
c
        200   end do
          Sn=Sn+sum
c
c        create output file
c
          write(11,1000) realj/(c*aT),Sn
c
        1000      format(e25.14,e25.14)
        100 end do
        end
```

APPENDIX THREE

Power law Fortran fatigue model with damage

```
      implicit double precision (a-h,o-z)
      integer i,j,k,N
c
c-----define functions
c       aT=time shift factor
c       f(x,y)=function being integrated
c       g(z) is function before integral
      h(u)=sigmean+sigamp*sin(w*u)
      diff(t)=(h(t)-thresh)*step
      g(z)=d0*b+d1*(1-exp(-z/tau1))+
     .d2*(1-exp(-z/tau2))+d3*(1-exp(-z/tau3))
     .+d4*(1-exp(-z/tau4))+d5*(1-exp(-z/tau5))
c
      f(x,y)=g(x-y)*w*sigamp*cos(w*y)*(1+(s+dc*y**dm)*diff(y))
     .+g(x-y)*h(y)*(dm*dc*y**(dm-1)*diff(y)+
     .(s+dc*y**dm)*w*sigamp*cos(w*y)*step)
c
      k=100
c
c-----defining constants
c
      pi=3.14159265358979323846
      sigamp=490.
      sigmean=600.
c       temp in kelvin
      temp=296.
      tref=296.
      d0=1.94
      d1=.65
      tau1=20.
      d2=.9
      tau2=1000
      d3=.8
      tau3=12000
      d4=1.126
      tau4=148641
      d5=1.8748
      tau5=3000000
      freq=.5
      offset1=1./(4.*60.*freq)
      w=2.*pi*60.*freq
      dm=0.15
      s=.00
      dc=.0011
c       threshold stress of .43% Sut
```

```
      thresh=670.
      aT=10.**((-20.534*(temp-tref))/(128.78+temp-tref))
c
      if (sigamp+sigmean.gt.thresh) then
      b=.000563*(thresh)+.8225
      c=-.00171*(thresh)+1.8555
      else
      b=.000563*(sigamp+sigmean)+.8225
      c=-.00171*(sigamp+sigmean)+1.8555
      end if
c
c     write format for output file
c
      iin=10
      iout=11
      open (unit=11,status='unknown',file='23C70%62',form='formatted')
c
c     evaluate integral using simpson's rule
c
      do 100 j=0,k
       realj=(j+offset1)
       Sn=0.
       sum=g(realj/(c*aT))*sigmean
            N=j*15000
            realn=N
c
      do 200 i=2,N
            reali=i
c           realn=N
c     continuing with simpson's rule
c
c           sum=sum+(realj/(6.*realn))*(f(realj,realj*(reali-1.)/realn)+
c     .     4.*f(realj,realj*(reali-.5)/realn)+f(realj,realj*reali/realn))
c
c
c---- loop for calculating max strain for first cycle of each minute
c
      if (h(realj*(reali-1.)/realn) .le. thresh) then
            step=0.
      else
            step=1.
      end if
      sum1=f(realj,realj*(reali-1.)/realn)
c
      if (h(realj*(reali-.5)/realn) .le. thresh) then
            step=0.
```

```
        else
                step=1.
        end if
        sum2=f(realj,realj*(reali-.5)/realn)
c
        if (h(realj*(reali)/realn) .le. thresh) then
                step=0.
        else
                step=1.
        end if
        sum3=f(realj,realj*(reali)/realn)

        Sn=(realj/(6.*realn))*(sum1+4.*sum2+sum3)+Sn
c
c
c
        200   end do
         Sn=Sn+sum
c
c        create output file
c
         write(11,1000) realj/(c*aT),Sn
c
        1000      format(e25.14,e25.14)
        100 end do
        end
```

APPENDIX FOUR

Prony series Fortran fatigue model with damage

```
      implicit double precision (a-h,o-z)
      integer i,j,k,N
c
c-----define functions
c       aT=time shift factor
c       f(x,y)=function being integrated
c       g(z) is function before integral
      h(u)=sigmean+sigamp*sin(w*u)
      diff(t)=(h(t)-thresh)*step
      g(z)=d0*b+d1*(1-exp(-z/tau1))+
     .d2*(1-exp(-z/tau2))+d3*(1-exp(-z/tau3))
     .+d4*(1-exp(-z/tau4))+d5*(1-exp(-z/tau5))
c
      f(x,y)=g(x-y)*w*sigamp*cos(w*y)*(1+(s+dc*y**dm)*diff(y))
     .+g(x-y)*h(y)*(dm*dc*y**(dm-1)*diff(y)+
     .(s+dc*y**dm)*w*sigamp*cos(w*y)*step)
c
      k=100
c
c-----defining constants
c
      pi=3.14159265358979323846
      sigamp=490.
      sigmean=600.
c       temp in kelvin
      temp=296.
      tref=296.
      d0=1.94
      d1=.65
      tau1=20.
      d2=.9
      tau2=1000
      d3=.8
      tau3=12000
      d4=1.126
      tau4=148641
      d5=1.8748
      tau5=3000000
      freq=.5
      offset1=1./(4.*60.*freq)
      w=2.*pi*60.*freq
      dm=0.15
      s=.00
      dc=.0011
c       threshold stress of .43% Sut
      thresh=670.
```

```
      aT=10.**((-20.534*(temp-tref))/(128.78+temp-tref))
c
      if (sigamp+sigmean.gt.thresh) then
      b=.000563*(thresh)+.8225
      c=-.00171*(thresh)+1.8555
      else
      b=.000563*(sigamp+sigmean)+.8225
      c=-.00171*(sigamp+sigmean)+1.8555
      end if
c
c     write format for output file
c
      iin=10
      iout=11
      open (unit=11,status='unknown',file='23C70%62',form='formatted')
c
c     evaluate integral using simpson's rule
c
      do 100 j=0,k
       realj=(j+offset1)
       Sn=0.
       sum=g(realj/(c*aT))*sigmean
            N=j*15000
            realn=N
c
      do 200 i=2,N
            reali=i
c           realn=N
c     continuing with simpson's rule
c
c           sum=sum+(realj/(6.*realn))*(f(realj,realj*(reali-1.)/realn)+
c     .     4.*f(realj,realj*(reali-.5)/realn)+f(realj,realj*reali/realn))
c
c
c---- loop for calculating max strain for first cycle of each minute
c
      if (h(realj*(reali-1.)/realn) .le. thresh) then
            step=0.
      else
            step=1.
      end if
      sum1=f(realj,realj*(reali-1.)/realn)
c
      if (h(realj*(reali-.5)/realn) .le. thresh) then
            step=0.
      else
```

```
            step=1.
        end if
        sum2=f(realj,realj*(reali-.5)/realn)
c
        if (h(realj*(reali)/realn) .le. thresh) then
            step=0.
        else
            step=1.
        end if
        sum3=f(realj,realj*(reali)/realn)

        Sn=(realj/(6.*realn))*(sum1+4.*sum2+sum3)+Sn
c
c
c
        200   end do
         Sn=Sn+sum
c
c        create output file
c
         write(11,1000) realj/(c*aT),Sn
c
        1000     format(e25.14,e25.14)
        100 end do
        end
```